Development of Novel Advanced Flow Control Systems on Centrifugal Microfluidic Platforms for Nucleic Acid Testing

Jennifer Gaughran, B.Sc. (Hons)

School of Physical Sciences

Dublin City University

A thesis submitted to Dublin City University for the degree of

Doctor of Philosophy (Ph.D.)

Research Supervisor

Prof. Jens Ducrée

January 2016

Declaration

I hereby certify that this material, which I now submit for assessment on the programme of study leading to the award of Doctor of Philosophy, is entirely my own work, and that I have exercised reasonable care to ensure that the work is original, and does not to the best of my knowledge breach any law of copyright, and has not been taken from the work of others save and to the extent that such work has been cited and acknowledged within the text of my work.

Signed: _____

ID No.:57530978

Date: _____

For my parents,

Sandra and Stephen

Acknowledgements

There are so many people I would like to thank and inevitably many more that I have forgotten at this moment. I can only hope that they know they are greatly appreciated.

First of all, I would like to thank my supervisor Prof. Jens Ducrée for giving me the opportunity to work in his group and for the advice and direction during my PhD.

My sincerest thanks to all the Microfluidics Group, past and present, who helped me along the way and made my time working in our lab so enjoyable. I'd particularly like to thank Nikolay for all his help and advice at the beginning of my PhD, Charles and Macdara for their highly useful insights and Lorcan for always having the answer to my questions. Special mention must go to Dave Kinahan, who not only proof read this document for me, but has been my sounding board and shared with me his considerable knowledge, as well as some excellent book recommendations.

I have to thank all the highly talented students who worked with me during their internships with the microfluidics group. Their enthusiasm and help with building all those discs will be forever appreciated. I would especially like to thank Dave Boyle who is one of the hardest workers I have ever met and has a very bright future.

Thank you to all those in the Biomedical Diagnostics Institute who I worked with in my time in DCU, particularly to the members of S252 for keeping me company during my long hours at the spin stand.

Many thanks to Declan McGlade for answering my endless stream of questions when I began my work with graphene oxide.

Thank you to all the members of the DCU School of Physics who have been such a huge part of my time in DCU. My sincerest thanks to Prof. Enda McGylnn and Prof. Colette McDonagh for their excellent advice and for always having an open door. Thanks to the technical and administrative staff in the School, in particular Lisa for always knowing where the form was supposed to go and for the excellent Christmas parties.

I am very grateful to the entire Bio-AT team, in particular Christine, Joan and Jane, for not only giving me this opportunity but for all the support and encouragement throughout my entire PhD. They also introduced me to all the other Bio-AT students, who I would also like to thank both for their friendship and for answering all my biology questions. I'd particularly like to thank Tríona for all of her support and help.

Thanks to all the postgrads in my office for their friendship of the last few years and for making every day fun. There are too many to name but I will mention Dan, Stephen, Paul, May, Danielle, Éanna and Leanne.

I've made and managed to hang onto some of the best friends during my PhD and I would like to sincerely thank them for their support. To Damien, who started out as a friend and became much more, thank you for the support and the laughter. To Mary and Sam, thank you for feeding me and for all the chats. To Ciarán, thank you for your friendship and for answering all my 'what now' questions. Finally, a specially mention must go to Adam, who has been my friend, roommate and sounding board for the past four and a half years. Thank you for listening to me give the same talks over and over again and for the many nights of TV watching and tea.

And most of all special thanks go to my family. To my brothers Glenn and Matthew, who have given me great support for years and who have always been there for me. To Eileen and Jonathan, for their constant encouragement and always telling me 'you'll get there'.

Most of all I would like to thank my parents, without whom none of this would have been possible. They believed in me every step of the way and they showed me there was nothing I couldn't do. I am eternally grateful for everything you have done for me and for the constant, unwavering support. As promised, I dedicate this one to the both of you.

Table of Contents

Glossary

μTAS	micro Total Analysis Systems
ADF	Aqueous Dissolvable Film
ADF	Annular Dark-Field
AFM	Atomic Force Microscopy
BF	Bright-field
BSE	Backscattered Electrons
cDNA	Complimentary DNA
CFU	Colony Forming Units
CNC	Computer Numerical Control
COP	Cyclo-olefin polymer
CVD	Chemical Vapour Deposition
DF	Dissolvable Film
DF	Dissolvable Film
DFV	Dissolvable Film Valve
DMEM	Dulbecco's Modified Eagle Medium
DNA	Deoxyribonucleic acid
dsDNA	Double Stranded DNA
DXF	Drawing eXchange Format
Eaq	Elute Collection Chamber
EB	Elution Buffer
EDTA	Ethylenediaminetetraacetic acid
EGOR	Event-triggered Graphene Oxide Router
EtOH	Ethanol
GO	Graphene Oxide
HM	Hydrophobic Membrane
HMV	Hydrophobic Membrane Valve
IPA	Isopropanol
L	Loading Chamber
LAMP	Loop-mediated isothermal amplification

LB	Luria-Bertani
L_E	Elution Loading Chamber
L_O	Organic Loading Chamber
LoaD	Lab-on-a-Disc
L_S	Sample Loading Chamber
LUOs	Laboratory Operating Units
n	Number of repeats
NA	Nucleic Acid
NC	Numerical Control
ODF	Organic Dissolvable Film
PCR	Polymerase Chain Reaction
PDMS	Poly(dimethylsiloxane)
PMMA	Poly(methyl methacrylate)
POC	Point of Care
PSA	Pressure Sensitive Adhesive
PTFE	Polytetrafluoroethylene
qPCR	Real-time PCR
RIN	RNA Integrity Number
rRNA	ribosomal RNA
RT-PCR	Reverse Transcription PCR
S/N	Signal to Noise
SE	Secondary Electrons
SEM	Scanning Electron Microscope
SPP	Solid Phase Purification
ssDNA	Single-stranded DNA
TE Buffer	Tris EDTA Buffer
TRI	Trizol
Tris	Trisaminomethane
Waq	Aqueouse Waste Chamber
Worg	Organic Waste Chamber

List of Figures

List of Tables

List of Publications

Papers

1. **Jennifer Gaughran**, David Boyle, James Murphy, Robert Kelly and Jens Ducrée. *Phase-Selective Graphene Oxide Membranes for Advanced Microfluidic Flow Control.* Nature Microsystems and NanoEngineering, 2:16008, 2016. Selected as feature article on journal cover. (Chapter 3)

2. Nikolay Dimov, Eoin Clancy, **Jennifer Gaughran**, David Boyle, Darren Mc Auley, Macdara Glynn, Thomas Barry, Louise Barrett, Terry J. Smith, and Jens Ducrée. *Solvent-selective fluid routing for centrifugally integrated solid-phase extraction of RNA.* Microfluidics & Nanofluidics, 18(5-6):859–871, 2015. (Chapter 4)

3. **Jennifer Gaughran**, Robert Kelly and Jens Ducrée. *Graphene Oxide Enabled Centrifugo-Pneumatic Routing of Flows for Nucleic Acid Purification.* [In preparation] (Chapter 5)

4. **Jennifer Gaughran**, David Kinahan and Jens Ducrée. *Event-triggered Graphene Oxide Router for Automated Nucleic Acid Purification.* [In preparation] (Chapter 6)

5. **Jennifer Gaughran**, Nikolay Dimov, Eoin Clancy, Barry Glynn, Thomas Barry, David Kinahan, Terry J. Smith and Jens Ducrée. *Rotationally automated fluid-fluid extraction of total RNA on-disc for early-stage point-of-care diagnostics from whole blood.* [In preparation] (Chapter 7)

Conference Manuscripts

1. **Jennifer Gaughran** and Jens Ducrée. *Graphene oxide enabled centrifugo-pneumatic routing of flows.* In Proceedings of the 18th International Conference on Solid-State Sensors, Actuators & Microsystems (Transducers 2015), June 21–25, Anchorage, Alaska, USA, pages 331–334, 2015. (Oral). (Chapter 4)

2. **Jennifer Gaughran**, David Boyle, James Murphy, and Jens Ducrée. *Graphene oxide membranes for phase-selective microfluidic flow control.* In Proceedings of the 28th IEEE International Conference on Micro Electro Mechanical Systems (MEMS 2015), January 18 – 22, Estoril, Portugal, pages 2–4, 2015. (Oral). (Chapter 5)

3. **Jennifer Gaughran**, Nikolay Dimov, Eoin Clancy, Thomas Barry, Terry Smith and Jens Ducrée. *Multi-stage, solvent-controlled routing for automated on-disc extraction of total RNA from breast cancer cell line homogenate.* In Proceedings of the 17th International Conference on Solid-State Sensors, Actuators & Microsystems (Transducers 2013), June 16–20, Barcelona, Catalonia, Spain, pages 305–308, 2013. (Chapter 3)

4. Nikolay Dimov, **Jennifer Gaughran**, Eoin Clancy, Thomas Barry, Terry Smith, and Jens Ducrée. *Automated on-disc total RNA extraction from whole blood towards point-of-care for early-stage diagnostics*. In Proceedings of the 17th International Conference on Solid-State Sensors, Actuators & Microsystems (Transducers 2013), June 16–20, Barcelona, Catalonia, Spain, pages 2548–2551, 2013. (Oral). (Chapter 7)

5. Nikolay Dimov, **Jennifer Gaughran**, Darren Mc Auley, David Boyle, David J. Kinahan, and Jens Ducrée. *Centrifugally automated solid-phase purification of RNA.* In Proceedings of the 27th IEEE International Conference on Micro Electro Mechanical

Systems (MEMS 2014), January 26 – 30, San Francisco, California, USA, pages 260–263. IEEE, 2014. (Chapter 3)

6. Charles Nwankire, Elizaveta Vereshchagina, **Jennifer Gaughran,** Mary O'Sullivan, Nikolay Dimov, Chandra Kumar Dixit, Maria Kitsara, Lorcan Kent, Gerson Aguirre, Macdara Glynn, David Kinahan, Robert Burger, Daniel Kirby, and Jens Ducrée. *Multi-force, multi-phase, multi-material, multi-component, multi-dimensional, multi-scale, multi-functional, multi-purpose microfluidic lab-on-a-disc platforms.* In Microfluidics Conference 2012 (μFlu'12) – 3rd European Conference on Microfluidics held in Heidelberg, Germany, December 03–05, 2012. Long oral presentation. (Chapter 3)

7. **Jennifer Gaughran**, David Kinahan, Rohit Mishra and Jens Ducrée. *Solvent-selective membranes for automating sequential liquid release of nucleic acid purification protocols on a simple spindle motor.* [Submitted to 20th International Conference on Miniaturized Systems for Chemistry and Life Sciences (μTAS 2016), October 9–13, Dublin, Ireland]. (Chapter 6)

8. **Jennifer Gaughran**, Robert Kelly, David Kinahan, and Jens Ducrée. *Disc-embedded grinding mill towards process-integrated hydro-mechanical cell lysis on centrifugal microfluidic platforms.* [Submitted to 20th International Conference on Miniaturized Systems for Chemistry and Life Sciences (μTAS 2016), October 9–13, Dublin, Ireland]. (Chapter 7)

Book Chapters:

1. Robert Burger, Maria Kitsara, **Jennifer Gaughran**, Charles Nwankire, and Jens Ducrée. Novel approaches in immunoassays, chapter *Automation of immunoassays through centrifugal lab-on-*

a-disc platforms, pages 72–92. Future Science Group, London, UK, 2014.

2. Rohit Mishra, **Jennifer Gaughran**, David Kinahan and Jens Ducrée. *Functional membranes for enhanced rotational flow control on centrifugal microfluidic platforms.* Reference Module in Materials Science and Materials Engineering. Elsevier Inc. [In preparation, expected publication August '16]

Additional Publications during PhD term:

1. Kevin T Sweeney, Edmond Mitchell, **Jennifer Gaughran**, Thomas Kane, Richard Costello, Shirley Coyle, Noel E O'Connor and Dermot Diamond. *Identification of sleep apnea events using discrete wavelet transform of respiration, ECG and accelerometer signals.* Body Sensors Network (BSN), 2013 IEE International Conference.

2. Monika Czugala, Robert Gorkin III, Thomas Phelan, **Jennifer Gaughran**, Vincenzo Fabio Curto, Jens Ducrée, Dermot Diamond, and Fernando Benito-Lopez. *Optical sensing system based on wireless paired emitter detector diode device and ionogels for lab-on-a-disc water quality analysis*. Lab on a Chip, 12(23):5069–5078, 2012.

3. Charles Nwankire, Di sien S. Chan, **Jennifer Gaughran**, Tríona O'Connell, Robert Burger, Robert Gorkin III, and Jens Ducrée. *Fluidic automation of nitrate and nitrite bioassays in whole blood by dissolvable-film based centrifugo-pneumatic actuation.* Sensors, 13(9):11336–11349, 2013.

Oral Presentation

1. **Jennifer Gaughran** and Jens Ducrée. *Graphene oxide enabled centrifugo-pneumatic routing of flows.* In Proceedings of the 18th International Conference on Solid-State Sensors, Actuators & Microsystems (Transducers 2015), June 21–25, Anchorage, Alaska, USA, pages 331–334, 2015.

2. **Jennifer Gaughran**, David Boyle, James Murphy, and Jens Ducrée. *Graphene oxide membranes for phase-selective microfluidic flow control.* In Proceedings of the 28th IEEE International Conference on Micro Electro Mechanical Systems (MEMS 2015), January 18 – 22, Estoril, Portugal, pages 2–4, 2015.

3. Nikolay Dimov, **Jennifer Gaughran**, Eoin Clancy, Thomas Barry, Terry Smith, and Jens Ducrée. *Automated on-disc total RNA extraction from whole blood towards point-of-care for early-stage diagnostics*. In Proceedings of the 17th International Conference on Solid-State Sensors, Actuators & Microsystems (Transducers 2013), June 16–20, Barcelona, Catalonia, Spain, pages 2548–2551, 2013.

4. Charles Nwankire, Elizaveta Vereshchagina, **Jennifer Gaughran,** Mary O'Sullivan, Nikolay Dimov, Chandra Kumar Dixit, Maria Kitsara, Lorcan Kent, Gerson Aguirre, Macdara Glynn, David Kinahan, Robert Burger, Daniel Kirby, and Jens Ducrée. *Multi-force, multi-phase, multi-material, multi-component, multi-dimensional, multi-scale, multi-functional, multi-purpose microfluidic lab-on-a-disc platforms.* In Microfluidics Conference 2012 (μFlu'12) – 3rd European Conference on Microfluidics held in Heidelberg, Germany, December 03–05, 2012.

5. **Jennifer Gaughran** and Jens Ducrée. *Just a Pinprink: The Next Generation of Disease Detection.* Institute of Physics, Ireland Frontiers of Physics Conference, Dublin, 2014. Invited speaker.
6. **Jennifer Gaughran.** *Spinning a Yarn: Quick and Easy disease detection.* SFI Annual Summit, Athlone, Ireland 2014. Invited speaker.
7. **Jennifer Gaughran** and Jens Ducrée. *Micro-opto-fluidic Biosensors for Advanced Global Diagnostics.* Bio-Analysis and Therapeutics (Bio-AT) Research Day, Royal College of Surgeons Ireland, June 2012.
8. **Jennifer Gaughran** and Jens Ducrée. *Automated On-Disc Total RNA Extraction from Whole Blood towards Point-of-Care Early Stage Diagnosis*. Bio-Analysis and Therapeutics (Bio-AT) Research Day, Dublin City University, June 2014.

Poster Presentations

1. **Jennifer Gaughran**, Nikolay Dimov, Eoin Clancy, Thomas Barry, Terry Smith and Jens Ducrée. *Multi-stage, solvent-controlled routing for automated on-disc extraction of total RNA from breast cancer cell line homogenate.* In Proceedings of the 17th International Conference on Solid-State Sensors, Actuators & Microsystems (Transducers 2013), June 16–20, Barcelona, Catalonia, Spain, pages 305–308, 2013.

2. Nikolay Dimov, **Jennifer Gaughran**, Darren Mc Auley, David Boyle, David J. Kinahan, and Jens Ducrée. *Centrifugally automated solid-phase purification of RNA.* In Proceedings of the 27th IEEE International Conference on Micro Electro Mechanical Systems (MEMS 2014), January 26 – 30, San Francisco, California, USA, pages 260–263. IEEE, 2014.

3. **Jennifer Gaughran** and Jens Ducrée. *Multi-stage, solvent-controlled routing for automated on-disc extraction of total RNA from breast cancer cell line homogenate.* Bio-Analysis and Therapeutics (Bio-AT) Research Day, IT Tallaght, June 2013.
4. **Jennifer Gaughran** and Jens Ducrée. *Graphene Oxide Membranes for Phase-Selective Flow Control.* Bio-Analysis and Therapeutics (Bio-AT) Research Day, NUI Maynooth, June 2015.
5. **Jennifer Gaughran**, Nikolay Dimov, Eoin Clancy, Thomas Barry, Terry Smith, and Jens Ducrée. *Multi-stage, solvent-controlled routing for automated on-disc extraction of total RNA from breast cancer cell line homogenate*. BOC School of Physical Sciences, Poster Competition, Dublin City University, 2015.
6. **Jennifer Gaughran**, Nikolay Dimov, Eoin Clancy, Thomas Barry, Terry Smith, and Jens Ducrée. *Multi-stage, solvent-controlled routing for automated on-disc extraction of total RNA from breast cancer cell line homogenate*. Institute of Physics Ireland, Annual meeting, Dun Laoghaire, 2014.

Awards

1. Winner of the National Thesis in Three 2014 Competition.
2. Winner of the Tell-It-Straight 2014 Competition.
3. Winner Institute of Physics Ireland, Rosse Medal 2014.
4. Outstanding Student Paper Finalist, IEEE International Conference on Micro Electro Mechanical Systems (MEMS) 2015.
5. 3rd Prize at BOC Physics Poster Presentation Competition 2015.

Abstract

Development of Novel Advanced Flow Control Systems on Centrifugal Microfluidic Platforms for Nucleic Acid Testing

Jennifer Gaughran, B.Sc. (Hons)

In this work the development of novel flow control methods in centrifugal microfluidic systems for the nucleic acid testing are demonstrated. Nucleic acids make excellent biomarkers for the identification of numerous diseases, but their detection is a lengthy and labour intensive process. Centrifugal microfluidics has emerged as a highly useful tool in the area of biomedical diagnostics; however there are still limitations when it comes to sample preparation on these Lab-on-a-Disc systems. This is especially important in nucleic acid testing, where the main bottleneck in performing these processes on microfluidic devices is in sample preparation. Nucleic acid testing can be broken into three stages; extraction, purification and detection. To this end, this work outlines the development of two novel centrifugal routing systems for nucleic acid purification, through the integration of functional materials. The first is a solvent-selective router which integrated two solvent specific membrane valves. The capability of the system to purify total RNA with significant integrity and concentration was shown. The second system integrated multi-layer Graphene Oxide (GO) membranes into our Lab-on-a-Disc devices. Using this, two unique properties of the GO were investigated; its solvent selectivity and air impermeability. Finally, a novel, centrifugo-pneumatic scheme for solvent-selective routing of organic and aqueous flows was demonstrated. Also shown is the development of two separate extraction platforms. The first was a centrifugo-pneumatic 'μHomogenizer', which implements a 3-phase fluid extraction protocol of RNA. This system integrates chemical lysis and separation of the RNA containing aqueous phase and shows significant improvement over its time-consuming and labour intensive benchtop alternate. The second was the development of a mechanical lysis method that utilises a rotor stator grinding mill driven by the spindle motor. This system can be used for general lysis of a wide range of bacteria but would be of significant benefit for armoured cells.

Chapter 1

Introduction

1.1 Overview

1.1.1 Point of Care Diagnostics

In recent years a substantial push in disease detection has been moving away from the traditional centralised laboratory approach to Point of Care (POC) diagnostics approach. A POC system is a laboratory standard test which is designed to be used in-situ, directly at the site of patient care (1). This could comprise of anywhere from a physician's office, to an ambulance, to emergency room and even patient's homes. It has a significant benefit when used in poor resource areas like the developing world, where people may have to travel great distances to receive medical care. If the test can be run and the disease diagnosed then and there, this would allow for much better and more tailor

treatments. There are numerous other significant benefits to the development of POC systems, for example:

1. Personalised medical treatment, designed to fit the individual patient's needs, not just the standard group treatment.
2. De-centralisation of laboratory testing. There would be a reduced need for centralised labs.
3. Early disease detection. Though the benefits of early diagnosis is somewhat in question for diseases like cancer, early identification of other disease types such as bacterial meningitis has significant benefits for patient prognosis, as well as reduction in long term neurological defects (2), (3).
4. Shorter sample-to-answer time, allowing faster treatment of disease.
5. Reduction of cost. There would be a reduction in sample and reagent consumption as well as a reduction in emergency room time and outpatient clinical visits, ensuring optimum usage of professional time.

It is clear, however, that in order to implement these practices and receive these benefits POC systems must meet certain criteria (4):

1. The systems must be at least as effective as the current laboratory standard.

2. It must be straightforward and easy to use. Extensive training or instruction should not be required for its operation.
3. The system should be fully automated and require minimal user input.
4. The system should be cost-effective. This aspect is essential if POC technologies are to be used in developing regions.

In order to achieve these goals POC systems must condense the complex fluid handling processes, normally performed manually, into simple automated devices. Microfluidic systems offer a means of achieving this.

1.1.2 Technological Advancements in POC Systems

Perhaps the most successful POC diagnostic device used today is glucose test strips, which are used to measure glucose levels in the blood and is now one of the main tools in managing diabetes. This simple test allows patients to make decisions about their diet and medication dosage by giving patients their glucose levels in a matter of seconds (5).

Other commercial POC devices have been developed to test for a range of diseases and conditions. Siemens have developed a wealth of diagnostic technologies for use in clinical settings, including their RAPIDSystems, used for blood gas analysis and their CLINITEK Status+ Analyzer used for POC urine analysis (6). Radisens Diagnostics

have developed their Gemini™ platform, a multimode system that uses centrifugal microfluidics to detect for various chronic diseases, e.g. chronic diabetes, heart disease and thyroid function (7). The Piccolo Xpress® by Abaxis uses a lab-on-a-disc system which can perform up to 15 different tests simultaneously in approximately 12 minutes (8). Multiplexing of immunoassays on-disc (9) and parallelized biochemical analysis have also been demonstrated (10).

Figure 1.1: Example of technological advancements in POC diagnostics. a) Piccolo Xpress® by Abaxis (8). b) Gemini™ platform by Radisen (7).

There has been an increasing demand in recent years for POC diagnosis and monitoring of patients using Nucleic Acids (NA), DNA and RNA. These are arguably some of the most difficult tests to perform in a POC environment as there are considerably more sample pre-treatment steps than with other bio-testing methods such as immunoassays (11).

Lee *et al.* developed a new NA based assay which is integrated into a cartridge system for HIV-1 (12). A simple rotary microsystem developed by Park *et al.* enabled the purification of RNA from viral lysate with frequency-controlled release of reagents (13). By pre-storing reagents through their gelification, Sun *et al.* were able to enhance the capabilities of reagent storage for POC analysis (14). The emergence of alternative detection techniques such as isothermal amplification have also helped to advance NA testing of diseases like malaria (15).

These are just some of the advancements being made in this area and a recent review by Chin *et al.* stated that there are over 32 companies currently active in the field of POC diagnostics (16).

1.2 Motivations and Objectives

With the increasing need for robust, automated sample-to-answer devices for POC diagnostics, especially in the area of NA testing, systems must be developed to combat the difficult and time-consuming sample preparation procedures. As sample preparation is the greatest bottleneck in NA testing, the aim of this thesis is to address this issue. The ultimate goal is to develop advanced flow control mechanisms for microfluidic systems capable of performing the complex fluid handling requirements of NA testing (notably cell lysis and purification), all using simple and automated devices. In particular this work focuses on:

1. The investigation and integration of functional materials within centrifugal microfluidic structures and using those materials for advanced flow control.
2. Use of these functional materials for solid phase purification of nucleic acids.
3. Development of nucleic acid extraction solutions.

1.3 Centrifugal Microfluidics

Microfluidics deals with the science and technology of fluid flows on the micron or submicron scale (17). Centrifugal microfluidics is an area of science which has been of interest for the past 40 years. The concept of it is a simple one, through the spinning of a disc, which as has been fabricated to contain microscopic structures, fluid is propelled from the centre of the disc due to centrifugal forces.

The main force involved in centrifugal microfluidics is the centrifugal force, f_ω, where

$$f_\omega = \rho r \omega^2 \qquad \text{(eqn. 1.1)}$$

where ρ is the mass density of the fluid, r is the radial position and ω is the angular velocity of the disc. This force is always directed out from the centre of the disc. Another less influential force is the Coriolis force, f_c,

$$f_c = 2\rho\omega v \qquad \text{(eqn. 1.2)}$$

where v is the planar velocity of the fluid, and the Euler force, f_E,

$$f_E = \rho r \frac{d\omega}{dt} \qquad \text{(eqn. 1.3)}$$

where $d\omega/dt$ represents the angular acceleration. All these factors, among others (such as the capillary force which will be discussed later), affect the way in which fluids flow when put on a disc (18).

Centrifugal microfluidics has emerged as highly useful tool in the area biomedical diagnostics as many of the necessary processing steps in fluidic analysis, such as mixing or metering of the fluids, can be miniaturised and incorporated into these Lab-on-a-Disc (LoaD) technologies. Also because of this miniaturisation multiple analysis steps can be incorporated onto the one disc, which has allowed for the development of sample-to-answer systems or micro total analysis systems (μTAS).

The advantage of using centrifugal microfluidics over traditional microfluidics is that propulsion of fluids can be achieved without the use of many external technologies. A simple motor can generate all the forces necessary to move the fluid through the disc. Other fluidic functions like valving, which will be discussed in detail below, have also been incorporated into the discs. Also, with developments in both the materials and manufacturing technologies of these discs, a cheap and fast method of testing can be achieved (19).

1.4 Microfluidic Flow Control

Due to the ubiquitous nature of the centrifugal field during rotation, flow control constitutes a particular challenge on integrated LoaD platforms. For example, in the design shown in Figure 1.2a, there are fluids stored in all three of the chambers, which need to be released sequentially to the bottom chamber. That will not be possible in the current configuration, as all three fluids are experiencing the same force, as they are at radially equal distances. However, if the radial distance of the chamber is increased (Fig. 1.2b), then the fluids farther out from the centre will experience a greater force and so flow first. This constitutes a simple example of flow control but the coordination of sequential or parallelised Laboratory Unit Operations (LUOs) (such as the sample and reagent storage) requires more complex, high-performance flow control such as: valving, routing, pumping, metering and mixing.

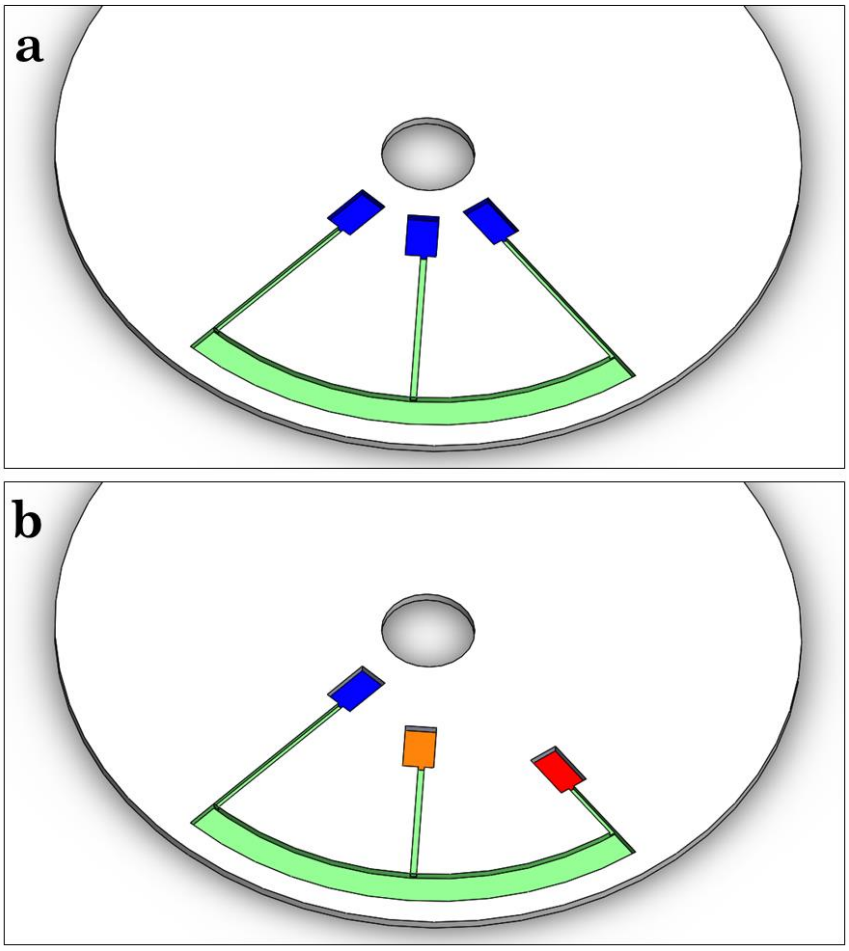

Figure 1.2: Example of simple method of flow control. a) Each of the three chambers on the disc is experiencing the same force and so all three fluids will flow simultaneously. b) By increasing the radial distance of the chambers sequential release of the three fluids can be achieved.

1.4.1 Passive Valving

It is commonly known that valving is perhaps the most important flow control method in centrifugal microfluidics. There are many different systems that can be used as valves, each with their own advantages and inefficiencies. The main systems will be examined here. They can be broken down into two groups: passive and active valves. Passive valving systems include capillary valving, siphoning and

hydrophobic valving. These types of valves are controlled primarily by the rotational frequency of the disc, its surface properties and channel design (20). However, these valving schemes only control the fluid phase, but not its vapour, thus making them unsuitable for long-term reagent storage, which would be a common requirement of fully automated commercial point-of-use systems.

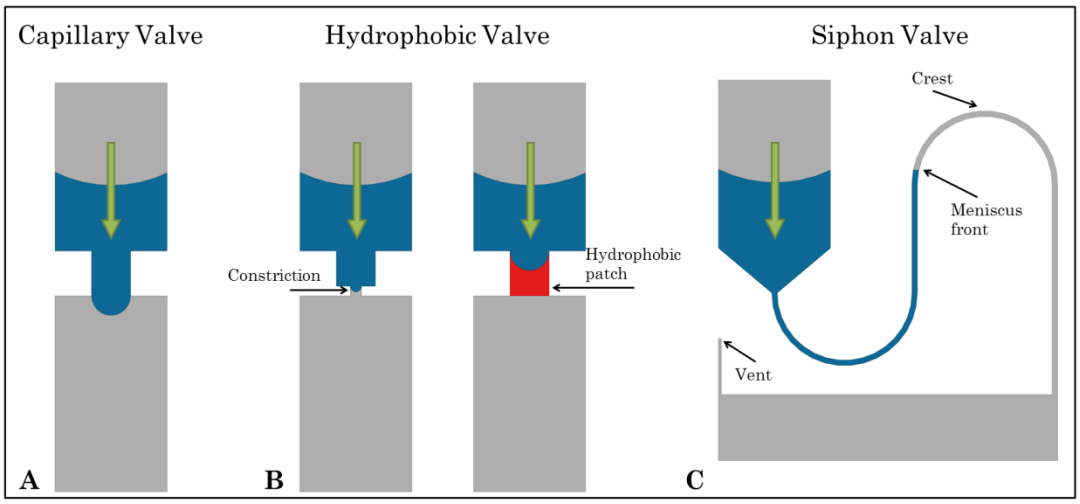

Figure 1.3: Microfluidic valving systems. A) Shows a capillary valve, B) shows a hydrophobic valve and C) shows a siphon valve. The operations of these valves are described below (19).

1.4.1.1 Capillary valving

Capillary valving is perhaps the most commonly used type of valve (Fig. 1.3A). It is based on a balance between the centripetal force and surface tension force (20). With hydrophilic microchannels fluids can be transported using capillary action. The rotation of the disc can aid with this action. When the fluid encounters a transition from a small

microchannel into a larger chamber, a large surface tension force develops. At this point, if the centrifugal force is less than that of the surface tension force, the flow of the fluid will cease. In order for this stoppage to be overcome, the rotation of the disc must be increased, therefore increasing the centrifugal force. At some spin speed, known as the burst frequency, the surface tension force is overcome and the fluid will continue to flow. In this way the flow through the disc can be controlled simply by varying its rotational frequency (21). Much research has been done into investigating the parameters of the burst frequency (22). The burst frequency is given by the Equ. 1.4,

$$\upsilon(Hz) = \frac{1}{\pi}\sqrt{\frac{\sigma|cos\Theta|}{\rho\bar{r}\Delta r d}} \qquad \text{(eqn. 1.4)}$$

where ν is the burst frequency, σ is the surface tension of the fluid, Θ is the contact angel at the interface between the small microchannel and the larger chamber, ρ is the density of the fluid, $\bar{r}$ is the mean radial position of the interface, Δr is the length of the liquid plug and d is the diameter of the microchannel (18).

There are some limitations involved with using capillary valves. The first of these is the need for the surfaces to be hydrophilic and therefore the disc needs to be surface treated. Though this can be done at the assembly stage, the process is not permanent and does wear-off after some time. Also, the burst frequency of the valves can limit the spin profiles of the disc, as it does not allow for high spin frequency operations (23).

1.4.1.2 Hydrophobic valving

Another method for stopping fluid flow is the use of a hydrophobic valve. The idea of this system is quite simple. A small hydrophobic patch is placed along the channel as shown in Figure 1.3B. There are two different methods for using hydrophobic valves, the first is the narrowing of a hydrophobic channel and the second is the hydrophobic patch placed in functional areas in the microchannels of the structure which impedes the flow of the fluid (19). As with the capillary valving, increasing the rotational speed to a certain burst frequency will allow the fluid to flow again (21). However, also like with the capillary valve, hydrophobic valves burst at relatively low frequencies not allowing for any high spin speed operations.

1.4.1.3 Siphon valving

The siphon structure, as shown in Figure 1.3C, can be used as both a means to transport the fluid around the disc and as a valve (19). The siphon consists of a fluid filled chamber connected to a siphon channel which first extends higher than the radial position of the chamber then back down to another chamber at lower radial position (21).

At high rotational speeds the level of the fluid in the initial chamber and in the siphon channel is maintained at a constant level. The centrifugal force keeps the meniscus front below the level of the

fluid in the chamber (19). When the spin speed is slowed down the centrifugal force is no longer strong enough to stop the capillary action in the siphon channel and meniscus front moves up and over the crest and down to the entrance of the radially lower chamber. The siphon channel is now primed (21). The rotational speed is then increased again allowing the entirety of the fluid to flow to the second chamber.

Siphon valving is useful when high initial spin speeds are necessary; however, siphoning requires that the siphon chamber be primed using capillary action, therefore the channel must also be hydrophilic. Also, a siphon structure requires a lot of surface area on the disc (19).

Siegrist *et al.* took steps towards a more integrated system by implementing a robust serial siphoning method of fluid handling (23).

1.4.2 Active Valving using Functional Materials

Active valves rely on the use of sacrificial materials for functional enhancement of microfluidic systems. Sacrificial valves are destructible barrier layers that can be placed strategically throughout the structure and can be used for functions such as long term on-board fluid storage (20). These physical-barrier based flow control elements are removed on demand by physical or chemical stimuli (24), (25). Wax valves, for instance, can be actuated by exposure to a heat source (25). Another

example is hydrogels, which can act as valves actuated by size change in the presence of water (26).

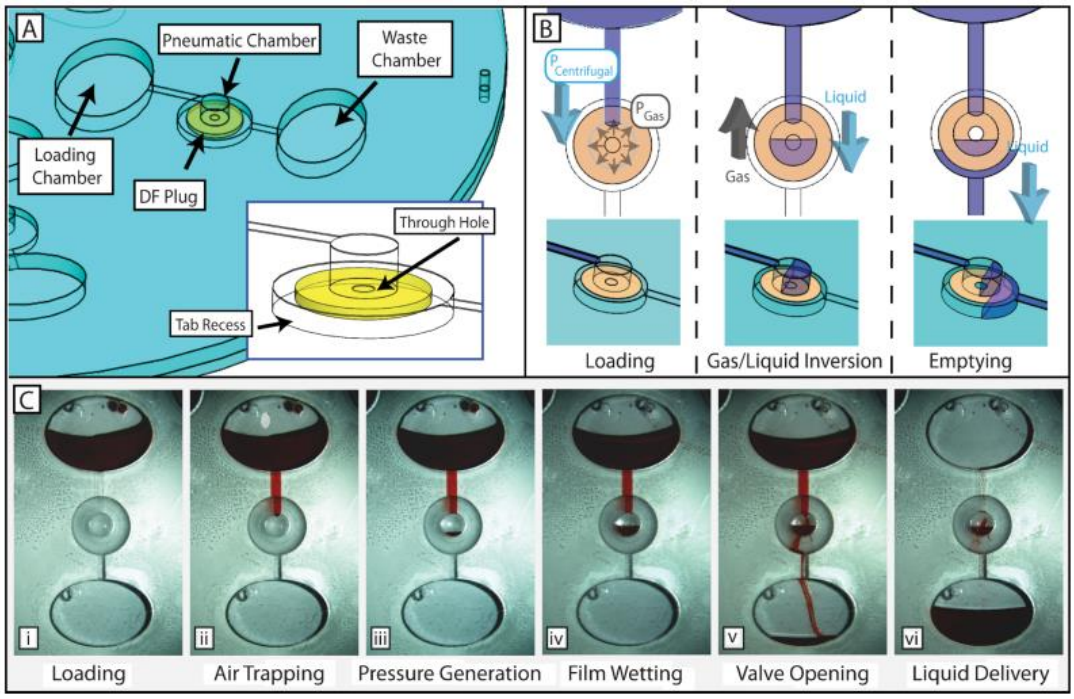

Figure 1.4: Centrifugo-Pneumatic DF valving. A) Structural design of DF valve in disc design. B) Actuation of DF valve under centrifugal field. C) Demonstration of DF valve operation using coloured dyes. Adapted from Gorkin *et al.* 2012 (24).

Gorkin *et al.* used a dissolvable-film material which opens upon contact with the on-board fluid in conjunction with a pneumatic structure to develop a novel valving system on a centrifugal microfluidic platform (Fig. 1.4) (24). Kinahan *et al.* advanced this sacrificial technology to an event-triggered valving paradigm which allows for more dynamic control of fluids on a centrifugal microfluidic platform (27). Mishra *et al.* recently integrated a sacrificial lipophilic membrane

which dissolved in the presence of a suitable oleophilic (a substance which has an affinity for oils) solvent, but remained intact in the presence of water. This allowed for the implementation of an enzyme-linked immunosorbent assay (ELISA) (28).

1.4.3 Routing

Fluidic routing to direct flow to a selected output at a junction between a waste and an elution outlet is critical for centrifugally implemented automation, especially in the area of nucleic acid purification where the sequence of fluids must be passed through a single channel, but each of these fluids must be routed away from the final collection chamber. Kim *et al.* developed a flow switch by using a capillary valve upstream of an open chamber and unique 3D junction geometry (29). A similar router, solely controlled by the rotationally actuated hydrodynamic Coriolis pseudo-force, was reported by Brenner *et al.* (30). This virtual routing concept was further sophisticated by Haeberle *et al.* who successfully extracted DNA from calf thymus using silica beads by alternating the sense of rotation (31). Automated extraction of human genomic DNA is demonstrated by Kloke *et al.* who implement novel ball-pen pierceable seals to route the sample lysate through an integrated silica membrane in a Lab Tube platform (32).

1.4.4 Pumping

Centrifugal pumping provides a means to regulate flow rates of a fluid around the structure, without the use of any external pumps. The basic principle is that by changing the rotational frequency of the disc, the flow patterns of a fluid can be manipulated. Pumping on a centrifugal disc is based mostly on the rotational speed, radial distance from the centre of the disc and channel geometry (21).

Centrifugal pumping also holds an advantage over other chip based pumping, such as electrokinetic platforms (33), in that it is not heavily dependent on the physicochemical properties of the fluid, for example, pH levels, ionic strength or chemical composition (34). Also it doesn't require large high voltage power supplies (19). A number of different fluids have been pumped using this system such as, aqueous solutions, solvents and biological samples (e.g., blood, milk, urine).

A method has also been shown which allows for pumping of fluids back towards the centre of the disc, using pneumatic energy (35). The method was developed in order to overcome some of the limitations involved in the centrifugal microfluidics process, namely space constraints and the one directional motion within a centrifugal system.

The structure of this system consists of two chambers: an intake chamber connected by a microchannel to a compression chamber. The operation of the system is shown in Figure 1.5 below.

Noroozi *et al.* have used pneumatic pumping as a method for mixing and accurate metering of reagents (36).

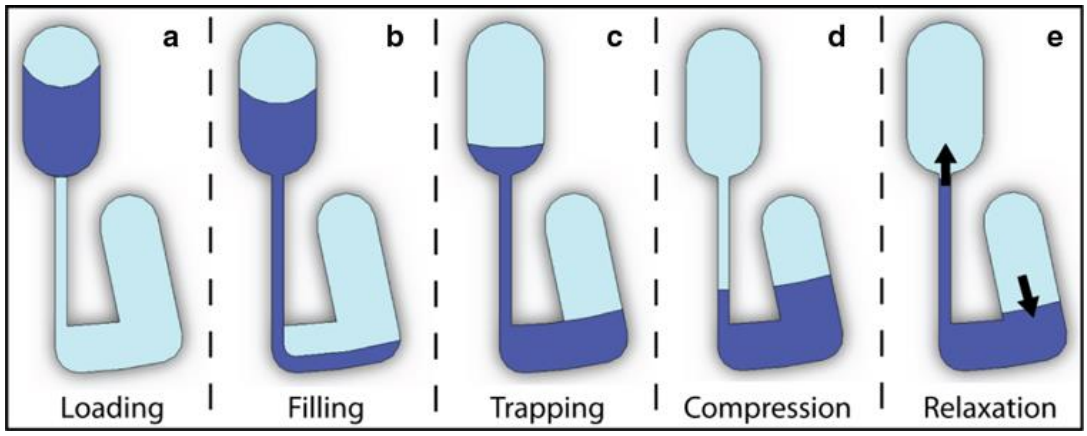

Figure 1.5: Operation of pneumatic pump. a) Fluid is loaded into the loading chamber, b) the disc is spun, the fluid moves down the channel and begins to fill the structure, c) the fluid creates a seal trapping the air, d) the disc is spun faster and the air is compressed and e) the spin speed is decreased allowing the trapped air to push the fluid back up the channel [18].

1.4.5 Mixing

Mixing is a necessary part of biomedical diagnostics but some problems occur when this has to be done on the microscopic scale (19). The problem arises due to the fact that the Reynolds number in small chambers is very low (36). The Reynolds number relates the ratio of the inertial forces to the viscous forces. In microfluidics, this number is usually less than 10, which means that the viscous forces play a significant part in the characteristics of the fluid flow (17). This low number also means that mixing within microfluidic structures can be

limited to diffusion mixing, which can be very slow (19). This process can take as much as seven minutes (37).

Methods for overcoming this problem have been investigated such as: the use of rapid oscillation of the disc (37), or the introduction of paramagnetic beads which are deflected by stationary magnetics on the surface of the disc (18). A combination of these two processes can decrease mixing times to as little as one second (37).

1.4.6 Metering

Fluid metering is a necessary step for testing of reagents in a microfluidic system. In its simplest terms volume metering is done using an overflow principle i.e. the fluid fills into a chamber of a certain size and the rest is passed on to some waste area (18).

1.5 Nucleic Acid Testing in Microfluidics

Microfluidic devices have significant advantages for uses with biological analysis, e.g. high throughput, small volume and shorter time-scales. Microfluidics can be used for a wide range of biological testing including immunoassays testing (38), cell capture and separation (39) and single cell analysis (40). While many of these biological methods address specific needs for disease detection, often times these tests only give positive results at a late stage of the disease. For example, when

detecting circulating tumour cells (CTCs), a tumour has already begun to break-up and metastasize around the body. With immunoassays there is a delay between when the patient is infected and when the body begins the production of antibodies to a detectable level. It is important, therefore, to develop tests capable of detecting diseases in a shorter time period. Nucleic acid testing can offer this. For an infectious agent NA testing has an analytical sensitivity of at least three orders of magnitude higher than immune reactions, cell culture or virus isolation and with considerably shorter timescale (41).

1.5.1 Nucleic Acids

Nucleic acids are chains of nucleotides that are biological molecules essential for known forms of life, including deoxyribonucleic acid (DNA) and ribonucleic acid (RNA). Both DNA and RNA make excellent biomarkers for the detection of numerous diseases. The usefulness of DNA as a marker has been widely known for some time (42), but the benefits of using RNA is a more recent find. RNA can be a more viable option for the detection of viruses or pathogens than DNA, for example when looking at the pathogen viability as RNA is less stable than DNA (43). One class of RNA species that has recently received a lot of attention is microRNA. These are non-coding small RNAs which are involved in regulating gene-expression. Their dysregulation has been shown to be involved in a significant number of human diseases

including cancer (44). For the detection of bacterial infections, ribosomal RNA (rRNA), most particularly 16S rRNA is the gold standard.

1.5.2 Nucleic Acid Testing Stages

Nucleic acid testing can be broken down into three stages: extraction, purification and detection.

1.5.2.1 Extraction

Extraction involves the rupturing of the cells (known as cell lysis) in order to collect the desired nucleic acid. There are numerous different methods depending on the type of cell being lysed and the type of nucleic acid you wish to extract.

Different types of cells have different cell-wall structures, which can exist in a wide range from very fragile to very tough. The tougher the cell-wall, the more shear force that is required to disrupt it. Mammalian cells and Gram-negative bacteria tend to be more shear-sensitive. Yeast and other fungi, as well as Gram-positive bacteria tend to have more rigid cell walls and require more rigorous methods of disruption (45).

The first isolation of DNA was achieved by Friedrich Miescher in 1869 and has since become a routine procedure in bioanalysis (46). Cells must first be lysed using one of four main methods: non-mechanical

disruption such as the use of detergents or freeze thawing, ultrasonication, high pressure homogenization or mechanical grinding (45).

For RNA a phenol-chloroform extraction procedure is usually observed. Commercial products are available for this procedure, such Trizol Reagent (TRI_Reagent). The cells are mixed with the TRI_Reagent and homogenized. The solution separates into phases: an aqueous phase, an interphase and an organic phase. The aqueous phase contains the RNA, the interphase retains the DNA and proteins and the organic phase retains the phenol from the lysate (47).

After the sample has been extracted it must be purified before detection.

1.5.2.2 Purification

Purification involves the cleaning of the extracted nucleic acid sample so that it is ready for detection. Through the course of this work the well-established Boom chemistry for solid-phase purification of the nucleic acids was used (48). This process involves three steps:

1. Mixing the extracted sample with a solid-phase (usually silica beads) under chaotropic conditions. A chaotropic agent (such as guanidinium thiocyanate which was originally used by

Boom *et al.*) is a substance which alters the surface structure of NAs making them capable of binding to the silica beads.

2. Washing the silica beads to remove contaminants. This usually involves multiple washes of the organic solutions isopropanol (IPA) and ethanol (EtOH). A drying step can help to enhance this.
3. Finally, the bound NA must be removed from the beads and re-suspended in a solution for detection. The NAs are eluted into a buffer (such as TE Buffer) which has low salt concentration and a pH > 7, which are the optimum conditions for NA separation from the silica beads.

The purified sample is now ready for detection.

1.5.2.3 Detection

There are various detection methods depending on the level of accuracy and the information required about the sample.

The simplest method of NA detection is absorbance spectroscopy. It is a simple quantitation method used to determine the concentration of DNA or RNA in a solution, as well as its purity. NAs absorb strongly at 260 nm and proteins at 280 nm, therefore the ratio between the two gives information about the purity of the sample. This will be discussed in greater detail in Section 2.4.2.2. Alternately, NA molecules can be

fluorescently tagged which can improve the sensitivity of the measurement.

The most widely used method of NA detection is Polymerase Chain Reaction (PCR). This is an amplification technique capable of taking a single copy of DNA and generating thousands or millions of copies of that particular DNA sequence. Quantitative Real-time PCR (qRT-PCR) can measure the accumulative effect of the amplification process as the reaction is taking place. This coupled with a fluorescently labelled probe hybridization used for the detection of a specific DNA sequence allows for very accurate DNA detection. For the detection of RNA, Reverse Transcription PCR (RT-PCR) is used. This creates a complementary DNA (cDNA) sequence from the RNA and amplifies it (49).

Other methods of detection include using isothermal amplification techniques such as nucleic acid sequence-based amplification (NASBA) or Loop-mediated amplification (LAMP). These techniques require heating the sample to a single temperature (instead of the cycling procedure required for PCR), which can reduce assay times (43).

1.5.3 Microfluidic Advancements in NA Testing

Microfluidics is of considerable use for NA testing. There have been some significant developments in this area. For nucleic acid detection using microfluidic devices, sample preparation remains the

biggest bottleneck (41). Haeberle *et al.* used a centrifugally driven system which routed the flows based on the Coriolis pseudo force which allowed the recovery of 16% of the DNA (31). Using centrifugal microfluidics, Cho *et al.* presented a device capable of one-step DNA extraction of pathogen-specific DNA from whole blood (50). A system was devised which significantly reduced the detection time (from 5 days to 30 minutes) of a common food-borne pathogen by combining an eight-chambered microfluidic chip with an optical reader and LAMP (51), (52).

These are just some examples of the use of microfluidics for nucleic acid testing. However, there is still significant room for advancement in this area, particularly with a focus on automation of sample preparation procedures.

1.6 Outline of Thesis

This thesis describes the development of novel flow control methods on centrifugal microfluidic discs to automate the numerous sample preparation steps of nucleic acid testing. A particular emphasis is given to the inclusion and characterisation of functional materials within the discs. These functional materials can help to enhance fluid flow control through their solvent selective properties. A brief outline of the remainder of the thesis is as follows:

Chapter Two, describes in detail the fabrication technologies used to manufacture the microfluidic discs (Laser ablation and CNC milling), as well as the cleaning and assembly process. The various materials used are discussed as well as the testing procedures. The characterisation techniques are discussed, including bio-analysis methods used throughout this work.

Chapter Three deals with the development of a solvent selective router for centrifugally automated solid phase purification of RNA. The design of a solvent-selective valving scheme is shown, along with the advancement of the system from a simple router to a fully automated design. The capability of the system to purify RNA to a high integrity is shown.

Chapter Four looks at the inclusion of Graphene Oxide (GO), as a functional material, in microfluidic systems. A method for inclusion of the GO membranes in polymeric microfluidic devices is described. The GO membranes are characterised using microfluidic structures and their range of unique capabilities is investigated. GO membranes are completely impermeable to organic solutions, air and oils, but yields to aqueous solutions above a certain threshold frequency.

Chapter Five shows the inclusion of the GO membranes as a flow control element in a centrifugo-pneumatic router. The evolution of the design of the system is shown, as well as its capability to purify DNA. The interaction of DNA with the GO membranes is also investigated.

Chapter Six shows the continued development of the GO router to a fully automated system capable of purifying DNA in less than eight minutes. The system incorporates an event-triggered design which uses three different functional materials to significantly reduce the labour intensive sample preparation requirements of DNA purification.

Chapter Seven looks at two separate methods for NA extraction. The first is a novel centrifugo-pneumatic 'μHomogenizer', which implements a 3-phase fluid extraction protocol of RNA. This system builds on the work of Linares *et al.* (53) to integrate chemical lysis and separation of the RNA containing aqueous phase and show significant improvement of its time-consuming and labour intensive benchtop alternate. The second is the development of a mechanical lysis method that utilises a rotor stator grinding mill driven by the spindle motor. This system could be used for general lysis of a wide range of bacteria but would be of significant benefit for armoured cells.

Chapter Eight outlines the final general conclusions of the thesis and includes some suggestions for further work on the topics in the thesis.

Chapter 2

Materials and Methods

The experimental work can be broken down into four stages: disc fabrication, biological sample preparation, disc testing and characterisation.

This chapter deals with the general materials and methods only. Anything specific to the individual disc designs will be discussed in the relevant results chapters. A full list of all materials and manufacturers is given in Appendix A.

2.1 Fabrication of Parts

The fabrication process has three steps: designing the layers, fabrication of parts and complete disc assembly. All designs were drawn using SolidWorks 2010 – 2015 (54).

2.1.1 Materials

There are many choices of materials for lab-on-a-chip systems, each with a different range of properties (55). Initially microfluidic chips were generally made from silicon or glass substrates. The use of these materials at the time was well known, and the optical transparency of glass was a highly desirable property (56). However, both of these materials were limited by their high cost and their harmful and complicated manufacturing procedures (57). The use of polymers such as Poly(methyl methacrylate) (PMMA) and Poly(dimethylsiloxane) (PDMS) were introduced as a replacement. Polymers are low-cost, disposable and far less complicated to fabricate (58). The microfluidic devices described in this report were fabricated from the polymer Poly(methyl methacrylate) (PMMA) or Cyclo-olefin polymer (COP) - Zeonor®.

PMMA is one of the most widely used polymers in microfluidics and is the least hydrophobic of the common plastic materials. It is low cost and so excellent for disposable microfluidic chips. It also has rigid mechanical properties and excellent optical transparency (56). PMMA can also be patterned effectively using laser ablation (59). PMMA is opaque to light transmission in the UV range, which can limit some of its sensing capabilities (60).

Zeonor® has excellent optical transparency (92% in the visible range 400-800nm) and is more chemically resistant than PMMA (61). As a relatively new type of thermoplastic it has low impurities which make

it highly useful medical equipment and biological analyse (62). However, the Zeonor® is more costly than PMMA and cannot be cut using a 30 W laser cutter, which makes it poor choice for rapid prototyping techniques.

The polymer layers are held together using Pressure Sensitive Adhesive (PSA). PSA is a class of adhesives which is used in adhesive tape. These adhesives are thin films of polymer which experience adhesive energy of ~100J/m^2 (63). Once attached these adhesives cannot be used again (17).

The discs shown in Chapters 3, 4, 5 and Section 7.3 were fabricated from PMMA with PSA and the discs used in Section 7.2 were fabricated from Zeonor with PSA.

2.1.2 Fabrication Processes

In general the polymer layers (PMMA or Zeonor) of the discs were fabricated by laser machine or Computer Numerical Control (CNC) milling (Fig.2.1). They were assembled together using PSA on an alignment rig and rolled with a laminator for sealing. The specifics of each of the fabrication processes are discussed in detail below.

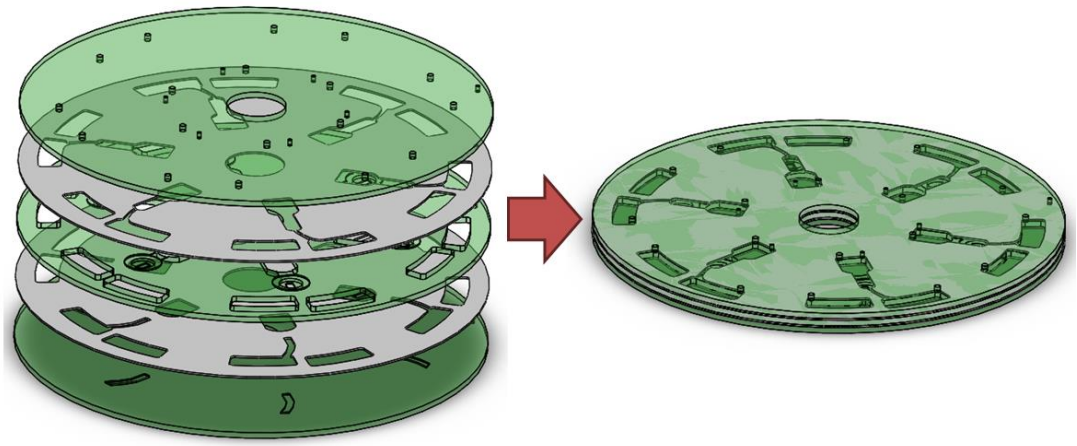

Figure 2.1: Example of assembly process using hard polymers. A disc consists of multiple layers of PMMA/Zeonor (green), held together using PSA (grey).

2.1.2.1 Laser Machining

The PMMA layers were fabricated by direct machining using laser microfabrication and/or milling. Laser cutting provides a rapid method of prototyping a disc (64,65). The basic principle is that a direct-write CO_2 laser can be used to fabricate microstructures onto a PMMA substrate. The user designs a pattern using some common drawing tool and uploads the design to system for automatic machining (59). When the focused CO_2 laser beam (with a wavelength of ~10.6 µm) (66) meets the material it rapidly heats it at that point causing the material to melt and vaporise. As the laser moves along its directed path, it vaporises the PMMA, hence cutting out the desired design. The depth of the cut is determined by the laser power, speed and number of passes it makes; however, studies have shown that the molecular weight of the PMMA can also have an effect (65). Due to the nature of the rapid heating of the polymer, bulges can form along the sides of cut channels. This can cause

issues when bonding the PMMA to other layers of the disc. Chung *et al.* have proposed a means of reducing this problem by attaching a cover layer on top of the PMMA which is being cut (67).

The laser cutting machine used for this work was an Epilog Zing 16 (Epilog Laser, USA). It has a working area of 406 x 305 mm and a maximum material thickness of 114 mm. It has a digitally controlled, air-cooled 30 W CO_2 laser (Fig. 2.2a).

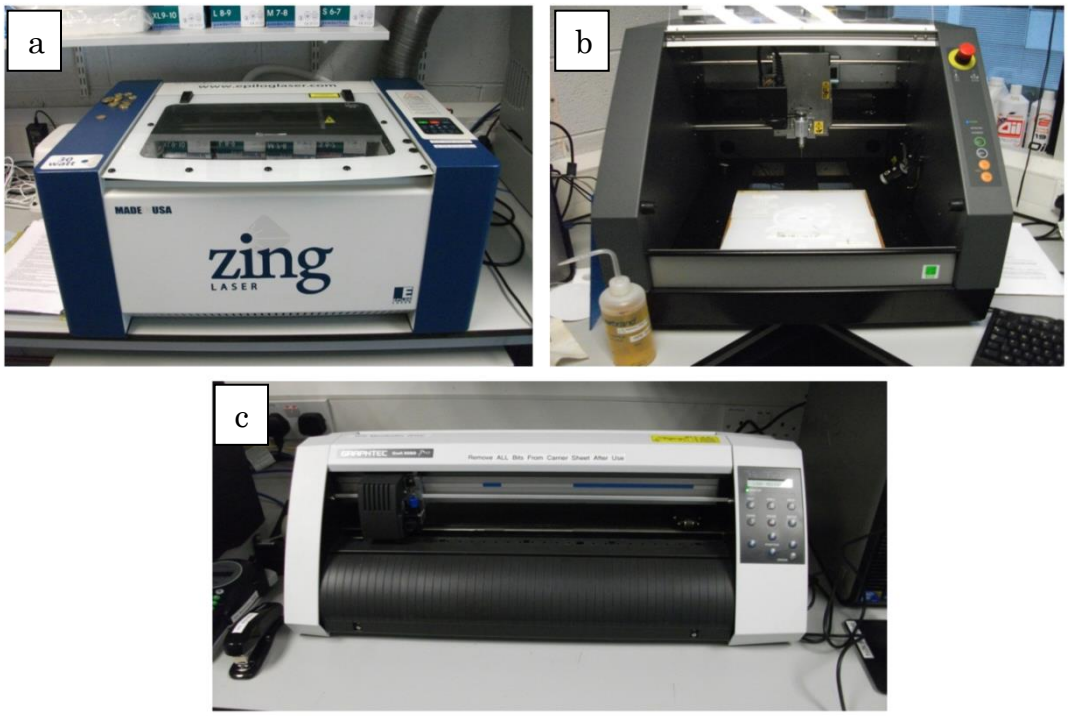

Figure 2.2: Equipment used for microfluidic disc fabrication. a) Laser cutter used to cut polymer layers of the disc. b) CNC milling machine used for precision cutting of polymer layers. c) Knife cutter used for cutting the PSA layers of the disc.

The procedure for operating the laser cutter is as follows. First a large sheet of PMMA was placed onto the support material within the device. The plastic packaging on the PMMA sheet was removed before use, as it would not allow for a clean cut with the laser. The focus and origin position of the laser were set on the device and the lid was closed. For safety, an exhaust vent fan was activated to remove any harmful fumes. The machine was now ready for cutting. Next a DXF file was uploaded to the CorelDraw software. Any final adjustments were made to the software and the file was sent to the laser cutter by clicking the 'Print' button. Finally, pressing the 'GO' button on the laser cutter machine initiates the cut.

2.1.2.2 CNC Machining

For designs which require more precise machining a Computer Numerical Control (CNC) milling machine was used (Fig 2.2b). CNC is the development of Numerical Control (NC) which is the technique of controlling a machine's movements and other functions by instructions in the form of a code. CNC is the term used when those instructions are supplied by a computer (68).

CNC machining can be performed on a range of substrates including metals and polymers and is useful in the production of smooth, precise features. A vertical spinning tool bit is used to engrave chambers and channels into the substrate surface (69).

The machine used for this work was a Roland Modela MDX-40A (Roland DG Corporation, Japan). It is a mid-range device with three axis of movement and a workable area of 305 x 305 mm. Its mechanical resolution is 0.002 mm/step (70). The size and shape of the features to be milled are controlled by the built in software and designs can be uploaded from a DXF file. The minimum feature size is limited by the tool part, which is Ø 0.1 mm.

The benefit of CNC milling is in its increased precision over laser machining and it has been shown to be capable of generating devices on-par with their commercial counterparts (71). However, when compared with laser machining it is a very slow process. Coolant must be manually supplied regularly during the milling process to combat the build-up of swarf. Swarf is formed when the supply of coolant is inadequate, causing the tool to overheat and melt the polymer substrate onto the tool surface, thus changing its shape and reducing the accuracy of the cut (69).

For these reason the CNC was used only when precision cutting was required and for use with the Zeonor substrates that cannot be cut using the laser cutter.

The procedure for operating the CNC is as follows. When cutting discs the substrates must first be cut to the Ø 120 mm size with a Ø 15.05 mm inner hole. In the case of PMMA this was performed on the laser cutter and with Zeonor, the substrates were purchased that way.

The cut disc was then adhered to the CNC stage in the provided disc slot. The disc was adhered to the surface of the stage using a hot glue gun, around the edges of the disc and in the centre. Next, the desired tool part was loaded into the machine. On the software, the X-Y position was set, as was the Z-position. Finally, coolant was added to the disc surface. The coolant was topped-up/replaced at regular intervals through the cutting process.

2.1.2.3 Knife Cutting

The PSA layers were cut using a precision knife cutter (Fig 2.2c). The machine used for this work was a Graphtec Craft Robo Pro (Graphtec America Inc., USA). The PSA sheet was adhered to a moderately 'sticky' carrier sheet and inserted into the knife cutter machine. The origin was set on the machine and the RoboPro software was used to upload a DXF file. The central loading hole and the alignment holes were set to double cut by copy and pasting the lines in the software. When the design was ready to cut, it was sent to the knife cutter using the 'Cut' option on the software. The cut force was adjusted on the cut dialog screen depending on the thickness of the PSA being cut.

2.1.2.4 3D Printing

3D printing is a method by which a solid free form 3D model can be built using three dimensional CAD data sets. It is referred to as a rapid prototyping method as it can complete parts without the need for additional assembly. The machine builds the structure based on data from the CAD drawing, laying down successive layers of material and in this way building a model up from a series of cross-sections (72). He *et al.* recently 3D printed microchannels using a 3D printer to build a sugar scaffold used as the structure in a PDMS cast chip (73).

The 3D printer used for this work was a Dimension uPrint Plus (Stratasys, Germany). It has a build size of 203.2 × 203.2 × 152.4 mm, a layer thickness of 0.254 mm and a resolution of 0.254 mm. It was used to make a holder unit which will be discussed in detail in Section 7.3.2.

2.1.3 Cleaning Procedure

The polymer layers were cleaned using an Ultrasonic bath (Grant Instruments, Cambridgeshire, UK) which removed any particulates which may have been attached to the discs. This step is also important for any biological testing. First the discs were placed within a sealed container, with 2% Micro90 solution in DI water. The container was placed into the sonicator at 50 ^{0}C for 30 min. The discs were then removed from the sonicator and rinsed with DI water. The Micro90 solution was replaced with DI water and the discs were returned to the

sonicator for another 30 min at 50 ^{0}C. The discs were once again removed and rinsed with DI water. They were then blown dry under nitrogen stream to reduce drying time and residual water marks. The discs were then placed in the oven for one hour at 80 ^{0}C.

The PSA layers were cleaned with a wipe and 70 % Isopropanol.

2.1.4 Assembly

Once all parts have been cut and cleaned they were assembled to form a disc. This process was done under clean room conditions and the required equipment is shown below in Figure 2.3. The PMMA layers were adhered to the PSA layers using transfer film as backing support. Once all layers were assembled they were passed through a heated roller multiple times, in order to ensure good adhesion. The disc was then ready for testing.

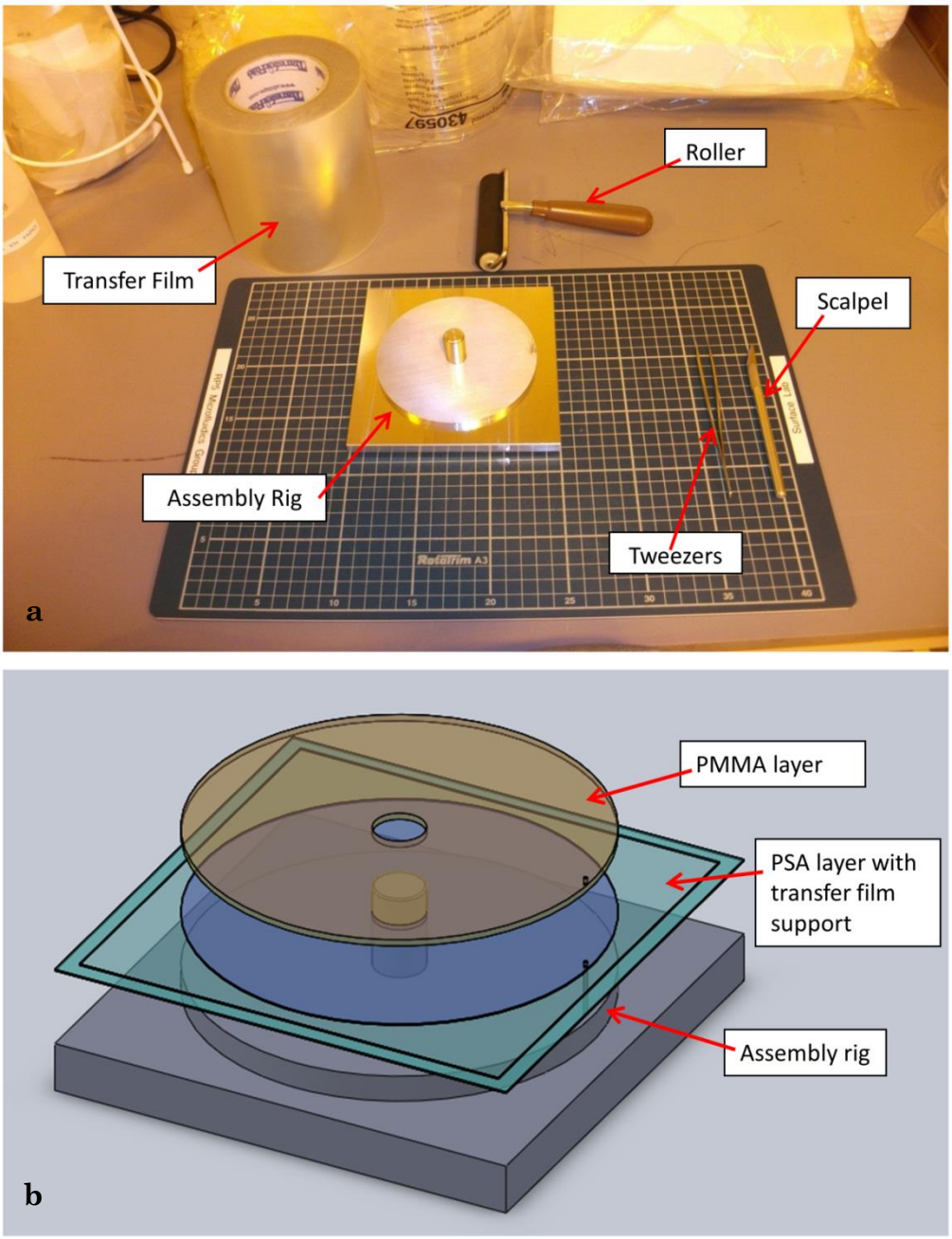

Figure 2.3: Equipment used for microfluidic disc assembly. a) Image of the various instruments required for the assembly process. b) Illustration of the assembly rig used to align the various layers of a disc.

2.2 Biological Sample Preparation

2.2.1 Bacterial Cell Culture

E.coli cells were cultured in Luria-Bertani (LB) medium overnight at 37°C and 400 rpm, 1 mL was transferred from the stock solution into 9 mL of fresh LB. The bacteria were collected in their log phase reaching a density of 3.75×10^4 colony forming units (CFU) per mL, based on a plate count.

2.2.2 DNA Purification Procedure

As a means of testing the viability of some of the systems discussed in the upcoming chapters for nucleic acid purification a QIAquick® PCR Purification Kit (Qiagen, Manchester, UK) was used. The kit contains a series of Buffers (PB, PE and EB) which have been developed to optimise DNA binding, washing and elution through a silica membrane. It can be used for the efficient recovery of single- or double-stranded DNA fragments from 100 bp (base pairs) to 10 kb (kilobase).

The kit contains spin columns which consist of a silica membrane and collection tube. The protocol is shown in Figure 2.4. The sample is mixed in a 1:5 ratio with Buffer PB, which contains high concentrations of guanidine hydrochloride and isopropanol. The solution is passed through the silica membrane using a centrifuge (Mikro 200R, Hettich,

Germany). The DNA in the solution binds to the silica membrane in the presence of high concentrations of salt, due to the Buffer PB, while any contaminants pass through the column. Next, the remaining salts are washed away by a 96% Ethanol containing Buffer PE (750 µL). An additional centrifugation step is required to remove any remaining Buffer PE, which may interfere with subsequent enzymatic reactions.

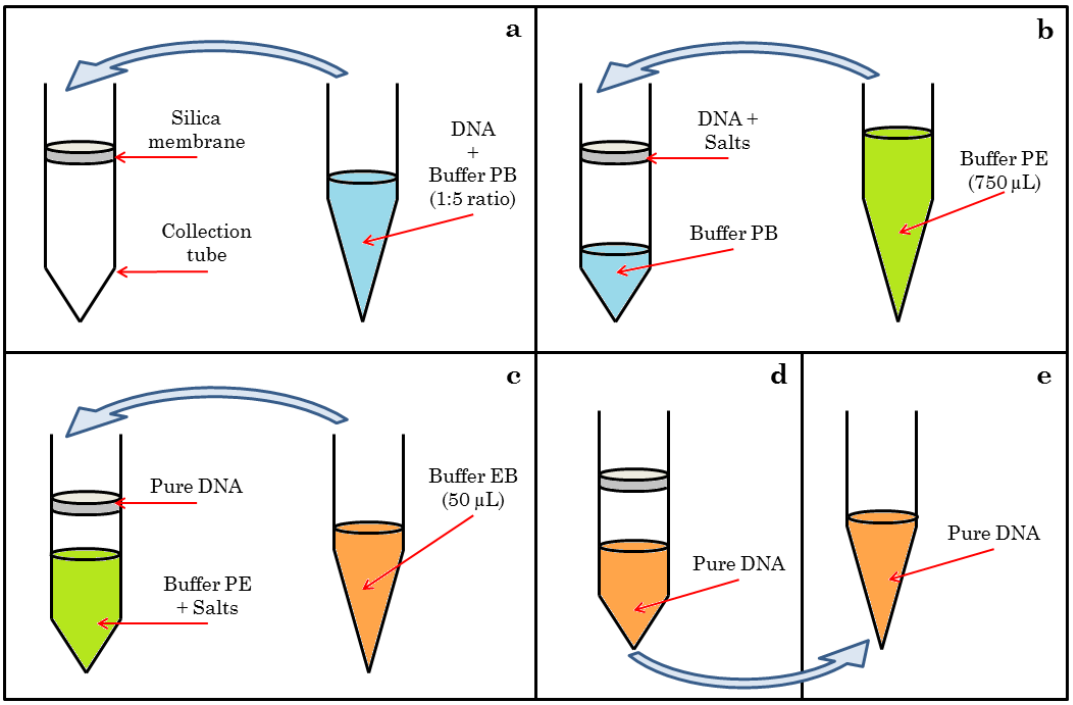

Figure 2.4: Protocol of purification of DNA using QIAquick® PCR Purification kit. a) DNA and Buffer PB solution are passed through a silica membrane, b) To clean the sample, Buffer PE is passed through the membrane which now has DNA and salts bound, c) The elution buffer, Buffer EB is passed through the membrane to collect the pure DNA, d) The pure DNA is collected from the membrane, e) The purified DNA sample can be removed for analysis.

Finally, the DNA is eluted in a low-salt buffer solution, Buffer EB (50 μL). The elution efficiency is highly dependent on the salt concentration and pH of the elution buffer and unlike with binding is best performed under basic conditions and low-salt concentrations. The Buffer EB contains 10 mM Tris-Cl, pH 8.5, with maximum elution efficiency being achieved between pH 7.0 and 8.5.

All centrifugation steps are carried out at 13,000 rpm, at room temperature for 60 seconds. For DNA purification on-disc, the Qiaquick buffer solutions were used and the silica membrane was replaced with acid-washed silica beads. One other variation when using the disc was the reduction in volume of the Buffer PE wash. In the standard benchtop protocol a 750 μL volume is used. This is a far too large a quantity to use in the small microstructures of the discs. Therefore, two 60 μL Buffer PE washes were instead used on the disc. In order to ensure that this would not adversely affect the results, the spin column procedure was performed with the original and reduced volumes. The collected final samples were then analysed using fluorescence (Section 2.4.2.3). The outcome is shown in Figure 2.5.

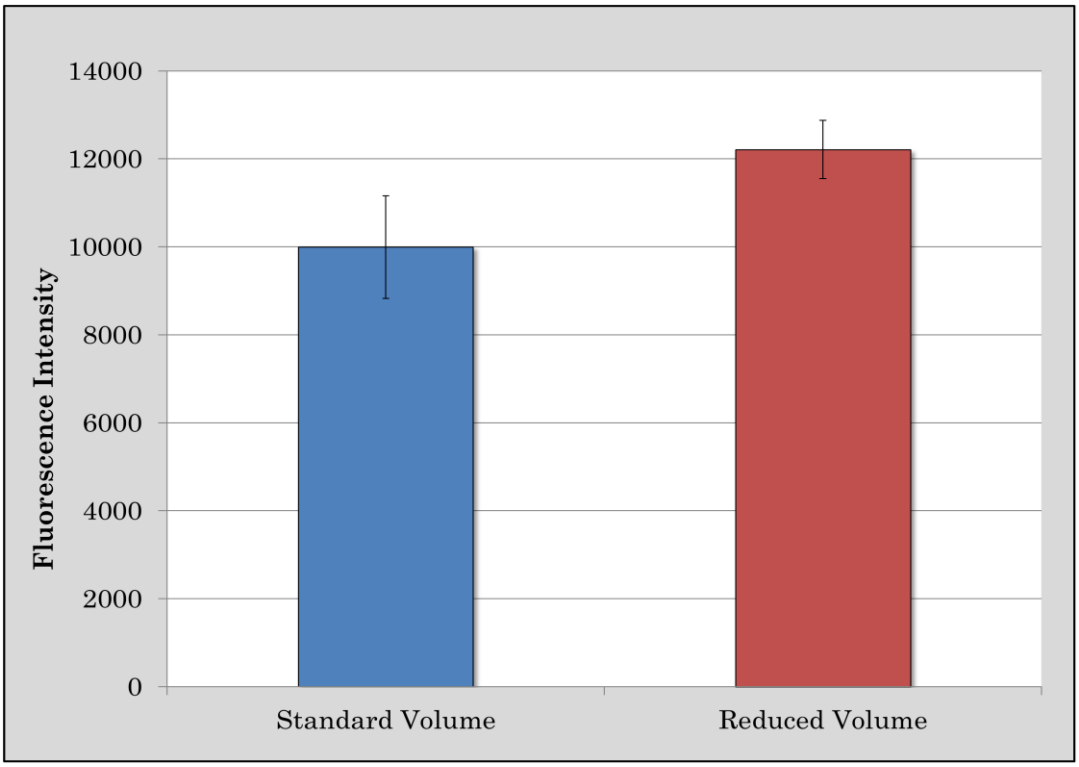

Figure 2.5: Comparison of standard Buffer PE volume versus reduced Buffer PE volume. The standard volume is 750 µL and the reduced volume is 120 µL. The reduced volume gives larger quantity of DNA than the standard volume. Data points are mean ± 1 standard deviation, n=3.

The result shows that reducing the volume on the disc to two 60 µL washes of the Buffer PE has no detrimental effects on the quantity of DNA recovered. In fact, more DNA was recovered when using the reduced volume versus the standard 750 µL volume. It was, therefore, concluded that using a reduced volume of Buffer PE for on-disc testing was acceptable.

2.3 Testing

As the discs use the centrifugal force, a spin stand was used for testing. The test point is displayed in Figure 2.6. The disc is attached to the spindle motor (CMMS-AS Servo Motor, Festo, Germany) and spun slowly. A Labview programme designed in-house was used to control the speed at which the disc is spun. The height and position of the strobe light was manually adjusted for optimum brightness and visibility. The position and focus of the camera (PCO Pixelfly) was adjusted as necessary. When the desired parameters had been achieved the disc was stopped and fluid can then be loaded. The test can now proceed.

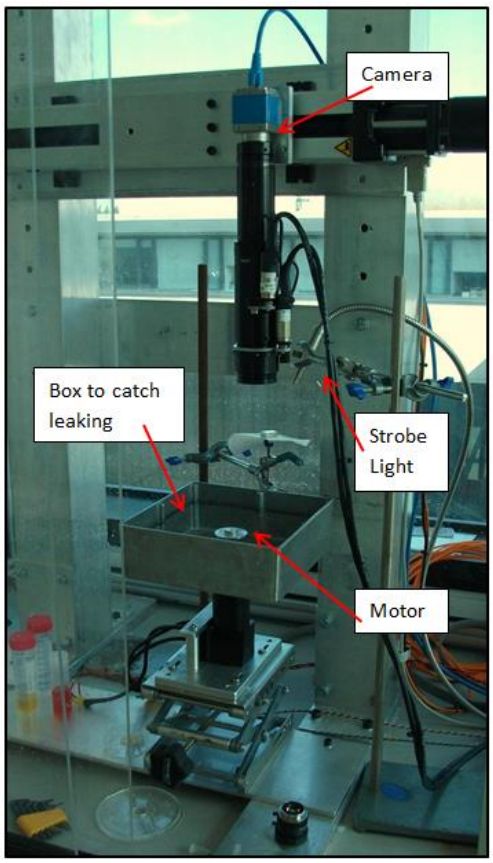

Figure 2.6: Test point set-up.

2.4 Characterisation Techniques

2.4.1 Disc Analysis

In order to ensure reliability and repeatability of the discs various characterisation techniques for the disc structure were used. Sometimes this was as simple as using an optical microscope to examine a cut. For example, as shown in Figure 2.7, if the blade of the knife cutter was not maintained to a sharp standard, an uneven cut of the PSA layers could be observed. These uneven cuts could then impede the clean flow or empting of the fluid in a channel.

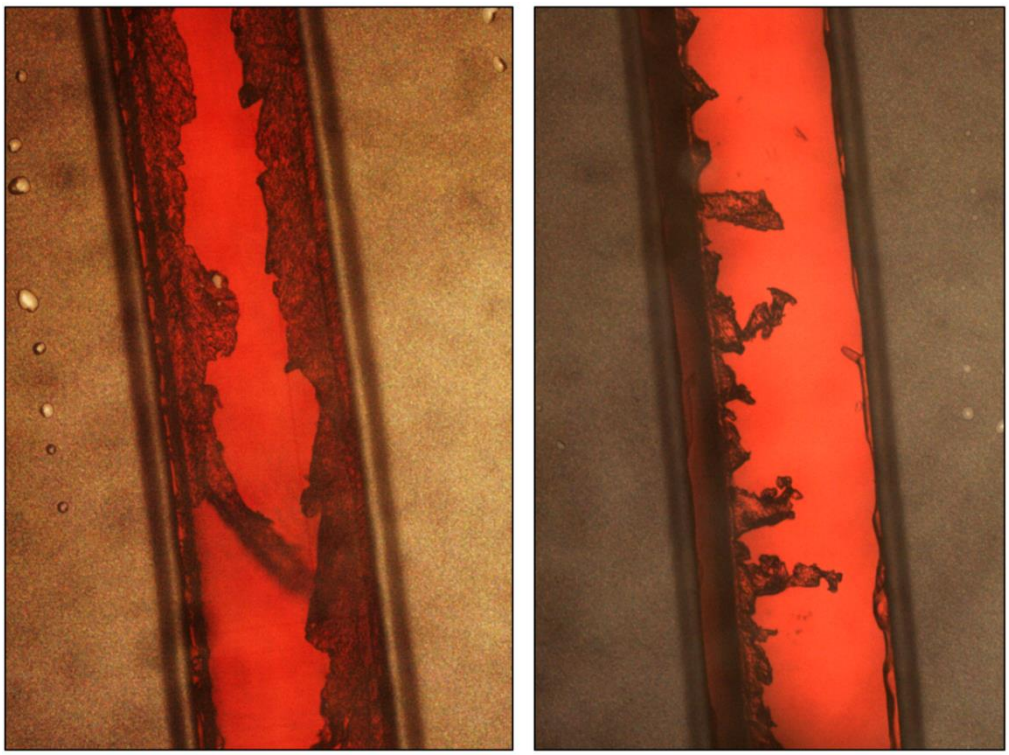

Figure 2.7: Image of uneven cut of PSA channel.

2.4.1.1 3D Microscope

3D microscopy is digital microscopy technique which takes high-resolution images of a sample by taking cross-sectional images and stitching the images together to form a three dimensional structure.

The 3D microscope used in this work was a Keyence, VHX-5000 series, Digital Microscope (Keyence, Illinois, USA). It has an 18 megapixels × 3CMOS camera and a resolution range of 1600 × 1200 to 4800 × 3600. It has a frame rate of 50 fps for fast operating and processing and a magnification range of 1x to 5000x (74).

2.4.1.2 Scanning Electron Microscopy

Scanning Electron Microscopy (SEM) refers to an instrument which uses a beam of high-energy electrons to image the surface of a sample. It is widely used for characterisation of surfaces, materials and devices to give surface topography information (75).

In SEM, a beam of high energy electrons interact with the atoms of the sample under investigation, giving information about its morphology and composition, as well as other physical properties and traits. An SEM is typically made-up of an electron gun, various beam deflection coils, a detector and display or recording device. Tungsten is usually the source of choice for the filament of the electron gun due to its high melting point and low vapour pressure. Other emitters include lanthanum hexaboride cathodes. Current passes through the source,

emitting the electron beam. The beam with an energy range of 0.5 to 40 eV is focused through the magnetic deflection coils or scanning coils and a final magnetic lens. This deflects the beam in the x and y axis by applying a small current to the coils, so that it scans over the sample surface. A SEM also typically contains an objective lens, used to focus the small probe on the sample surface (75).

The electrons interact with the sample producing a number of different signals which can be interpreted to give information. It allows for the simultaneous acquisition of bright-field (BF), annular dark-field (ADF) and secondary electron (SE) images. With BF and ADF, transmitted electrons are used to generate the image. This gives structural information about the sample's interior. In contrast, SE which is the most common mode of imaging with SEM, are formed when incident electrons collide with the outer shell electrons in the sample, ejecting these electrons. These secondary electrons are usually low energy and give topographical information about the sample surface. Electrons directed away from the surface of the inelastic scattering process are known as backscattered electrons (BSE) and are dependent on the mass of the atoms in the sample; higher atomic mass means more BSE. This mode therefore gives information about the composition of the sample (75).

The SEM used in these experiments was a Hitachi S-3400 (Hitachi Ltd, Japan).

2.4.2 Bioanalysis

2.4.2.1 BioAnalyzer

The concentration and integrity of the purified total RNA was determined by capillary electrophoresis (RNA 6000 Pico kit, BioAnalyzer 2100, Agilent technologies, USA) as per the manufacturers' instructions. Electrophoresis is a technique used to separate DNA and RNA fragments by size and charge. NA molecules move through an electrophoretic gel under an electric field. The negatively charged NA molecules move through the gel with the shorter molecules moving faster and farther. In this way it is possible to receive information about the NA molecules being detected.

The quality of the purified RNA was assessed by the RIN (RNA Integrity Number). This is given by a built-in algorithm of the Agilent Expert Software. The RIN algorithm analyses the entire electrophoretic trace generated from an RNA sample. The algorithm builds regression models using indicated peak positions, heights, areas, area ratios, S/N ratio, maximum and minimum values, and waviness of the electropherogram trace to assign a 1–10 score (76). RIN score of 1 means the sample is degraded, and 10 scores for completely intact RNA. According to the description of Agilent, the RIN algorithm is developed to utilize neural networks and adaptive learning in conjunction with a large database of eukaryote (organisms whose cells contain a nucleus)

total RNA samples. The RIN score is largely independent of the amount of RNA used and the origin of the sample.

2.4.2.2 Nanodrop

In order to quantify nucleic acid presence in samples a UV-Vis spectrophotometer was used. Nucleic acids absorb ultraviolet light in known ways. In a spectrophotometer, the sample is exposed to light at 260 nm and the transmitted light is detected. The more light that is absorbed by the sample indicates a greater nucleic acid concentration. For quantification purposes the built in software uses a modified Beer-Lambert equation to calculate the sample concentration *c,*

$$c = \frac{(A * \varepsilon)}{b} \qquad (eqn.\ 2.1)$$

Where c is the nucleic acid concentration in ng/μL, A is the absorbance in machine units, ε is the wavelength-dependent extinction coefficient in ng-cm/μL and b is the pathlength in cm. A typical absorbance spectrum is shown in Figure 2.8.

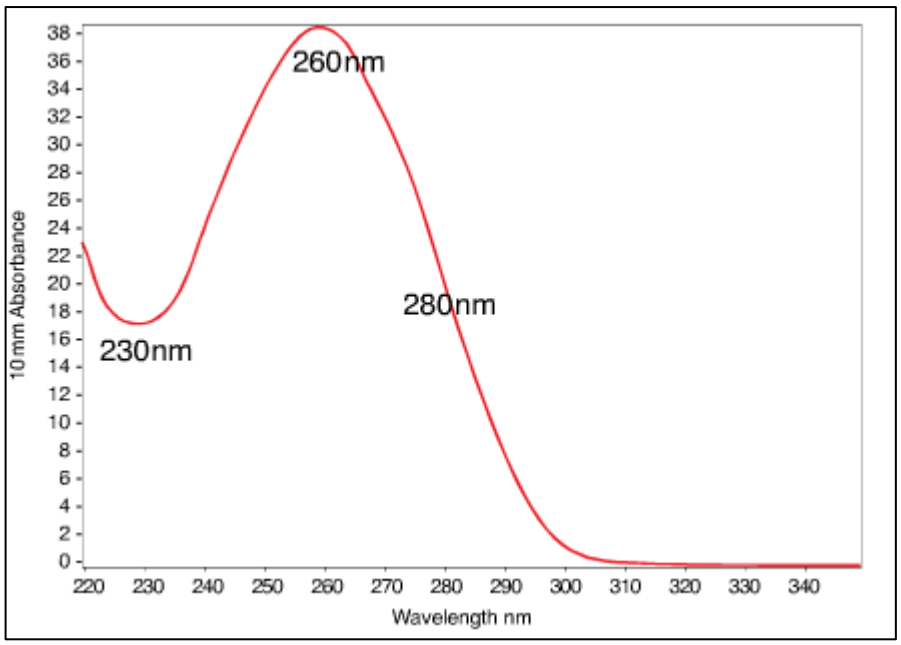

Figure 2.8: Typical absorbance spectra of nucleic acid. Wavelengths of interest are at 230 nm, 260 nm and 280 nm. Adapted from Nanodrop Handbook (77).

The ratio of absorbance at 260 nm and 280 nm gives information about the purity of the nucleic acids, as proteins have an absorbance maximum at 280 nm. A ratio of ~1.8 is generally accepted as 'pure' DNA and a ratio of ~2.0 as 'pure' RNA. Alternatively, absorbance at 230 nm is generally due to some form of contamination within the sample. Therefore, the A260/A230 ratio is also useful. Expected values of 260/230 are usually in the range of 2.0 - 2.2 (74).

Shifts in the 260/230 ratio can show an issue with the sample or the extraction procedure. For example, a low 260/230 ratio can be an indicator of residual phenol from the extraction process or residual guanidine from the purification process. The 260/280 ratio is heavily dependent on the pH and ionic strength of the buffer used to make the

sample measurement. Acid solutions under represent the ratio by 0.2 - 0.3, while basic solutions over represent it by 0.2 – 0.3. Also a low 260/280 ratio may indicate low concentration (> 10 ng/μL) of nucleic acid (78).

The spectrophotometer used in this work was a Nanodrop 2000c (Thermo Scientific, Ireland). The pedestal measurement of the device requires only 0.5 – 2 μL of sample. The droplet is suspended between the pedestals and stretched to form a known pathlength (Fig. 2.9). Optical fibres are embedded within the upper and lower measurement surfaces. The device has a wavelength range of 190 – 840 nm and a wavelength accuracy of 1 nm. It has a lower limit of detection of 2 μg/mL for dsDNA and an upper concentration limit of 15,000 μg/mL.

Figure 2.9: Droplet stretched on pedestal of Nanodrop spectrophotometer to give a 1 mm pathlength. Adapted from Nanodrop Handbook (77).

2.4.2.3 Fluorescence Detection of DNA

In order to detect the quantity of DNA present post-purification a Quant-iT™ PicoGreen® dsDNA Assay (Life Technologies, Dublin,

Ireland) was used. The kit allows the detection of as little as 25 pg/ml of dsDNA in a background of RNA, ssDNA and free nucleotides and is orders of magnitude more sensitive than UV absorption methods. It uses a standard spectrofluorometer and fluorescein excitation and emission wavelengths (excite at 480 nm and emission intensity measured at 520 nm). The kit has a linear detection range which extends over four orders of magnitude from 25 pg/mL to 1000 ng/mL.

The DNA is suspended in a TE Buffer solution (10 mM Tris-HCl, 1mM EDTA, pH 7.5). The buffer comes as 20X TE Buffer solution which must be diluted down to 1X TE Buffer using sterile, DNase-free water.

The Quant-iT™ PicoGreen® dsDNA dye used for fluorescence must be prepared on the day of the experiment. The aqueous working solution is acquired by making a 200-fold dilution of the concentrated DMSO solution in 1X TE Buffer. The solution should be prepared in a plastic container, instead of glass as it may absorb to the glass surface, and must be protected from light as it is susceptible to photodegradation.

To analyse the sample, a 1:1 quantity of sample and dye is placed into a clear 96-well plate (Nunclon MicroWell, Sigma Aldrich). The solutions are allowed to incubate for five minutes in the dark, and then the plate was placed into the spectrofluotometer plate reader (Tecan Safire 2, Tecan Group Ltd, Switzerland). The plate reader performs a fluorescence intensity scan, exciting at 485 nm and detecting emission at

520 nm. The software outputs a fluorescence intensity signal for each of the 96-wells.

2.4.2.4 Cell Counting

In order to identify the number of cells in a suspension a haemocytometer was used. This gives the number of cells in a given volume and is counted by direct examination under a microscope. The haemocytometer is a glass chip which has a precise grid carved into it (Fig 2.10). A cover slip is placed on top of the grid area, until Newton's rings are visible. This indicates that a chamber of precise depth has been formed. Haemocytometers were originally developed for counting blood cells but have also been designed for counting bacterial cells, as was used in this work. The ruled grid area consists of 9 large square, each 0.05 × 0.05 mm = 0.0025 mm^2. The depth of the chamber is 0.01 mm. This gives a volume of each large square as 0.0025 mm^2 × 0.01 mm = 2.5×10^{-5} mm^3. The four corner squares are subdivided into 16 smaller squares and the centre square into 25 smaller squares (with each of those 25 squares divided into a further 25 squares).

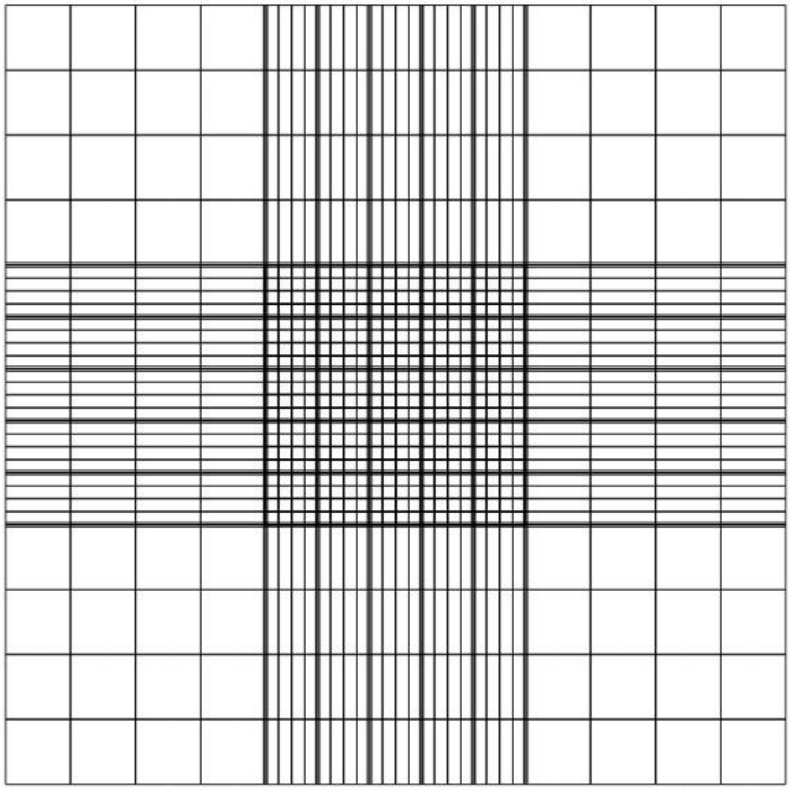

Figure 2.10: Grid structure of haemocytometer cell counter. Each of the 9 larger squares has an area of 0.0025 mm^2.

A 7 μL volume of cell suspension is placed at the edge of the coverslip so as to allow the solution to flow into the chamber by capillary action. The slide is then viewed under an optical microscope. Depending on the size of the cells under examination, the optimum area of the grid is identified: the outer squares for large cells and the central squares for small cells. The cells within a given square are counted, using a predetermined method, i.e. count the cells within the square and those touching the top and left line, but not those touching the bottom and right lines. This procedure is repeated for a number of squares and the

average number of cells per square is calculated. The volume of a square is a known quantity so the number of cells per mL can be identified (79).

2.5 Conclusion

The various methods for fabricating, testing and characterising the microfluidic systems used as part of this work were given. The main fabrication techniques are laser ablation and CNC milling. All testing of the discs was performed on a spinstand. Structural analysis of the discs and their components was performed using an optical microscope, 3D microscope and SEM. Analysis of the biological samples collected from the various devices was achieved using a BioAnalyzer, Nanodrop, platereader and haemocytometer.

Chapter 3

Solvent Selective Router for Centrifugally Automated Solid-Phase Purification of RNA

3.1 General Introduction

As discussed in detail in Chapter One nucleic acid testing is of vast interest to the scientific community. The process can be broken down into three stages: extraction, purification and detection. One of the most common methods of purification is Solid-Phase Purification (SPP). For the course of this work we used the well-established Boom chemistry method (48). Nucleic acid purification has been implemented on centrifugal microfluidics with relative success (31). One of the

underlying challenges for the on-disc integration of bench-top purification protocols is the sequential routing of fluids to designated waste and elution reservoirs (30). We developed a new centrifugal microfluidic router that utilised differences in pressure drop across the microchannels in combination with solvent-specific flow control. As an additional benefit, the fluid handling on the centrifugal microfluidic platform is entirely controlled by the spin frequency of the disc. No external actuation or stimulus is required.

We adopted Trizol extraction for preparing homogenate of MCF7 breast cancer cells. The reagent contains phenol that ruptures the cells and guanidine that strips the protein complexes from the RNA. Due to differences in the solubility DNA is retained in the organic phase whilst the RNA is concentrated in the aqueous phase which also contains salt contamination. This procedure is done on the bench. To meet the purity requirements for downstream analysis of RNA, it is imperative that the extracted RNA remain free of contaminants such as salts and phenol. To this end, we implemented a four stage purification protocol (Fig. 3.1) on-disc. We then validated the device using MCF7 cells.

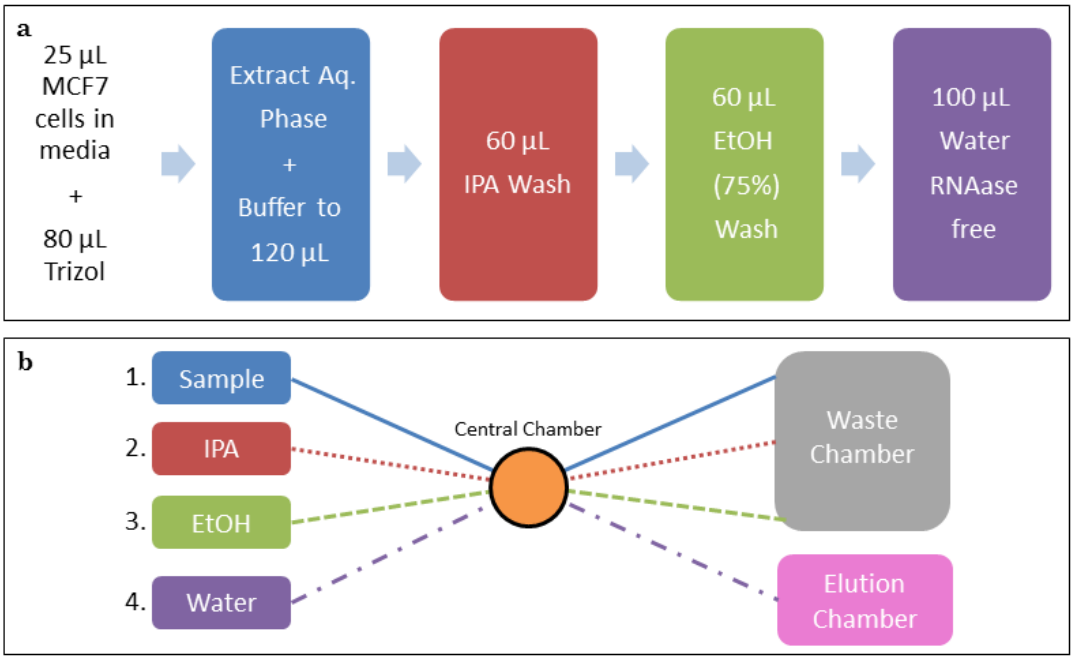

Figure 3.1: Protocol for total RNA isolation from breast cancer cells (MCF7 cell) using Trizol_Reagent. a) MCF7 cells are lysed using TRI reagent and the aqueous phase is isolated and mixed with a buffer. This is followed by an IPA wash and an EtOH wash. Finally RNAase free water acts as an elution buffer. b) The four solutions are all washed through a central chamber which contains the solid phase. The first three flows are routed to the waste collection and the final solution is routed to the elution collection.

3.2 Working Principle

3.2.1 Valve Design

In order to handle the four different fluids (Fig 3.1), two organic and two aqueous, and collecting the phases separately we developed two solvent-specific valves. The first was a Dissolvable Film Valve (DFV), which uses a water dissolvable film. It was discovered that the DF is unreactive to organic solvents, i.e. it will not dissolve in two of the four purification steps, the Isopropanol (IPA) and Ethanol (EtOH) steps. The

ratio of organic to aqueous solution does however effect the dissolution time of the film.

The second valve was a Hydrophobic Membrane Valve (HMV). This HMV is made up of a PTFE-supported membrane which permits the passage of the organic phase but remains impermeable to aqueous solutions. The DFV is single-use and dissolves once in contact with water whereas the HMV remains intact preventing water from passing through. Using a method similar to Gorkin *et al.* (24) the valves were assembled into a tab structure using two pieces of Pressure Sensitive Adhesive (PSA). The precision knife cutter defined through holes in the PSA. The rounded rectangular holes, cut into the PSA layers, were identified as the optimum shape for flow through the tab. This was determined by experimental validation. When a circle was used, (as done so by Gorkin *et al.*), in our structure the presence of an air bubble could sometimes block the passage of fluid through the tab. A smaller square piece of HM or DF was then placed between the PSA layers (Fig 3.2a,b). This sandwich structure allowed for better reliability of the tabs as the HM/DF are completely sealed in between the 'sticky' PSA layers.

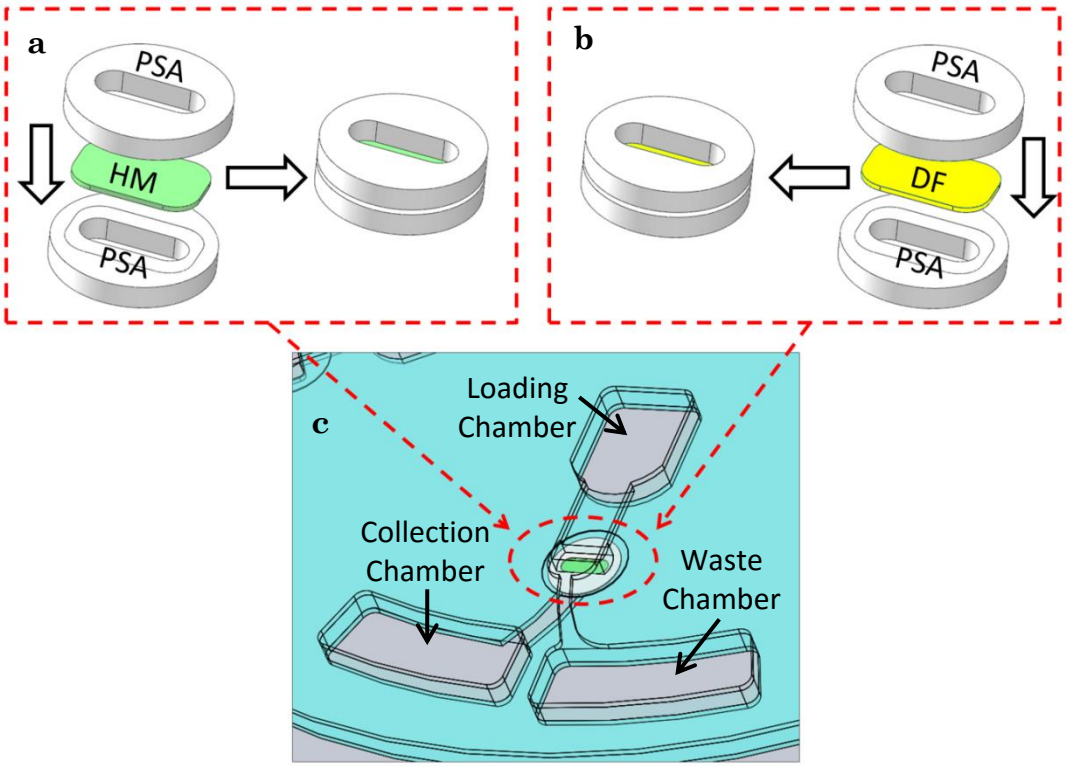

Figure 3.2: Principle of fluid routing. a,b) Assembly of pressure-sensitive adhesive (PSA) and dissolvable-film/hydrophobic-membrane (DF/HM) tab, c) Schematic of the simple router structure and location of tab placement within the disc.

3.2.2 Proof-of-Principle Router

A simple router was designed in order to test the principle of using the valves for routing of flows on a centrifugal microfluidic platform. The design of the simple router is shown in Figure 3.2c, as is the placement of the tabs within the disc. The design consisted of a loading chamber connected to two collection chambers via microchannels. The 3-dimensional architecture of these discs means that the two channels can be placed in two separate layers and connected via a through hole. The through hole connecting these chambers was sealed

using one of the tabs, in this case a HMV. In an open system, under centrifugation, the fluid will preferentially travel to the left collection chamber due to a lower pressure drop across the channel, achieved by making the channel shorter with a larger cross-section. However, the HMV is impermeable to aqueous solutions; the first aqueous flow is thereby routed to the right collection chamber. Organic solutions can pass freely through the valve and were routed to the left collection chamber. Flow through the system is shown in Figure 3.3. The HMV is interchangeable with a DFV. In that case, the organic solution would be unable to pass whereas the aqueous solution would dissolve the film and continue to the left collection chamber. As these valves are interchangeable, precise control of fluid routing can be achieved.

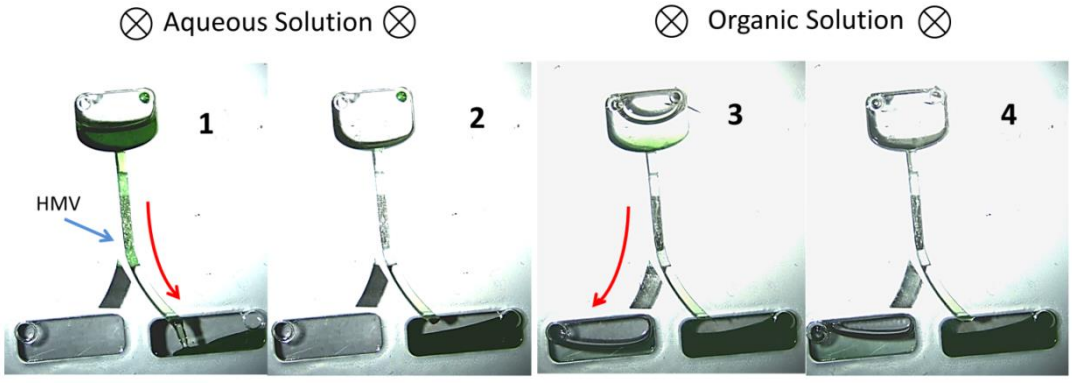

Figure 3.3: Routing of aqueous and organic flows using HM tab. The HM is impermeable to the aqueous phase. The fluid, therefore, travels over the 'closed' membrane and is collected in the right collection chamber (1, 2). The organic solution is loaded next; it passes through the 'open' membrane and is collected in the left collection chamber (3, 4). The centre of rotation is indicated above each image.

3.2.3 Combination Valve

In an attempt to adapt the simple router to handle the four fluids required for SPP, a combo-valve was developed. The valve consisted of a stacked structure of DF and HM tabs which would be inserted into the simple router. The order of the stack would determine which directions the fluids went and in which order. The design of the stacked combo-valve is shown in Figure 3.4.

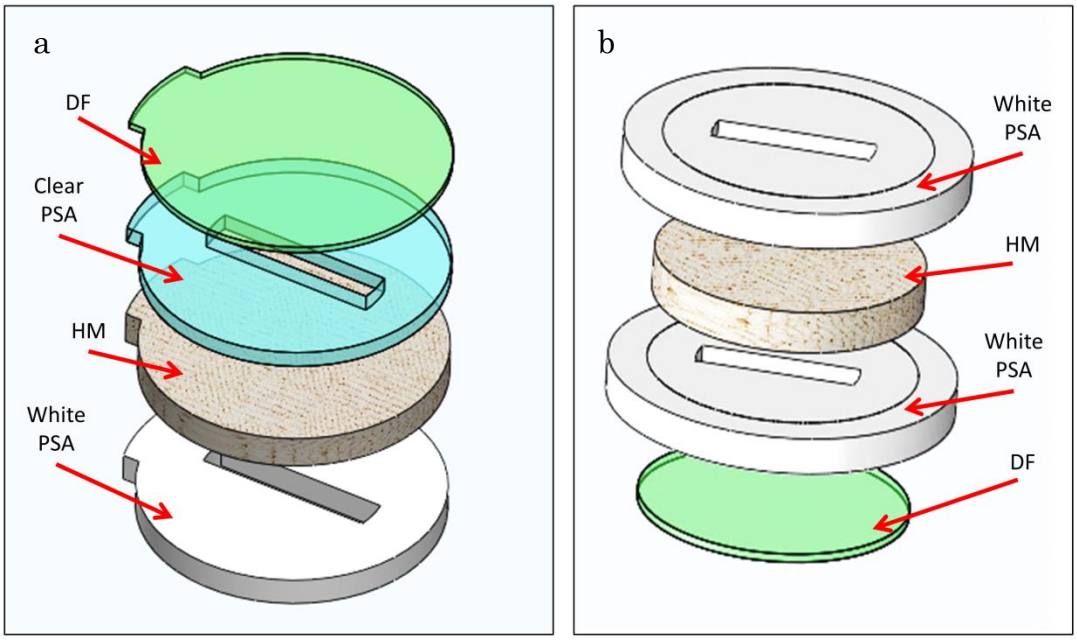

Figure 3.4: Combo valve designs. a) First configuration of the combo valve. A DF was adhered to thin clear PSA, which was subsequently adhered to a HM and thicker white PSA. All four layers were cut to the same diameter. b) Second configuration of the combo valve. In this case the HM is 'sandwiched' between two layer of white PSA, with a DF stuck to the other side. The clear PSA was abandoned due to difficulties with handling.

A number of different configurations were attempted. Firstly the individual layers were simply placed one on top of the other, with the DF and HM layers being held together by clear PSA with a through hole cut out (Fig. 3.4a). A white PSA layer was stuck to the underside of the HM and the backing of this was used to adhere the tab to the disc. The clear PSA is thinner than its white equivalent (~50 μm thickness versus ~86 μm). The overall thickness of the combo tab was ~250 μm which was a considerable thickness to insert into the disc, therefore the hope was that the clear PSA would remove at least some of this. Unfortunately, the clear PSA proved extremely difficult to handle and the structure shown in Figure 3.4a was prone to leaking especially in the HM layer, which seemed not to adhere as well to the PSA as the DF did.

It was therefore, determined that the 'sandwich', shown previously would solve the leaking issue and this was design was implemented into the disc (Fig. 3.4b). The working principle is shown in Figure 3.5.

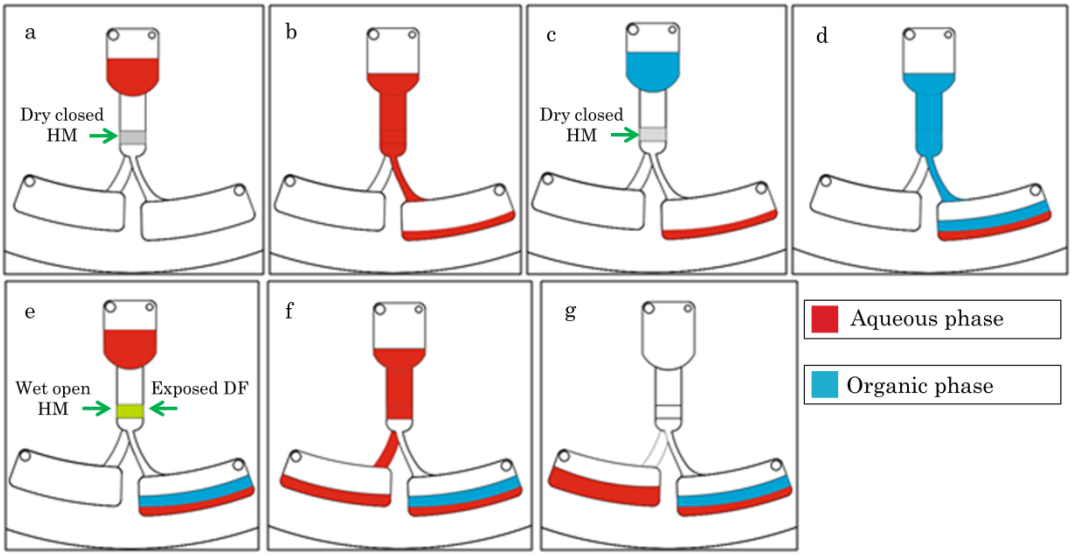

Figure 3.5: Working principle of combo valve in simple router structure. a) The combo valve was inserted into the disc with HM side up. The HM was yet to be wetted so was currently in a 'closed' state. An aqueous solution was loaded. b) The aqueous solution flowed down the channel, over the closed HM and is collected in the right chamber. c) An organic solution was loaded. The HM was still currently dry. d) The organic solution flowed down the channel, wetting the HM but unable to pass by the DF, it was therefore routed to the right chamber. e) The final aqueous solution was loaded. The HM has now been wetted, exposing the DF underneath. f) The aqueous solution flows down the channel, through the HM, dissolves the film and is collected in the left collection chamber. f) Final configuration of the combo valve design.

The concept relied on the discovery that once the HM had been wetted by passing an organic solution through it, it would then enter an 'open' state where it was possible for aqueous solutions to pass through. The combo valve was therefore inserted into the disc in the layout shown in Figure 3.4b, with a HM layer sitting on top of the DF layer. As per the four stage purification protocol (Fig. 3.1), an aqueous solution would be first loaded. It would travel down the channel, across the closed HM and

be collected in the right chamber. Next an organic solution would flow down the channel, through the HM but would not be able to pass the DF. It would therefore also be routed to the right chamber. A second organic solution would follow the same pathway. Finally, an aqueous solution would flow down the channel, through the now open HM, dissolve the DF and be collected in the left chamber.

Ultimately, this design proved unsuccessful for a number of reasons. Firstly, though it was shown that passing organic solutions through the HM turned it from a 'closed' to 'open' state, in the current configuration the organic solution did not seem to pass through the HMV at all. This was postulated to be because the DF was creating an airtight seal on the underside of the HM. This meant that the final aqueous solution was in fact interacting with a 'closed' HM. Secondly, the DF requires time to dissolve and in this time the flow was still occurring, therefore much of the sample would be lost to the right waste chamber.

It was therefore decided that though the inclusion of the two different membrane types within the one structure could handle all the necessary fluidic steps for SPP, a more complex structure was needed to accomplish this goal.

3.3 Router for RNA Extraction

This simple router was expanded upon for total RNA solid-phase extraction as it only allowed for the routing of two fluids. The full router was engineered to enable sequential handling of four separate fluids.

3.3.1 System Design

The final design (Fig. 3.6a) comprises of four chambers: the loading chamber (*L*), the organic waste chamber (W_{org}), the aqueous waste chamber (W_{aq}) and the eluate collection chamber (E_{aq}). The loading chamber is used for the loading of the sample and reagents. It also contains the solid-phase, for which we used glass beads. Within the chamber, we placed a baffle with laser ablated, 100-μm grooves, to retain the glass beads (diameter ≤106-μm) under centrifugal flow (Fig. 3.6a inset left). Without this baffle some beads could travel down the channel blocking the passage of fluid. The eluate collection chamber was used to collect the purified RNA in the final step of the solid-phase purification.

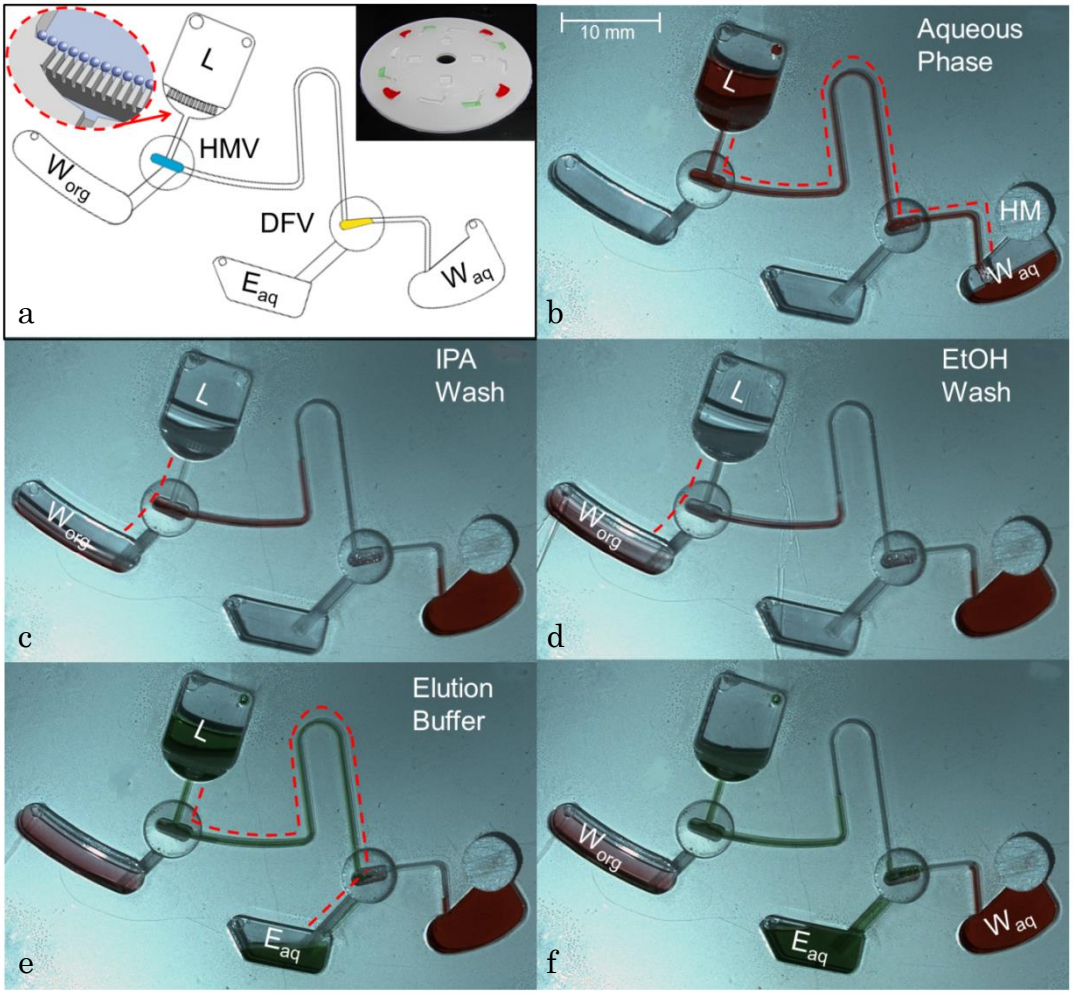

Figure 3.6: Working principle of flow router showing fluidic tests. a) Schematic of flow router showing chambers the loading chamber (L), the organic waste (W_{org}), the aqueous waste (W_{aq}) and the elution chamber (E_{aq}). Also shown are the Hydrophobic Membrane Valve (HMV) in blue and Dissolvable Film Valve (DFV) in yellow. Inset on the left shows a magnified view of the loading chamber containing the baffle. The baffle was used to retain the glass beads within the loading chamber. The inset on the right shows an image of the whole disc. b) Flow is directed from L to W_{ag}. The initially closed DFV is opened by the flow. c,d) 60 µL IPA and EtOH flows from L to W_{org} through the HMV, which is permeable to organic solutions. e) Routing of final elution buffer from L to E_{aq}, passed the HMV which is closed to aqueous solutions and through the now open DFV. f) Final configuration of fluids in router. Note that the E_{aq} remains free of organic solutions with is crucial for good quality extracted RNA.

Three different valves were implemented on the router: a HMV, a siphon valve and a DFV. These valves are controlled by the fluid levels and the spin frequency of the disc. Two of the composite "tabs" (HM and DF) were placed in the multi-layer architecture of the router. The HMV blocks access to the organic waste chamber (W_{org}) and the DFV seals the elution buffer collection chamber (E_{aq}). A single channel with a siphon valve leads the fluid over the HMV to the DFV. One microfluidic disc can contain up to four identical structures (Fig. 3.6a, inset right) permitting the extraction and enrichment of multiple samples simultaneously.

3.3.2 Fluidic Operation

First the system was tested fluidically using sequential loading of reagents along a series of intervals at specific spin frequencies (Fig. 3.6). To test the principle, we used a scaled-down version of the extraction protocol developed by Linares *et al.* (53) for total RNA. This extraction process (Fig. 3.1) requires sequential treatment of the aqueous RNA phase with 2-propanol (IPA), 75% ethanol (EtOH) and water. The loading chamber was packed with 25-mg of acid-washed glass beads (diameter < 106 μm). These beads represent the solid phase for the purification of total RNA based on charge-charge interaction in a solution that contains chaotropic salts.

The operating principle of the router was based on the following protocol: first 120-µL of the crude aqueous phase extracted from a lysed sample is added to the beads in the loading chamber (Fig. 3.6b). The RNA in the sample binds to the acid-washed glass beads due to charge-charge interactions, under chaotropic conditions. The acid-washed glass beads are positively charged due to the sodium on their surfaces; they interact with the phosphoric acid backbone of the RNA, which is negatively charged (48). Under centrifugation the RNA-depleted aqueous phase, travels down the channel and passed the HMV (which is impermeable to aqueous solution), up over the siphon in W_{aq}. As the flow passes over the DFV it dissolves the film. There is a time delay on the dissolution of the film and during this time all the fluid is collected in W_{aq} (Fig. 3.6b). Next the disc is stopped and IPA is pipetted into the loading chamber (L). The IPA precipitates any remaining unbound RNA. The disc is spun again, this time at a higher spin rate, in order to stop the fluid from passing over the siphon. The IPA contacts the HMV and passes through the PTFE-supported membrane, routing the fluid into W_{org} (Fig. 3.6c). Any fluid remaining in the channel from the first step passes through the now wetted PTFE-supported membrane. According to the supplier, organic solvents change the permeability of the membrane, thus making it possible for the remaining RNA-depleted aqueous phase to pass into W_{org}. The EtOH is loaded and follows the same path as the IPA. The EtOH rinses away any salts from the beads, it also removes any residue left in the pre-crest siphon channel (Fig.

3.6d). A drying step is required after the EtOH wash is order to allow the EtOH to evaporate from the pores of the PTFE-supported membrane, returning it to its originally closed state. For the final stage, the aqueous elution buffer is added to the loading chamber, the disc is spun at a low frequency as the fluid passes through the beads, collecting the purified RNA. The solution then passes over the now closed HMV, over the siphon and through the now open DFV (opened during the first stage), where it is collected in the E_{aq} reservoir (Fig. 3.6e).

3.4 Materials and Methods

3.4.1 Disc Fabrication and Assembly

The disc (Ø 120 mm) consisted of three layers of PMMA and two layers of PSA (Fig. 3.7). The PMMA layers were cut using the laser cutter, as described in Section 2.1.2.1. The loading holes and chambers were cut from the top and middle layers and the bottom layer had its draining channels ablated. Additionally, channels were milled (CNC milling as described in Section 2.1.2.2) into the top of the middle layer and valve grooves were milled into its underside. Milling was used for alignment purposes and to achieve a more reliable and reproducible cut than could be achieved by using the laser. The cleaning procedure, as outlined in Section 2.1.3, was observed. The PSA layers were cut using the precision knife cutter. Prior to assembly (described in Section 2.1.4)

the tabs were stuck into the valve grooves on the underside of the middle PMMA layer.

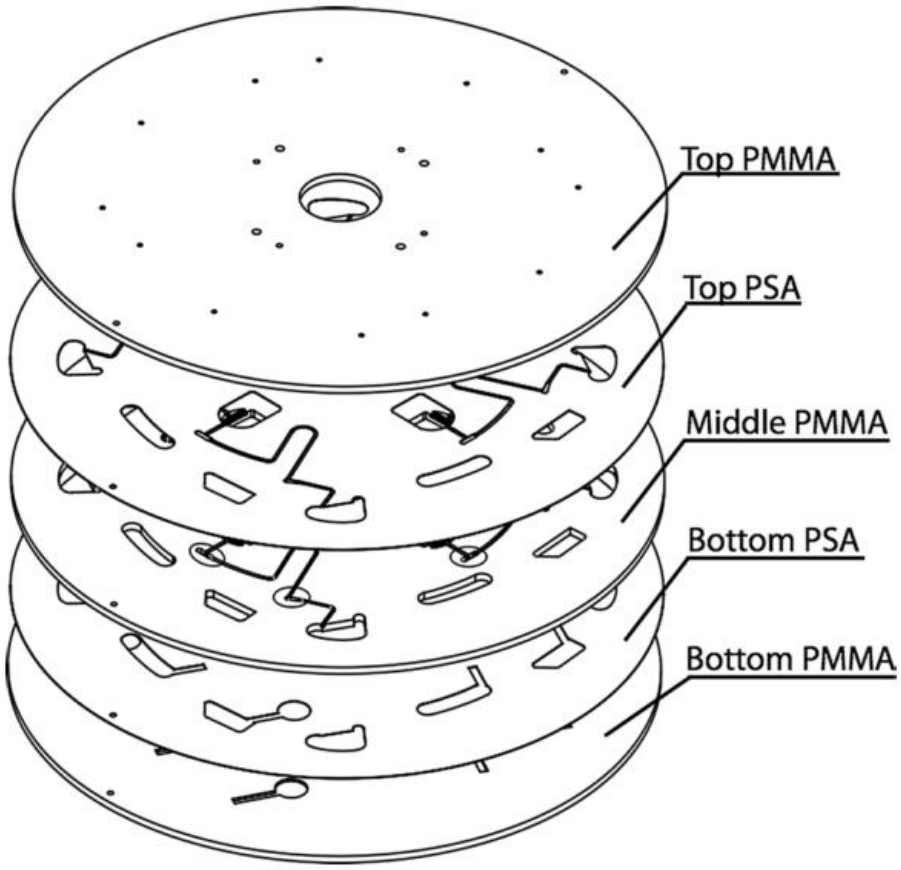

Figure 3.7: Exploded view of disc assembly. The (Ø 120 mm) disc consists of five layers: three PMMA layer and two PSA layers.

3.4.2 MCF7 Cell Culture

MCF7 cells (DSMZ, Braunschweig, Germany) were cultured in 75 cm flasks in Dulbecco's Modified Eagle's Medium (DMEM), supplemented with 10 % foetal bovine serum (FBS), 100 UmL^{-1} penicillin and 100 μgmL^{-1} streptomycin. The cultures were maintained at 37 °C with 5 % CO_2. Cells were harvested by incubation in 5 mL 0.25 % trypsin/0.1 % EDTA at 37 °C for 5 min followed by neutralization with

5 mL culture medium. Cells were centrifuged at 300×g for 4 min and resuspended in culture medium. The cells used in this study were collected between their 17 and 25 passages. Passaging, also known as subculturing, is the processes were by cultured cells are transferred to fresh growth media, thereby sustaining the cell line (80). This procedure was performed by Dr. Macdara Glynn.

3.4.3 Benchtop Lysis and RNA Extraction

Cells were lysed by mixing a 25 μL aliquot in growth media with 80 μL of TRI Reagent. The aliquots contained 2.96×10^5 – 7.4×10^4 MCF7 cells. This mixture was vortexed for 1 minute and left to incubate at room temperature for 9 minutes. To each of the samples 5 μL of 4-bromoanysole was added enhancing the phase separation and the extraction. All samples were centrifuged at 13000 RPM (14000 g) for 10 minutes at room temperature. During this process complete phase separation occurs with the aqueous, RNA containing phase, above the organic phase, containing DNA. The aqueous phase (60 μL) was removed for on-disc purification. The interphase between the aqueous and organic phases was not disturbed during the extraction as it could influence the quality of the purified RNA at the end. In parallel a negative control experiment was set up with an 'empty' sample containing only the growth media without cells.

3.5 Results and Discussion

3.5.1 Fluidic Analysis

Experimental validation was performed to determine the optimum fluid volumes and spin frequencies for each stage of the four step process. The final spin frequency protocol is shown in Figure 3.8. A five minute incubation period, while the disc was at rest was necessary to allow the RNA time to bind to the beads. Another five minute elution period was observed during the final stage, to allow the RNA time to detach from the beads and re-suspend in the elution buffer. It was determined that these two waiting periods enhanced the purification efficiency. During the course of testing it was also determined that a five minute drying step should follow the EtOH wash. This allows for the siphon to dry before the final elution step, thus improving the reliability of the system. When this drying step was omitted, the elution buffer would sometimes seep over the siphon and mix with the aqueous waste fraction.

After the initial waiting period, the disc was spun up to 12.5 Hz to allow the first aqueous sample to travel over the siphon. The IPA and EtOH washes were spun at a considerably higher frequency of 75 Hz, to stop these fluids from traveling over the siphon, which is a low-frequency pass valve, and contaminating the final sample. It takes approximately 3.5 minutes at this spin frequency for the PTFE-supported membrane (HM) to open, as the RNA depleted aqueous phase

prevents the IPA from directly accessing the HMV. Finally, the elution buffer was spun at a lower frequency of 7.5 Hz until it was collected into E_{aq}. The entire process requires less than 25 minutes but each disc contains four identical structures, so four samples can be run simultaneously.

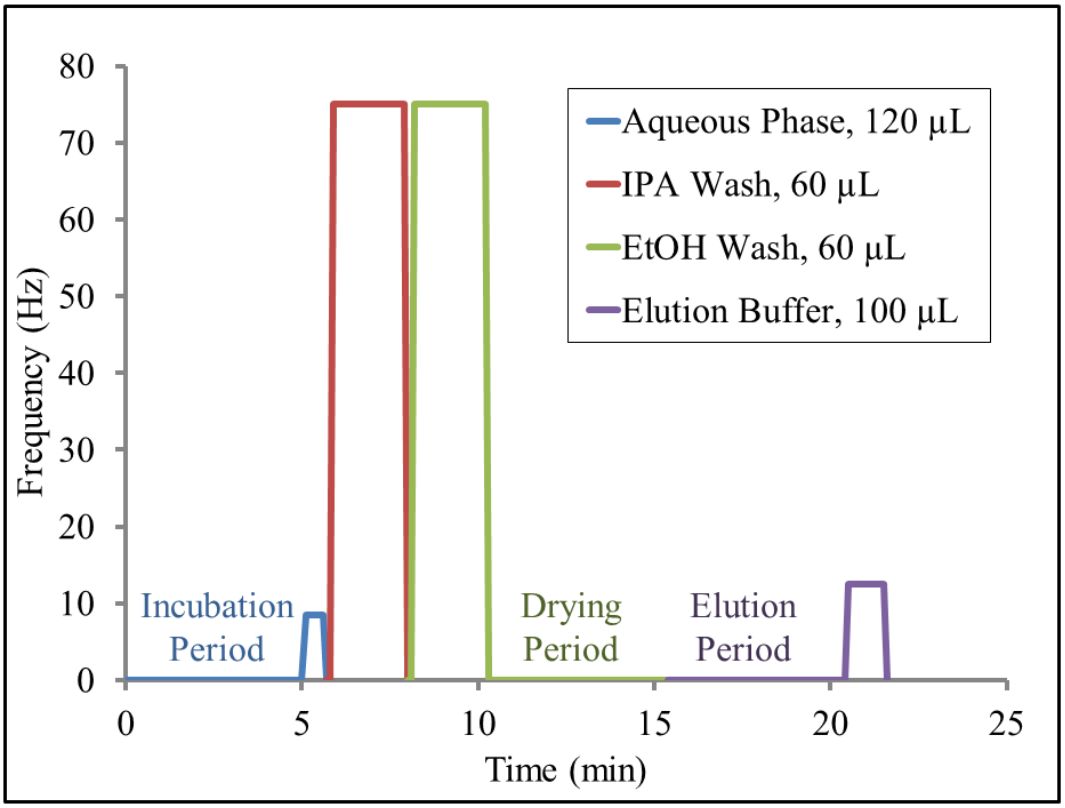

Figure 3.8: Spin frequency of the disc versus time for RNA extraction protocol. The disc is stopped for loading each of the four solutions. The three 5 minute waiting periods, where the disc is at rest, are required to: give the RNA time to precipitate unto the beads, allow the PTFE-supported membrane and siphon channel to dry, and allow the RNA time to re-suspend in the elution buffer. The simultaneous purification of four samples was achieved in less than 25 min.

An addition to the control given by the valving technologies and variation in spin rates, was the deliberate design of the interconnect between the elution collection chamber (E_{aq}) and the aqueous waste chamber (W_{aq}) (Fig.3.9). During the final elution stage, the centrifugally stabilized fluid volume already resident in the right chamber (W_{aq}) from the first flow through, blocks all vents, thus acting akin to a solid plug to practically create a dead-end channel. The system can be simplified because both fluids are aqueous solutions and have identical contact angles with the channel walls and the channel has uniform cross section on both sides of the air pocket. For the sake of clarity, we neglect capillary and inertial effects, so the flow into the right outlet will hence stop once the pressure in the interspersed air pocket balances the centrifugal pressure exerted by the incoming fluid. The air pocket thus acts as a fluidic capacitance (81) where the final pressure of the air pocket

$$P = P_{ini} \cdot \left(\frac{V_{ini}}{V}\right) \qquad (eqn.\,3.1)$$

depends on the initial (typically atmospheric) pressure P_{ini} and the ratio of the initial and final volumes V_{ini} and V, respectively (Fig. 3.9). The flow in the lateral channel stops once the pressure in the air pocket equilibrates the centrifugally induced pressure

$$P_{\omega} = \rho\omega^2\bar{r}\Delta r \qquad (eqn.\,3.2)$$

with the fluid density ρ, the angular frequency ω, the radial length $\bar{r}$ and the mean position Δr of the incoming fluid plug. So essentially, the here considered routing function is tightly linked to the sequence of fluids and sealing the air pocket formed between the advancing and the stationary fluids. To help with sealing the air pocket, we placed a PTFT-supported membrane (HM) over the air vent in W_{aq} (Fig. 3.6). The membrane allows air to be vented but is impermeable to aqueous solutions. In this way, it stops the fluid in W_{aq} from being centrifugally pumped out by the incoming air pocket.

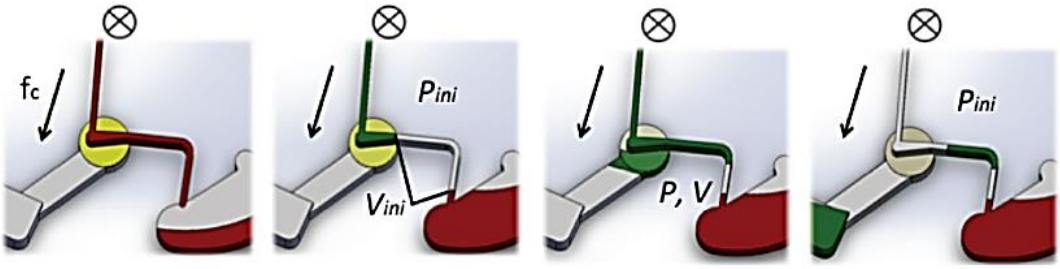

Figure 3.9: Schematic of the fluidic capacitance, dissolution of the DF (yellow) and routing of the aqueous flows, where P_{ini} is the atmospheric pressure, V_{ini} is the volume of the lateral channel and P with V is their centrifugally compressed counterparts under centrifugal force (fc), directed from the centre to the periphery of the disc (black arrows). The axis of rotation is denoted by ⊗ above each panel.

3.5.2 On-disc RNA Purification

To validate the functionality of on-disc SPP with our router, we performed cell lysis and RNA extraction on the bench, of MCF7 cells

with TRI Reagent. The extracted volumes were diluted with water to 120 μL with RNAase free water and the complete volume was loaded on-disc. The protocol described in Figure 3.6 was performed and the purified samples were extracted.

Samples were collected from both E_{aq} (the purified sample) and W_{aq} (unbound sample). These were also compared with the control sample where no RNA was detected. The results of this are shown in Figure 3.10. The electropherogram shows that the recovered RNA originated from the cells and not from the growth media. The quantity of total RNA extracted from W_{aq} is significantly less than the one recovered from the yield of E_{aq}. A concentration of 180 pg μL^{-1} was measured in the purified fraction (100 μL), against 37 pg μL^{-1} (120 μL) in the waste fraction. This is a solid proof for the successful retention of the RNA on the glass beads.

Furthermore the electropherogram for the rRNA peaks (18S and 28S) of the sample from W_{aq} is shifted left in relation to the typical migration times. We relate this behaviour to the residual salts in the W_{aq} (82). Extending on the purity of the sample, from the RNA integrity numbers (RIN) in Table 3.1 one can deduce that the sample from E_{aq} is less degraded than the one eluted in W_{aq}.

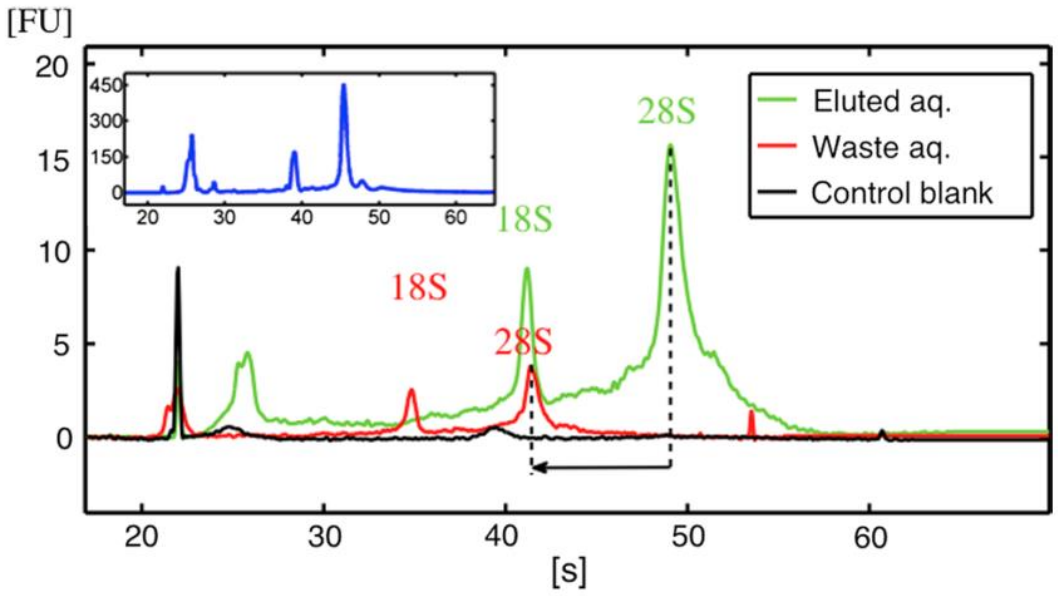

Figure 3.10: Electropherograms showing solid-phase purification efficiency on-disc. Total RNA content was measured from the purified sample Eaq (green), the waste sample Waq (red) and a control blank (black). The dashed line indicates the shift in waste sample which is attributed to residual salts in the Waq. The inset displays the bench-top extracted sample using 2-propanol precipitation and the position of the peaks of pure total RNA (blue).

Table 3.1: Summary of electropherogram for the above samples. An Integrity Number (RIN) of 10 corresponds to intact RNA, while 1 indicates completely disintegrated RNA.

Total	RIN	28S/18S	pg/uL
E_{aq}	7.7	2.6	180
W_{aq}	6.4	1.8	37
Control	1	NA	10

As part of our investigation, bench-top extraction was performed lysing 9.5×10^4 MCF7 cells. IPA precipitation was used, followed by two

consecutive washes with EtOH. We measured total RNA of 32.3 ng from this bench-top sample. The RNA recovered from an identical sample after on-disc extraction resulted in 3.9 ng of total RNA. By normalising the results and assuming that the bench-top extraction was 100% efficient, our purification efficiency was 12.1 % (by weight) of extracted total RNA from an identical sample using a purification protocol on bench without beads. The percentage of purified RNA on-disc varied between samples with different cell counts. For the 1.48×10^5 cells, 43 % of the total RNA was retained on the beads, from which 7.2 % was recovered from the elution fraction. Variations in the packaging of the solid phase would inevitably lead to fluctuations of the amount of recovered total RNA. Further investigation and optimization of the solid-phase extraction protocol should follow in order to further raise both the capture and elution efficiency of total RNA.

The electropherograms obtained for the varying number of MCF7 cells are show in Figure 3.11. These show that high-quality RNA was recovered from the eluted fraction. For the MCF7 RNA studied (n = 8), RIN values were in the range of 7.2–9.2. An average of 16.8 ng was recovered from the 2.96×10^5 cells, which was less than the 23.1 ng from 1.48×10^5 MCF7 cells. Evidently, the cell number and the amount of ribosomal RNA (18S and 28S) are not correlated as indicated by the peak height variations in Figure 3.11. According to previous studies, random fluctuations of ribosomal RNA are not uncommon (83). However, the RIN is the criterion used here to evaluate solid-phase

extraction and RNA quality on our disc. Based on qualitative analysis of the rRNA, we conclude that the purified RNA has preserved high integrity after on-disc purification with the solvent-specific router.

Further analysis indicates that the quantity of recovered small RNAs is proportional to the number of cells in a starting sample. From the integrated area of the peaks with migration time between 24 and 28 s, the small RNA fraction was quantified for four different cell concentrations. We focused on this region as many potential biomarkers have been identified as small RNAs. Figure 3.11b compares the purified small RNA concentrations to cell content.

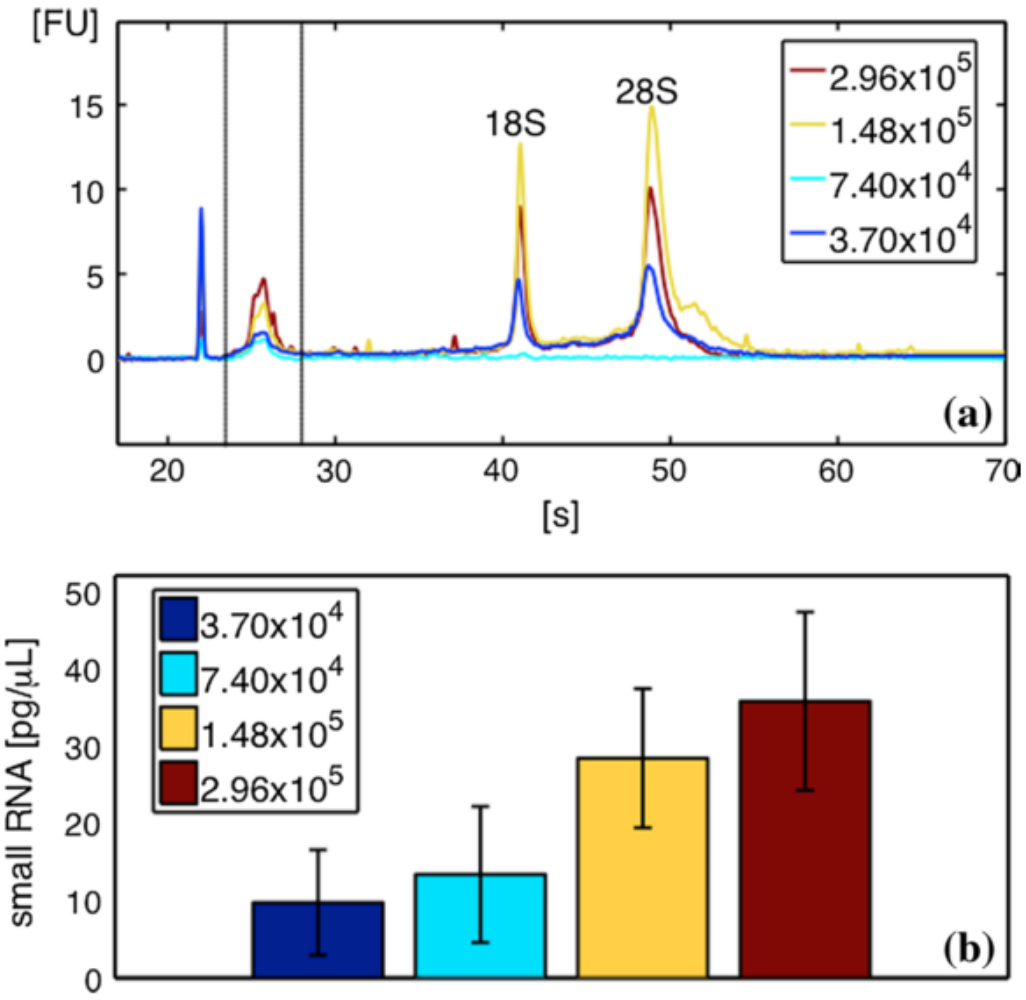

Figure 3.11: Electropherogram of the total RNA purified on-disc from four different aliquots of MCF7 cells. a) Vertical lines between 24 and 28 s designate the region of small RNA (size range 30–200 nt). B) Mean values and standard deviations from triplicate samples containing (red) 2.96×10^5, (yellow) 1.48×10^5, (light blue) 7.4×10^4, (blue) 3.7×10^4 of MCF7 cells.

In spite of the significant loss of RNA, the results suggest that our platform is applicable for small RNA purification.

3.6 Automated Solvent-Selective Routing

Building on the full router system, an advanced design was developed that allowed for the fully automated RNA purification. The system built on the work of Kinahan *et al.* who established an event-triggered valving scheme which utilized the dissolvable films. This led to a system whereby the release of reagents from a chamber is triggered by the dissolution of a film in a previous chamber (27). This system is run at a constant angular velocity. We extended the functionality of the even-triggered release by adding a secondary control mechanism, variation of angular velocity (Fig. 3.12).

This work was preformed predominantly by Dr. Nikolay Dimov with assistance from the author and was published as a conference manuscript (84).

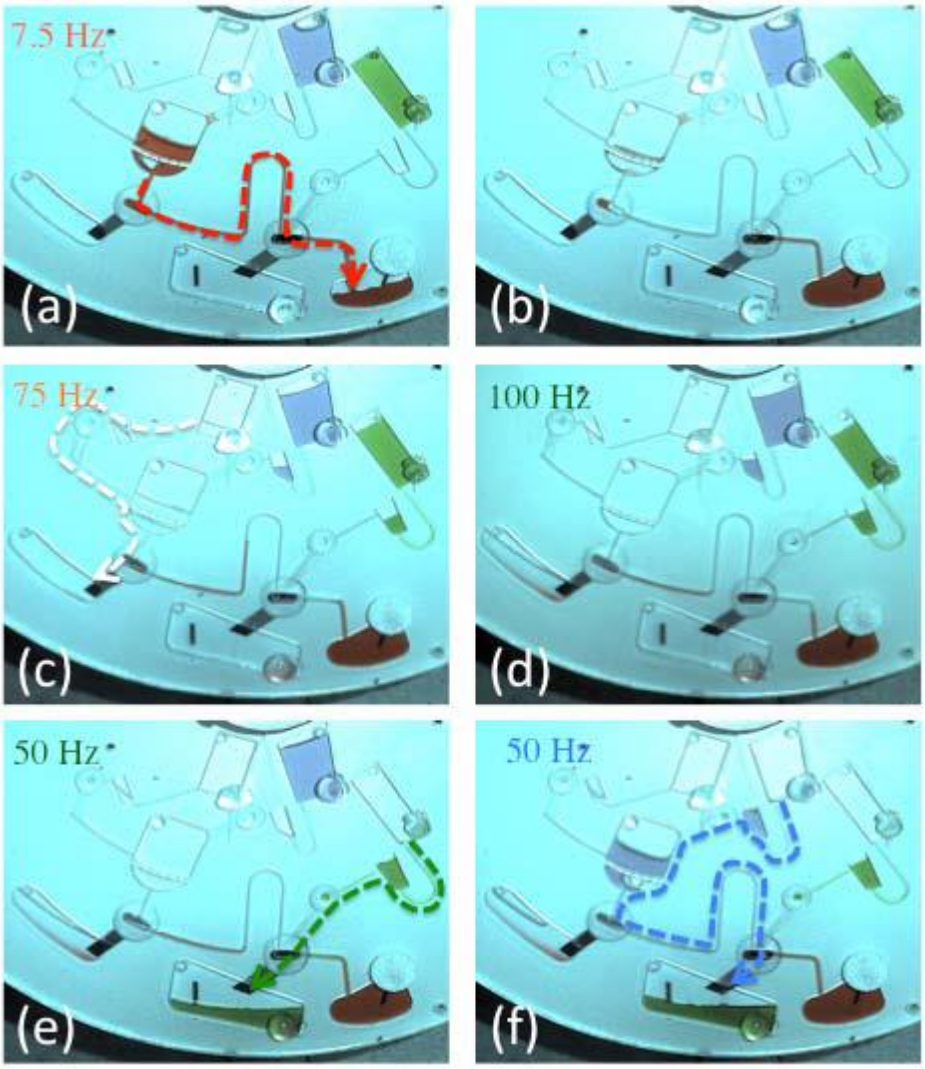

Figure 3.12: Fluidic operation of automated solvent selective router. All samples were initially loaded. The dashed lines show the path of the fluid flow. a, b) The aqueous phase (red) is directed to the aqueous waste chamber while the RNA remains on the glass beads in the loading chamber. c) An EtOH wash is released over the beads and directed to the organic waste chamber through the HMV. d) The spin frequency of the disc is increased actuating a primer solution (white) which is routed to the elution chamber through the DFV. e) This solution dissolves the valve within the chamber and triggers the release of the elution buffer. f) Aqueous elution phase (blue) re-suspends the RNA and mixes with the primer solution in the elution chamber. This sample can then be removed from the disc for analysis and detection. (84)

3.7 Conclusions

In summary, a novel centrifugal flow control method was developed which integrated two solvent specific membranes: the HM and DF. A simple router system was expanded upon to develop a full router which was capable of handling the four stage SPP protocol for RNA. We then purified total RNA with significant integrity and concentration. Finally an automated event-triggered system was developed.

Chapter 4

Characterisation of Graphene Oxide Membrane Properties for Advanced Microfluidic Flow Control

4.1 General Introduction

Since its discovery in 2004 (85), a wide spectrum of fascinating characteristics of graphene and its compounds, such as the here considered graphene oxide (GO), have been extensively investigated by the scientific community. In recent years, microfluidic systems have been used to characterise the distinctive properties of graphene, such as its electrochemical responses (86). Ang *et al.* used a graphene transistor array in a microfluidic chip for the detection of malaria-infected red

blood cells (87). Lo *et al.* included glycidyl methacrylate functionalized graphene oxide within a hydrogel which showed a significant increase in size change when exposed to infrared radiation (88).

However, while being explored by a broad scientific community, the wide spectrum of the often unique properties of graphene has so far not been implemented for microfluidic flow control; this is presumably due to the fact that it does not bind well to polymer surfaces. To leverage our experiments, we first developed a scheme for the integration of GO membranes in common, polymeric microfluidic devices.

A multitude of methods for graphene membrane fabrication have been developed with varying time scales and levels of repeatability. The first method used by Novoselov *et al.* was the scotch tape method, whereby layer upon layer of graphite was mechanically exfoliated away until a single layer (one atom thick) of graphene was achieved (85). Other methods include Chemical Vapour Deposition (CVD). This method allows for very pure graphene substrates to be made but it is a costly and lengthy process.

The properties of such integrated GO membranes are anticipated to enable a multitude of applications and advanced flow control. We demonstrate two such properties of the GO membranes: their solvent selectivity and air impermeability (Fig. 4.1). Beyond a specific burst pressure, GO membranes allow water to pass through at very low flow resistance; however, it completely blocks the organic solutions IPA and

EtOH, oil solutions and air, even at high pressure heads. Nair *et al.* postulated that due to the spacing between the flakes in the multilayer, stacked membrane being comparable to a monolayer of water (≈ 5 Å), this allows the spacing between the GO flakes to act as nanocapillaries which allow low friction flow of a monolayer of water (89).

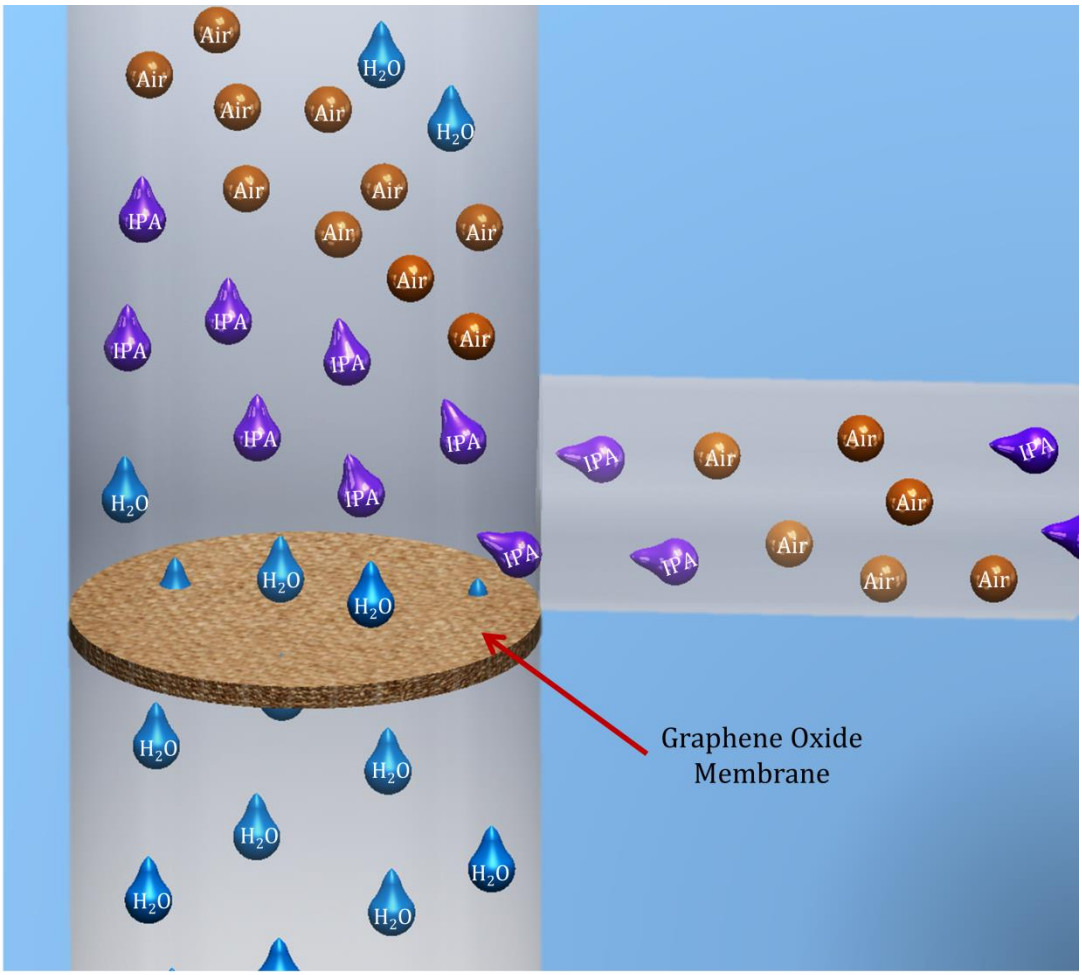

Figure 4.1: Illustration of the unique properties of GO. The GO membrane is entirely permeable to water (blue), but it completely blocks air (orange) and organic solutions (IPA and EtOH) (purple).

The various capabilities of GO membranes were investigated and these unique features were employed to show, for the first time, graphene-oxide enabled advanced centrifugal flow control.

4.2 Graphene Oxide Tab Fabrication

The membranes were synthesized from a suspension of GO flakes in water (Bluestone, Manchester, UK). The suspension was first compressed by vacuum filtration (Fig. 4.2) through a 0.45-μm pore size cellulose filter (Millipore, Cork, Ireland). As they fill the pores of the cellulose, the flakes form a multilayer structure across the entire filter surface.

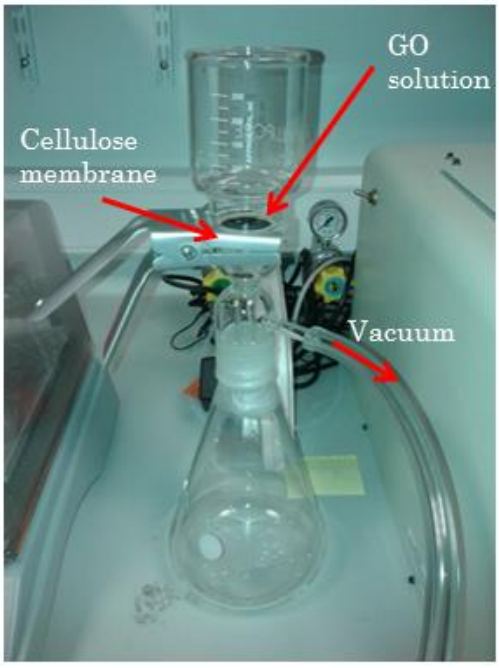

Figure 4.2: Vacuum filtration set-up. GO flake solution is water is filtered through a clamped cellulose membrane under vacuum.

This process eventually created a free-standing, 35-mm diameter GO-filter hybrid, whose diameter was defined by the vacuum filtration apparatus. The thickness of the membranes is governed by the volume and concentration of the GO flakes in suspension. The process time ranges from four to eight hours, depending on the volume being filtered (Fig. 4.3a).

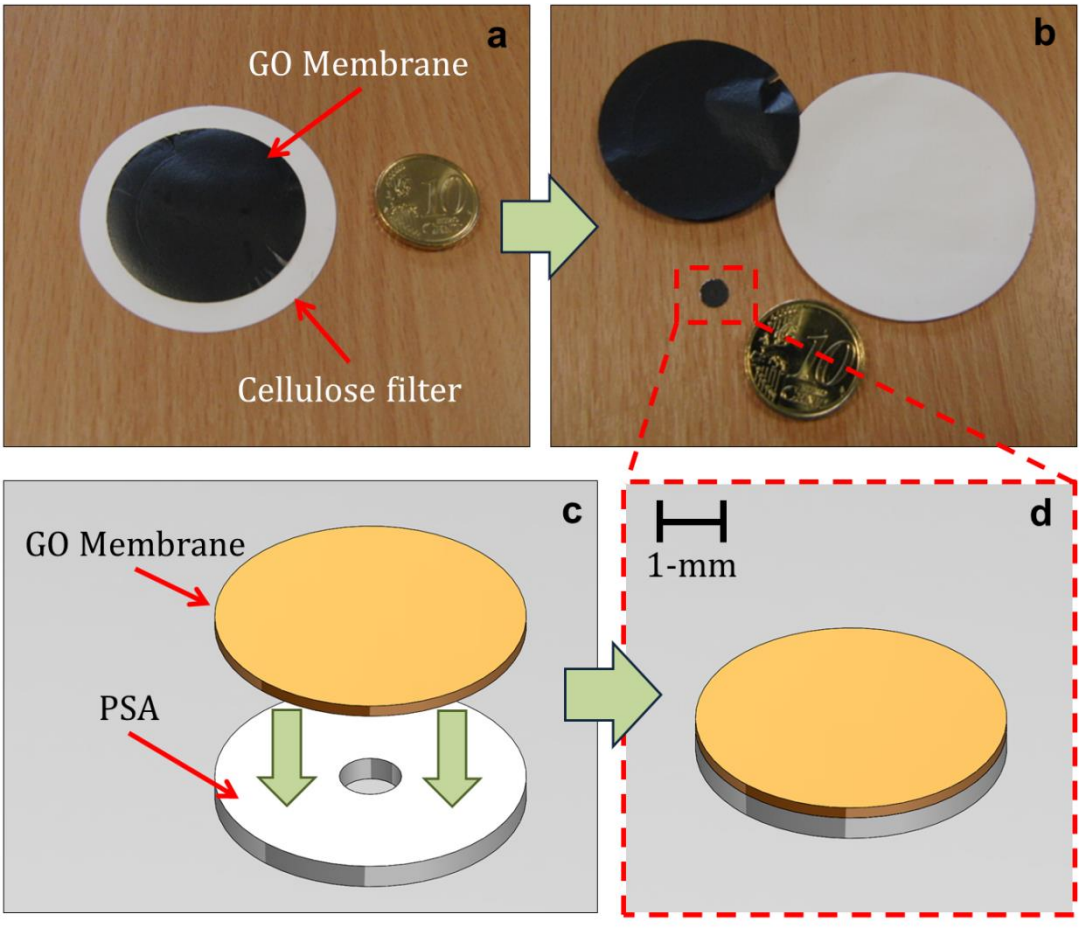

Figure 4.3: GO tab assembly and characterisation. a) Image of GO membrane and cellulose filter after vacuum filtration. b) Free standing membrane removed from filter after drying and a GO tab after fabrication. c, d) Assembly of GO tab. GO membrane is adhered to double-sided PSA with 1-mm through-hole cut out.

Once filtration was completed, the membranes were removed from the vacuum filtration set-up and left to dry for approximately four hours. During this time the membranes remained in contact with the cellulose filters. The completion of this drying step was crucial as prior handling of the membranes could lead to tearing. The membrane could then be peeled from the cellulose filters and be handled with ease (Fig. 4.3b).

In order to incorporate the GO into a microfluidic device a method for attaching the membrane to the polymer surface had to be devised. Once again, using a method first shown by Gorkin *et al.*, the membrane was adhered to double-sided Pressure Sensitive Adhesive (PSA), which featured a small, 1-mm diameter through hole. The contours and size of the GO and PSA tab was then flexibly defined using a precision knife cutter (Section 2.1.2.3). Next, the GO tab was integrated in a microfluidic system using the 'sticky' PSA backing (Fig. 4.3c, d).

4.2.1 Measuring the Thickness of a GO Tab

In order to evaluate the variation in thickness of the GO membranes a method for measuring that thickness had to be devised. Qualitatively, it could be determined that filtering a more concentrated volume of GO in water would result in a thicker tab, by the colour shift from a bronze to dark brown colour, but it was unclear how much

variation in thickness would be achieved. A number of methods for measuring the thickness were attempted, with varying levels of success.

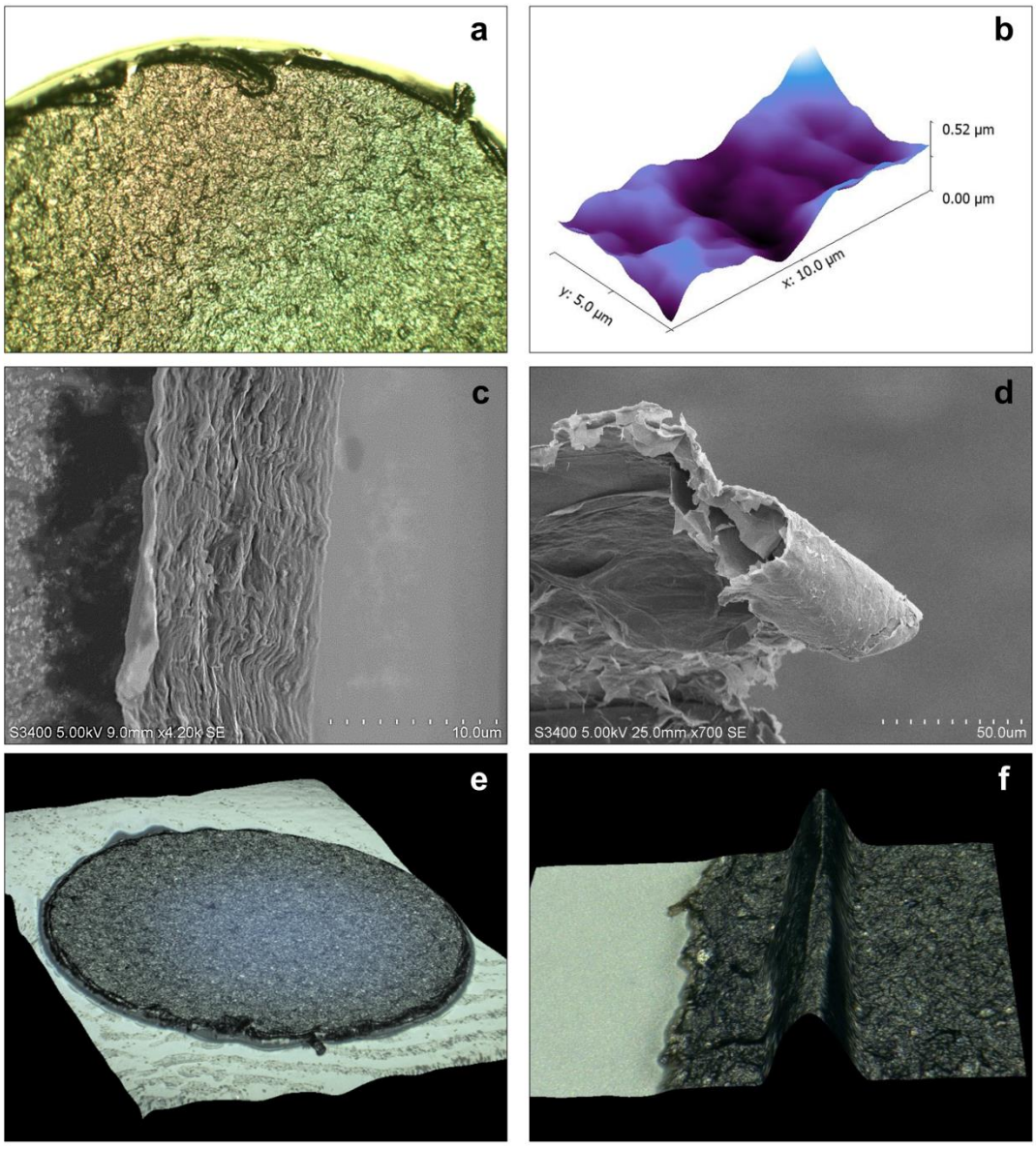

Figure 4.4: Various methods for determining membrane thickness and variation across the surface. a) Optical microscope image showing tab edge. b) AFM of small area of tab surface showing localised variation. c) SEM image of cross-section of GO tab showing a membrane thickness of ~ 10 µm. d) SEM image of 'curling' effect of slicing the membrane. e) 3D microscope image of entire tab. f) 3D microscope image of ridge encountered at edge of membrane.

First an optical microscope was used to view the GO after being cut by the precision knife cutter (Fig. 4.4a). From this the relative clean cut of the tab edge could be observed, as could the full coverage of the GO flakes across the tab surface. This did not however give any useful information about the thickness of the tab or the variations with the membrane surface.

Atomic Force Microscopy (AFM) (Dimension 3100, Bruker), which could give topographical information about the surface, was investigated next (Fig. 4.4b). This gave very accurate information of the thickness variance in a very small area (5.0 x 10.0 μm = 50 μm^2) but the through-hole of the GO tab has a 1-mm diameter giving a surface area of ~7.85 x 10^5 μm^2. This was far too large a surface area to image with AFM in any reasonable time frame.

Scanning Electron Microscopy (SEM) was used next. A section of GO tab was sliced using a blade in order to get a cross-sectional image. The membrane was then clamped between two pieces of copper to give it rigidity. This entire structure was then coated in a few layers of gold using a sputter coater. Figure 4.3c shows an SEM image of a cross section of a GO membrane clearly displaying the multilayer stacked structure. This membrane possesses a thickness of approximately 10-μm. From this, the even distribution of the flakes can be observed. This method for measuring the thickness worked well enough, however an issue often occurred during the processes. The slicing of the GO tab, in

order to get a cross-section, would often cause the flakes at the edge to curl in on themselves (Fig. 4.4d). This made it difficult to determine the thickness of that tab.

Finally, a 3D-Microscope (Section 2.4.1.1) was used. This set-up proved to be the most useful, as it was capable of taking a 3-dimensional image of the tab surface and, depending on the magnification, measuring the variation in depth across the surface. The tab was struck to a solid surface and a depth up image was taken. Figure 4.4e shows a 3D image of the entire tab structure. Using the in-built measurement capabilities of the Keyence software it was determined that the tab could have a variation of approximately ± 10 μm across the surface. If a tab was cut from the edge of a filtered membrane (Fig. 4.3a) there would be a ridge of approximately 100 μm high (Fig. 4.4f). This showed that only tabs cut from the centre of the filtered membrane should be used in order to avoid huge variations in thickness. The 3D microscope proved to be the most useful of the measurement techniques as it gave the most information about the entire surface of the tab.

4.3 Investigation of GO Properties

Three distinct properties of the GO were investigated: its air impermeability, solvent selectivity and wetting capabilities. These properties were tested over a given pressure range on three centrifugal microfluidic discs.

4.3.1 Air Impermeability

Figure 4.5 shows the design for testing the impermeability of the GO tabs to air. This disc consisted of three layers of PMMA and two layers of PSA. The discs contained four identical structures; each of them featured a loading chamber and two symmetric side arms which were connected via a common inlet channel. Both side arms exhibited a hole at the top which had been sealed by either a PSA or GO tab. For the sake of clarity in these tests, coloured food-dye in water was used, though the fluid would not make direct contact with the tabs.

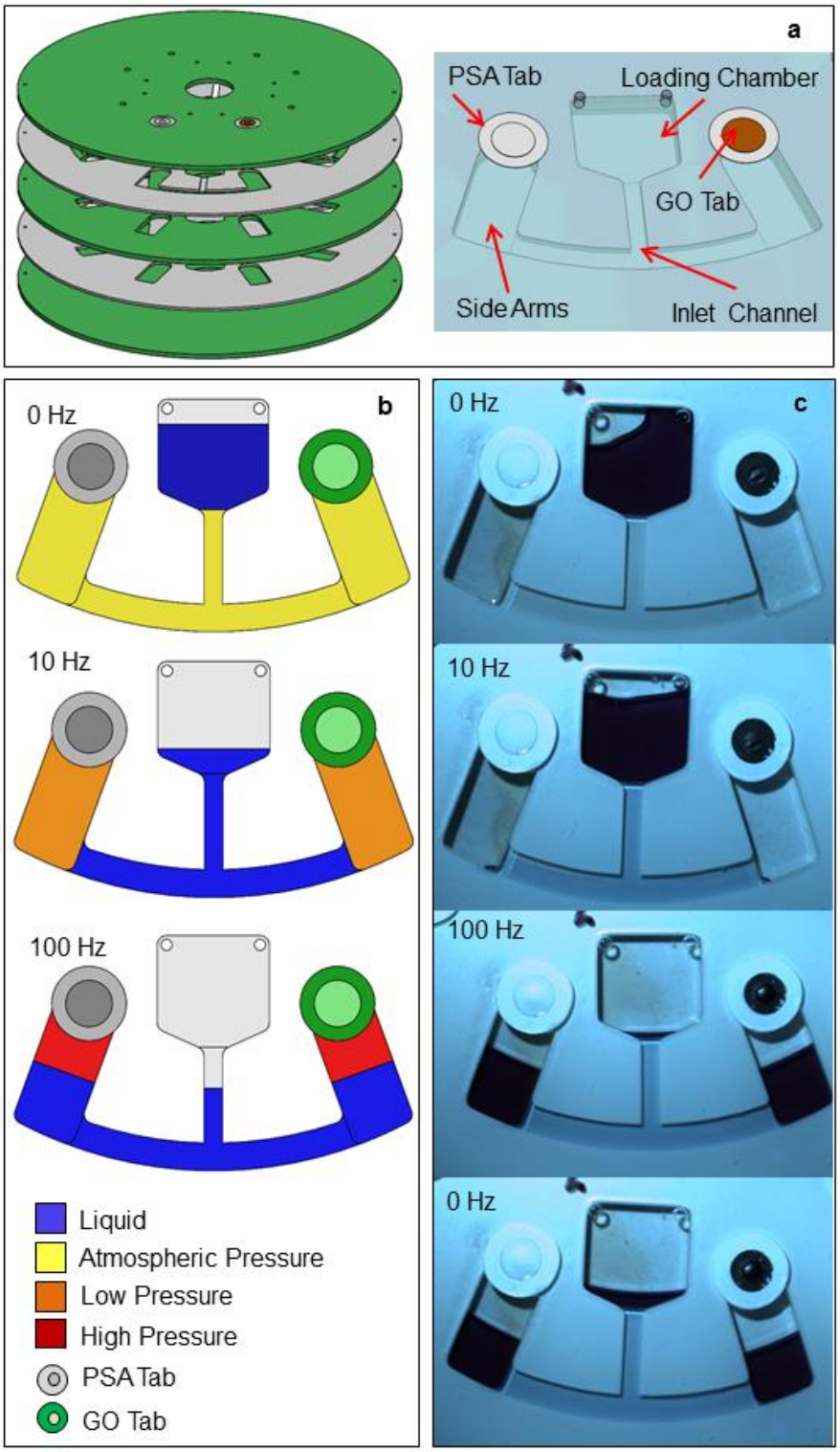

Figure 4.5: Design for measuring GO impermeability to air. The left and right arms are sealed by PSA and GO tabs, respectively. a) Operation under various air pressures. b) Image sequence showing that even at high centrifugally induced pressure-heads, hydrostatic equilibrium is maintained to demonstrate the impermeability of the GO membrane to air (as well as the integrity of the membrane and its seal with the disc substrate).

A 180-μL volume was added to the loading chamber. This fluid trapped and hence enclosed the air inside the inlet channel and side arms. With the increase of the rotationally induced centrifugal field, fluid extends down the inlet channel to compress the air in the side arms. The fluid reached the interface between the channel and side arm at a rotational frequency of 10 Hz. As the disc was spun faster up to a rotational frequency of 100 Hz, the fluid reached the side arms and continued to rise (Fig. 4.5a). Figure 4.5b shows that there was no discernible difference of the fluid levels in both side arms at the upper spin frequency, thereby proving the air-impermeability and pressure-tightness of GO tab.

Another interesting feature is the rather high, rotationally induced pressures,

$$\Delta p_{\omega} = \rho \Delta r \overline{r} \omega^2 \qquad \text{(eqn. 4.1)}$$

where $\Delta p_{\omega}$is the burst pressure in Pascals, ρ is the density of the fluid, Δr is the length of the fluid plug, $\overline{r}$ is the distance of the tab from the centre of rotation and ω is the angular frequency, that the tabs can withstand.

Upon loading, the fluid seals the air inside the channel and arms essentially under atmospheric pressure. As the spin frequency was increased to 10 Hz, the air pocket sealed by the GO tab was compressed to approximately 25 mbar (obtained using Boyle's Law). Finally, at 100 Hz, there was a significant increase in pressure of approximately

750 mbar. This verifies the sufficient mechanical strength of the integrated GO membranes. This can be observed in Figure 4.5b where the GO tab bends without disruption.

4.3.2 Solvent Selectivity

Figure 4.6 describes the disc used to test the solvent selectivity of the GO. The disc was made up of four layers of PMMA (green) and four layers of PSA (grey). It contained ten identical structures. Each structure consisted of a 3D architecture containing a Loading Chamber with a 1-mm hole at the base of the chamber. This vertical via is connected to a channel on the bottom layer of the disc. The hole was sealed by one of the GO tabs. The channel then connected to a Collection Chamber (Fig. 4.6b).

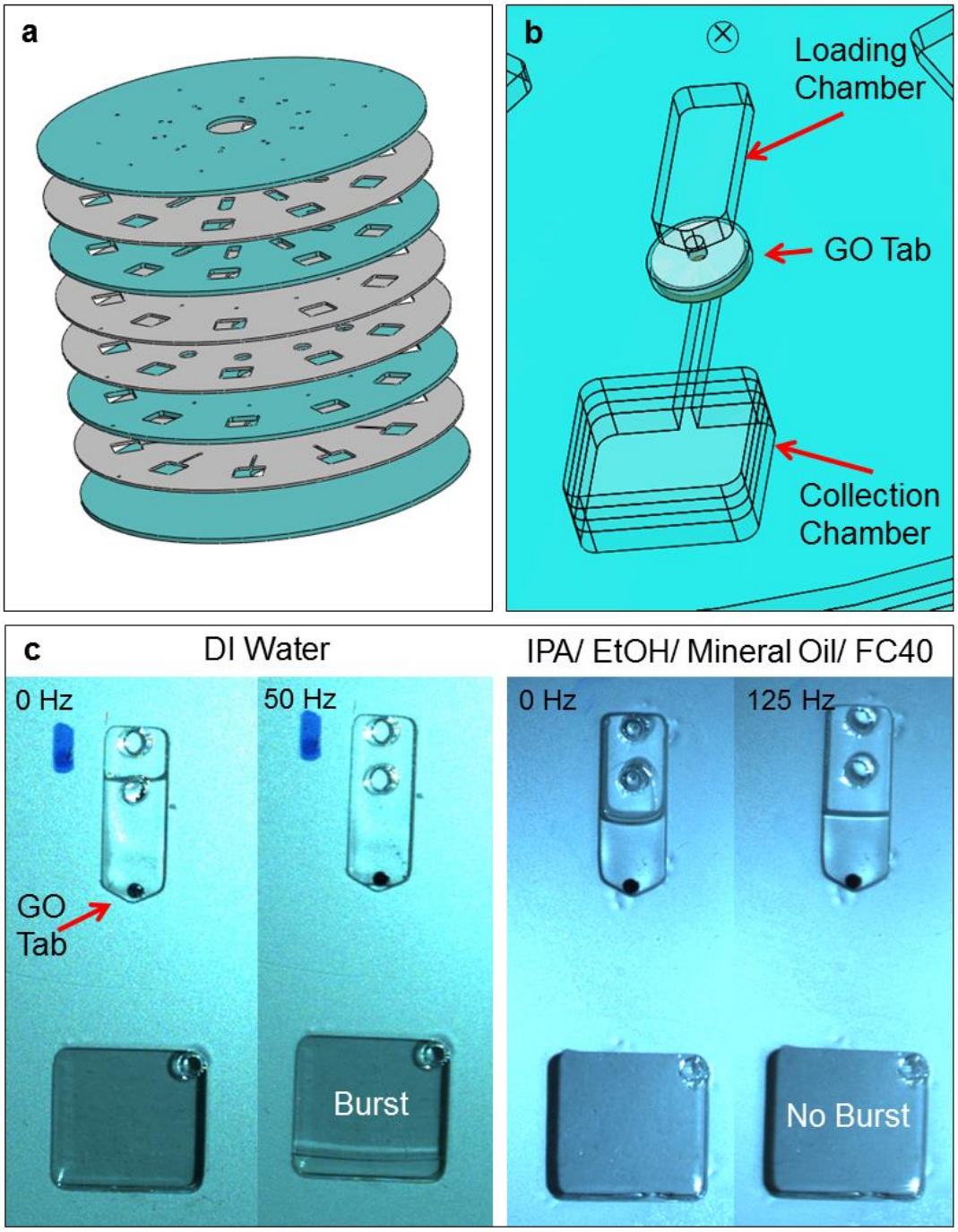

Figure 4.6: Design for testing the solvent selectivity of the GO. a) Multi-layer disc structure, with PMMA (green) and PSA (grey) layers. b) 3-dimensional architecture connecting loading chamber to collection chamber via a through-hole, sealed by a GO tab. c) Solvent selectivity of GO. DI water passes through at 50 Hz while the membrane is impermeable for the organic solvents IPA and EtOH, even at the much higher spin frequency of 125 Hz.

In order to test the solvent selective properties of the GO, three fluids were added to the chambers: deionized (DI) water, 2-propanol (IPA) and ethanol (EtOH). A 50-μL volume was added to the Loading Chamber. Under centrifugation the fluid generated a hydrostatic pressure head acting on the GO tab. The rotational frequency was increased at regular intervals until the membrane yielded. In the case of DI water the plug passed through the GO at approximately 50 Hz, or 8 mbar (Fig. 4.6c). Notably, once the 'burst' pressure was exceeded, the water penetrated with very low flow resistance. In contrast, the organic solutions IPA and EtOH were fully retained in the Loading Chamber, even at the highest spin frequency of 125 Hz, or 49 mbar, that we could implement on our test stand.

This simple test demonstrates the complete impermeability of the GO membrane to these organic solutions while offering very little flow resistance to water above a certain pressure threshold. Further experiments, using the structure shown in Fig. 4.6, gave evidence that the GO is also impermeable to oil solutions; both Fluorinert FC40 and mineral oil where incapable of passing through the GO tab even at the highest spin frequency of 125 Hz.

It should be noted that the tabs are single use. If a solution is flowed through the membrane it becomes mechanically weak and is no longer resistant to air or organic solutions.

4.3.3 GO Wetting Capabilities

Figure 4.7 shows the design used to test the wetting capability of the GO membrane. The objective was to test if wetting the underside of the GO membrane would change its permeability to air. To test this, a GO tab was stuck to the underside of a pneumatic chamber. The underside of the GO tab could be wetted by an ancillary actuation fluid.

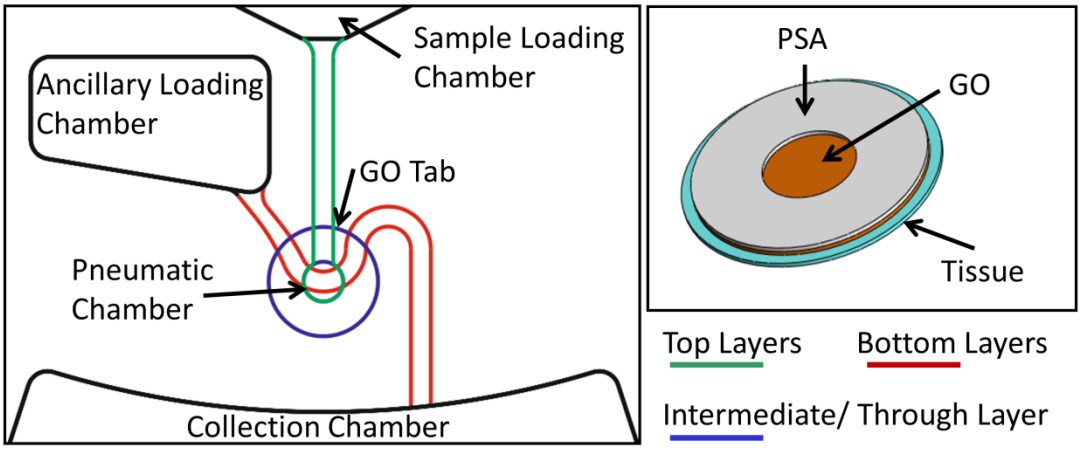

Figure 4.7: Design for testing the GO wetting capability. Colours indicate the position of the channels in the multilayer structure.

The design consisted of three layers of PMMA and three layers of PSA. Each of the four identical structures per disc consisted of a sample loading chamber connected by a channel to a small pneumatic chamber. The pneumatic chamber was sealed by a GO membrane, making the chamber air-tight. An ancillary loading chamber was connected via a channel on the lower levels of the disc to a collection chamber. This lower channel was used to flow the ancillary fluid past the GO

membrane. A thin cellulose 'tissue' was placed as a backing material to the GO membrane (Fig. 4.7b). The tissue acts as a sponge, keeping the ancillary fluid in contact with the GO and ensuring good wetting. To further enhance the wetting a small crest was placed in the channel after the tab position to increase the contact time of the GO tab with the fluid.

To determine if wetting one side of the tab would affect the air impermeability of GO membrane a coloured water sample was loaded into the sample loading chamber and water was loaded into the ancillary loading chamber. The disc was spun at a low frequency (10 Hz). Due to the radially increased position of the ancillary loading chamber the fluid in that chamber flowed first. The frequency was maintained at this level until the ancillary fluid had completely emptied to the collection chamber. The frequency was then increased at regular intervals until the coloured sample moved down the loading channel, where it compresses the air in the pneumatic chamber. As the disc was spun faster the pressure on the pneumatic chamber increased until a burst frequency, where the fluid begins to enter the pneumatic chamber, was reached. The frequency, at which the first drops of fluid enter the chamber, was recorded. The spin frequency was then increased at regular intervals again until complete inversion of the air and fluid occurred and the fluid flowed through the membrane to the collection chamber. The frequency that this occurs at was also recorded. The

results of the first drops and GO burst, for wetting and no wetting of the tab, were compared. The results are shown in Figure 4.8.

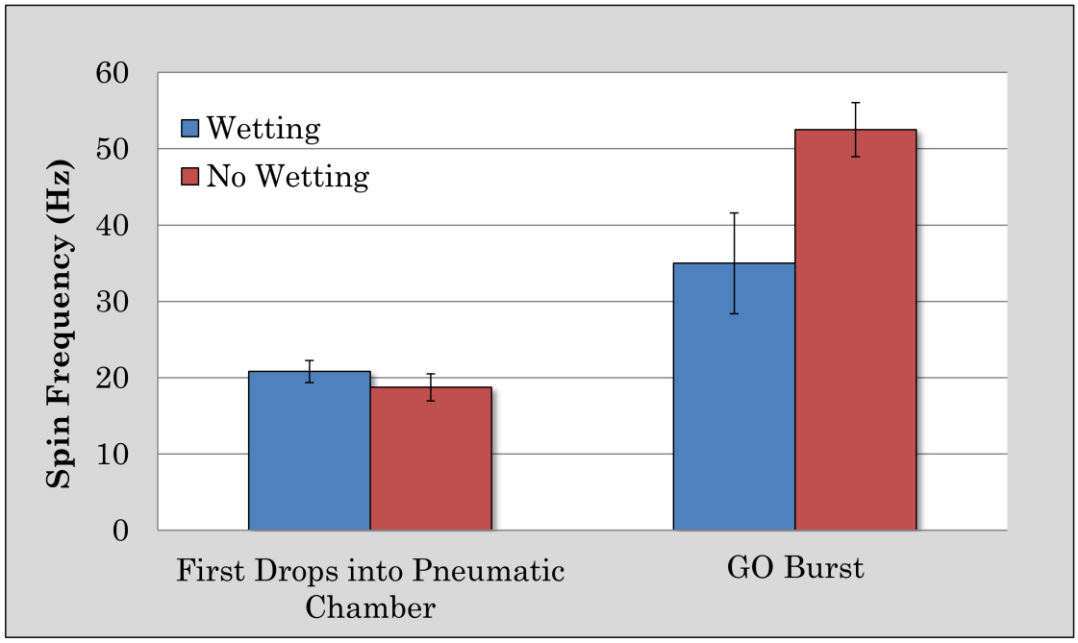

Figure 4.8: Effect of wetting GO tab on its air impermeability and mechanical strength. The data shows that the wetting the tab does not make it more permeable to air but does appear to decrease the strength of the membrane making it burst at a lower frequency.

The results show that wetting the GO membrane has little to no effect on the air impermeability of the membrane. The first drops entered the pneumatic chamber at the same frequency regardless of whether the tab had been wetted or not. This shows that there was no reduction in air pressure within the chamber; if the membrane had become permeable to air then the first drops would have occurred at a lower frequency. An interesting point though is that wetting the GO tab

appears to have weakened it somewhat mechanically so that the fluid would flow through the membrane at a lower frequency (and therefore pressure) than its un-wetted counterpart.

This experiment showed us that the GO tab could be placed within a structure where it is wetted and will maintain its air impermeability but will reduce its burst frequency.

4.3.4 Characterisation of GO Tabs

Using the structure shown in Figure 4.6, the capabilities of the solvent selective nature of the GO tabs were investigated. First, as the membranes had been shown to be permeable to water but completely impermeable to IPA, water and IPA mixtures were also tested. Solutions with varying water concentration in IPA were flowed through the GO tabs, up until the water concentration at which a burst could no longer be achieved. The tab used in these experiments was approximately 10-μm thick. The spin frequency was recorded and, using the geometry of the disc, the burst pressures were calculated using Equation 4.1. Each test was repeated five times per water concentration.

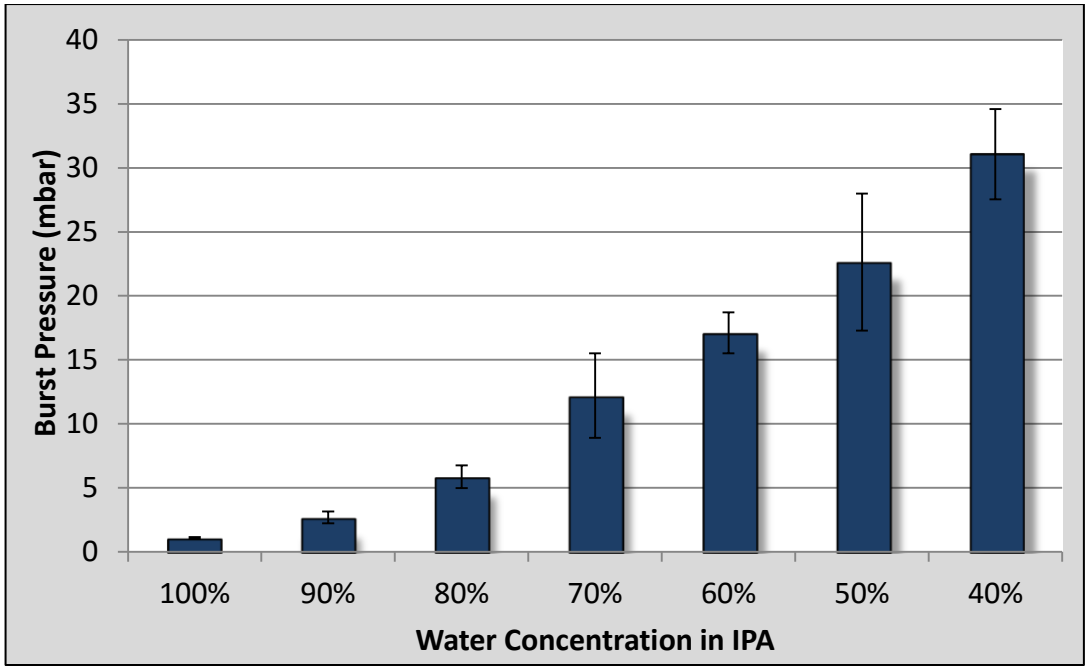

Figure 4.9: Change in burst pressure required for the passage of fluid with varying water concentrations in IPA. The data shows an inverse relationship between the water concentration in the solution and burst pressure require for flow. Data points are mean ± 1 standard deviation, n=5.

The burst pressure required for flow increases with reduction of the water content (Fig. 4.9). It was also determined that any solution with a concentration below 40% water was incapable of passing through the GO tab, even at the highest spin frequency we could realise for safety reasons.

The second experiment revealed the correlation between the thickness of the GO membrane and the burst pressure for water. The variation in the tab thickness was achieved by filtering different concentrations of GO flakes (Fig. 4.3). In this case four different membrane thicknesses were used with approximate thicknesses of 27 µm, 35 µm, 38 µm and 44 µm. The thickness of the GO membrane

was then measured using a 3-D Microscope (Section 2.4.1.1). For this experiment, a 100% DI water solution was used and once again the burst frequency required for flow was recorded and converted to burst pressure using Equation 4.1. According to Figure 4.10, the burst pressure rises with the thickness of the membrane.

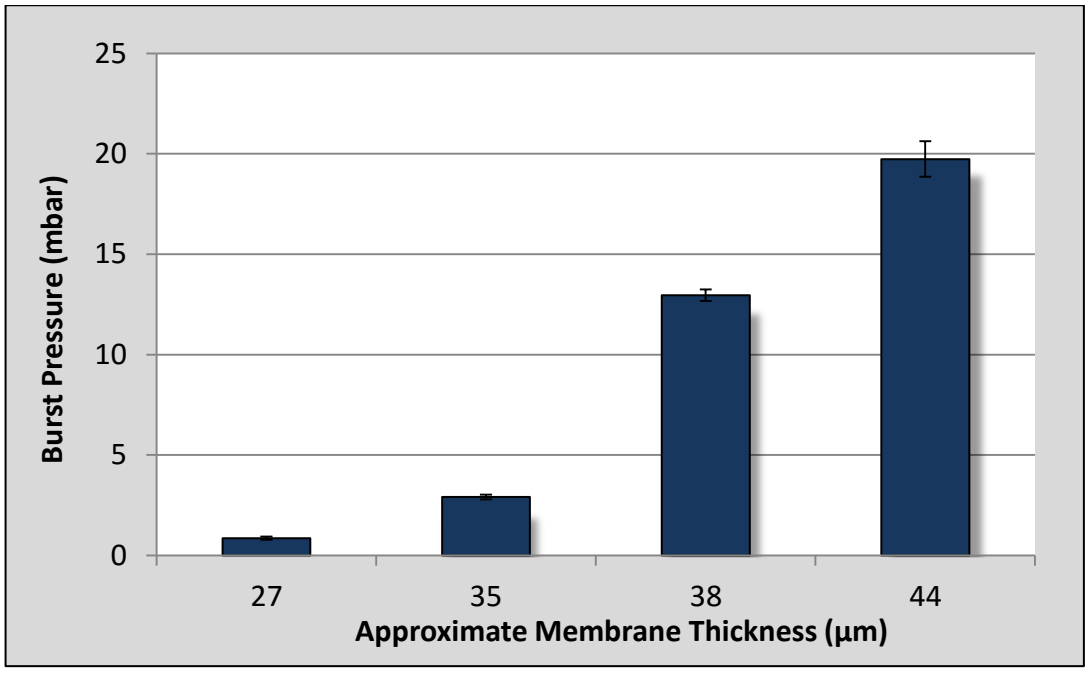

Figure 4.10: Change in burst pressure required for the passage of 100% water with varying membrane thicknesses. The data shows an inverse relationship between the thickness of the membrane and burst pressure require for flow. Data points are mean ± 1 standard deviation, n = 5.

These two experiments elucidate the dynamic range of capabilities of the GO tabs. By varying their thickness, the tabs can be tailored to work for multitude of designs within a centrifugal system.

4.4 Conclusions

A new method for the integration of a GO tab within a polymeric microfluidic structure was shown. Using centrifugal flow control, various unique features of GO, notably its solvent selectivity and air impermeability were investigated. This membrane is completely impenetrable to the organic solutions IPA and EtOH, as well as mineral oil and FC40, but yields at moderate spin rates to an aqueous phase. The solvent selectiveness of the membrane makes it an ideal material for robust automation of nucleic acid purification protocols on centrifugal LoaD platforms.

Chapter 5

Graphene Oxide Enabled Centrifugo-Pneumatic Routing of Flows for Nucleic Acid Purification

5.1 General Introduction

As previously discussed centrifugal microfluidic platforms can offer significant benefits for nucleic acid testing. In particular the highly-labour intensive process of nucleic acid purification could be incorporated and integrated into these systems. The solvent-selective router described in Chapter Three took significant strides towards this goal. The integration of the DF and HM valves opened up new avenues for fluidic flow control methods.

In order to allow for more condensed handling of fluids, new and more dynamic materials can offer diverse benefits for flow control. The work described in Chapter Four showed that Graphene Oxide (GO) displays unique properties, notably its solvent selectivity and air impermeability. Beyond a certain threshold burst pressure, GO membranes allow aqueous solutions to pass with very little flow resistance but are completely resistant to organic solutions and air. This holds true even at significantly high pressure heads.

The unique properties of the GO made it an excellent material to harness for performing on-disc nucleic acid solid phase purification (SPP) (48). As shown in Section 3.1, in this a sequence of different fluids some aqueous and some organic are passed through a single chamber which contains some solid phase, e.g. glass beads. Yet, each of these fluids must be routed away from the final collection chamber so as not to contaminate the sample for detection.

This chapter describes the design and testing of a centrifugal microfluidic disc which uses a centrifugo-pneumatic router and harnesses the unique properties of GO membranes for advanced flow control and uses it to perform on-board DNA purification.

5.2 System Design

5.2.1 Evolution from First Design

Figure 5.1 shows the evolution of the design of the centrifugo-pneumatic router which incorporates a GO tab for the solvent selective routing of aqueous and organic flows. There were a number of iterations, but the main three steps are shown here.

Initially, the design consisted of a loading chamber, connected by a channel to an air-tight pneumatic chamber. A siphon channel connected this to a waste chamber. The siphon was angled to encourage the fluid into the pneumatic chamber. At its base the pneumatic chamber has a hole which connects to a collection chamber by a channel on the bottom layer. This hole is sealed by a GO tab (Fig. 5.1a). This design allowed for the routing of the required fluids however there were some issues with certain aspects of the design. The sharp inclination of the siphon channel made it difficult for the fluid to empty. This made the fluid preferentially travel back up the inlet channel instead of over the siphon to waste. The waste chamber was also made too small and much of the waste fluid would leak out over the course of the spin cycle. This would be undesirable if harmful chemicals or biological samples were to be used.

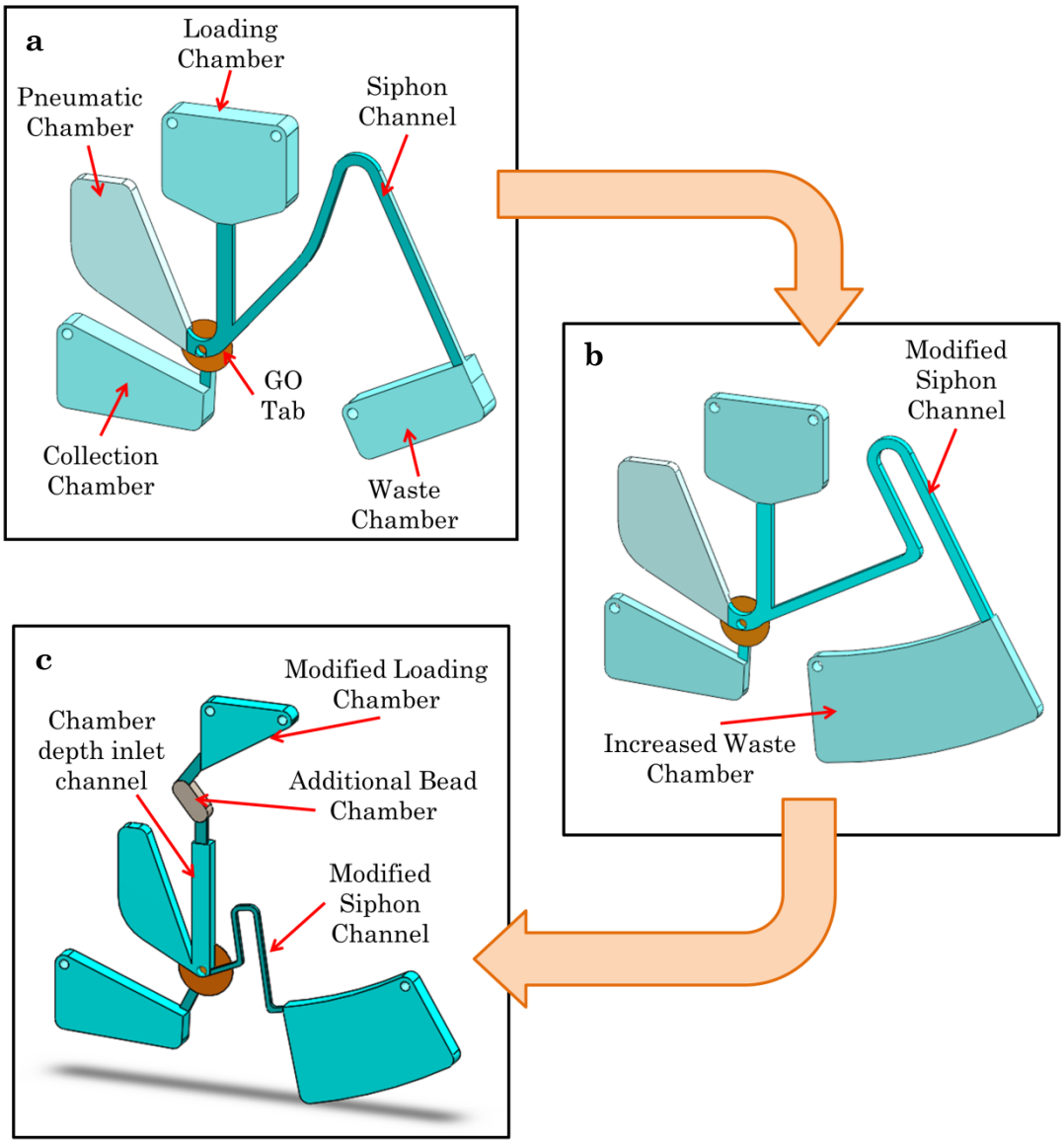

Figure 5.1: Evolution of design of centrifugo-pneumatic router which incorporates a GO router. a) First design iteration with all its functional components. b) Second design iteration showing modified siphon channel and waste chamber. c) Third and final design iteration showing modified loading chamber, inlet channel and siphon channel and addition of a bead chamber.

These issues were attempted to be dealt with for the second iteration (Fig. 5.1b). The angle and shape of the siphon channel was altered and the size of the waste chamber was increased. However, clean emptying was still not reliable. If the fluid did not fill over the siphon

uniformly, a large air bubble would form between the siphon crest and the entrance to the waste chamber. This occurred because of a filling problem when working under a centrifugal field. As the fluid travelled up the channel towards the crest of the siphon the bottom of the meniscus is experiencing a greater centrifugal force than the top. It therefore 'drips' over the edge first, making a pathway for the rest of the fluid to follow (Fig. 5.2a). The fluid then collects at the base of the channel as it encounters a capillary valve in the expansion of the channel into the waste chamber. This meant that there could be some residual fluid left at the base of the pneumatic chamber. This could lead to contamination of the final sample (Fig. 5.2b).

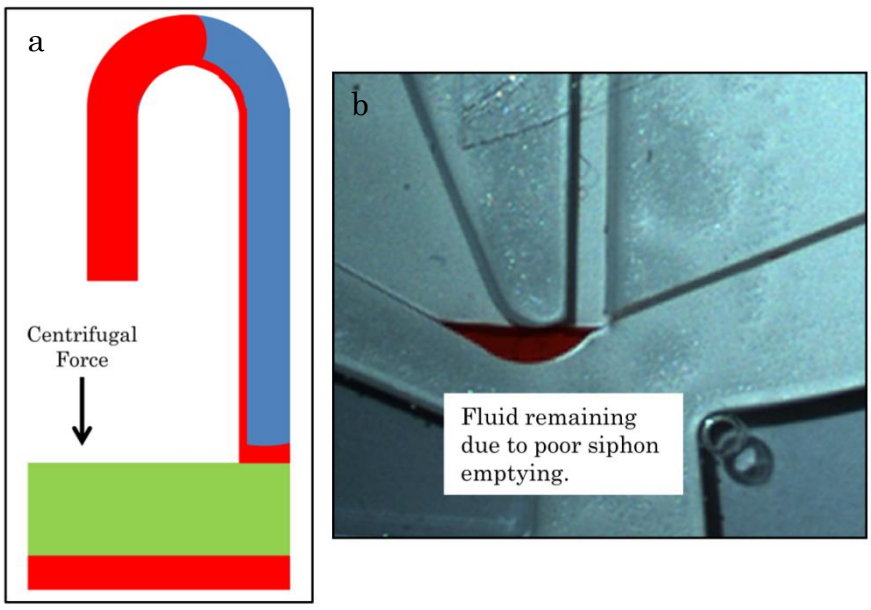

Figure 5.2: Illustration and image of siphon issues. a) The channel (blue) is connected to a chamber (green) which is significantly deeper. The fluid (red) moves over the crest where the bottom of the meniscus travels first and makes a pathway for the fluid to follow and a large air pocket is formed. b) Image of fluid remaining at base of pneumatic chamber due to poor emptying of siphon.

The final working design is shown in Figure 5.1c. Here the most drastic changes were introduced. Firstly, the inlet channel which leads to the pneumatic chamber was made chamber deep, i.e. it was cut to the same depth as the pneumatic chamber. This meant that once the fluid flowed down into this channel there was sufficient space for it not to re-enter the loading chamber. The through hole at the base of the pneumatic chamber was also shifted to be in line with the inlet channel. This meant that the maximum amount of fluid could be collect through the GO membrane during the final step. Next, a bead chamber was added. This was used to house the glass beads for the SPP. The beads had previously been housed in the loading chamber, but this seemed to restrict the flow. The loading chamber shape was modified to encourage all the fluid out of the chamber and through the beads. Finally the siphon was modified to correct the emptying problem. The inlet channel into the siphon was shortened and its height was reduced. Also an '*L*'-shaped bend was placed at the end of the channel at the entrance to the waste chamber to stop the fluid from collecting at the end of the channel. All of these changes lead to our final working design.

5.2.2 Working Principle

Figure 5.3 shows the flow schemes for sequential routing of aqueous and organic solutions. Initially, an aqueous solution is loaded (A). Under rotation, the fluid flows down the channel into the bead

chamber (B). The fluid then flows through the beads and down the inlet channel. The angle and position of the siphon valve directs the fluid into the pneumatic chamber where it traps and compresses the enclosed air pocket (C). The disc is spun below the threshold burst frequency (75 Hz) of the GO tab to maintain the seal of the tab. Upon reduction of the spin rate, the air expands to centripetally pump the aqueous solution back up into the inlet channel. The fluid is now at a level higher than the siphon crest and it flows over the crest point into the waste chamber (D). In a similar way, the organic solution is routed past the unaffected GO membrane through the siphon to the waste (E – H). For the final step, another aqueous solution is loaded. In this case the spin rate is elevated to a spin frequency beyond the threshold burst frequency (75 Hz) of the GO tab (I – K). Therefore, the solution penetrates through the solvent-selective GO membrane into the collection chamber (L).

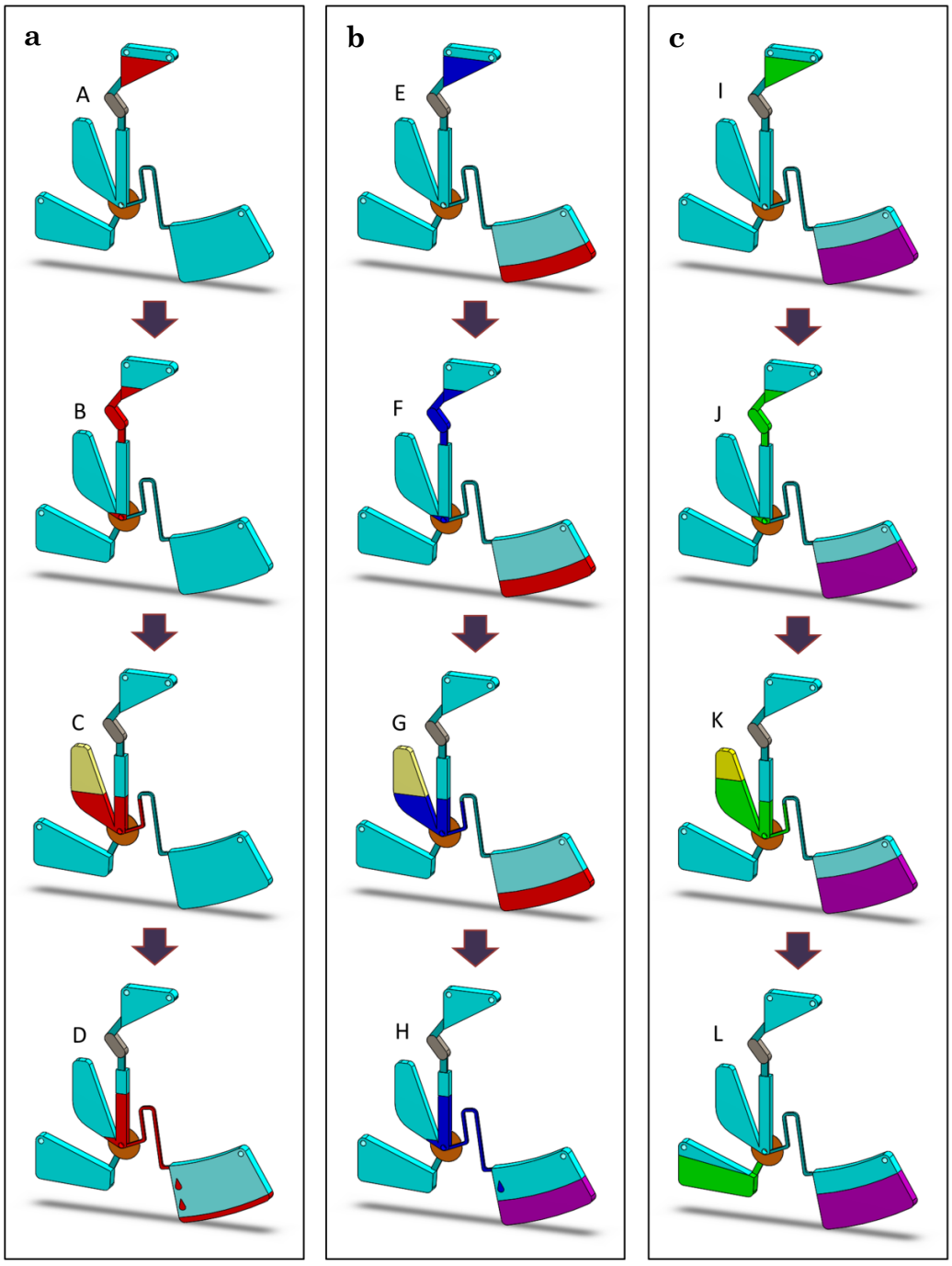

Figure 5.3: Working principle of the GO router. The individual components are labelled in Figure 5.1. (a) At moderate spin rates, water (red) compresses the air in the pneumatic side chamber (yellow). Upon deceleration, the entrapped air expands to pump the fluid over the siphon. (b) The organic solutions IPA / EtOH (blue) follow the same itinerary. (c) In the final step, a second volume of DI water is loaded. Compared to the first fluid, the spin rate is elevated to surpass the burst pressure of the GO tab for water. The fluid is directed into the left collection chamber. Letters (A – L) refer to spin rates shown in Figure 5.5.

5.3 Materials and Methods

5.3.1 Disc Fabrication and Assembly

The disc (Ø 120 mm) consisted of three layers of PMMA and four layers of PSA (Fig. 5.4). The PMMA layers were cut entirely with the laser cutter as described in Section 2.1.2.1 and the PSA layers were cut using the precision knife cutter. The cleaning procedure, as outlined in Section 2.1.3, was observed. The GO tab was fabricated as described in Section 4.2 and was fabricated to a thickness of approximately 45-µm for the fluidic tests (Section 5.4.1) and 35-µm for the biological tests (Section 5.4.2). Prior to assembly (described in Section 2.1.4) the tab was adhered to the underside of the 'Tab Cover PSA' layer, with the 'Tab Supported PSA' layer, giving adequate space to house the tab.

Once assembly of the disc was complete glass beads (diameter ≤ 106-µm) were packed into the 'Bead Chamber' (Fig. 5.1c), to its capacity, through a hole in the top layer of the PMMA. The hole was then sealed.

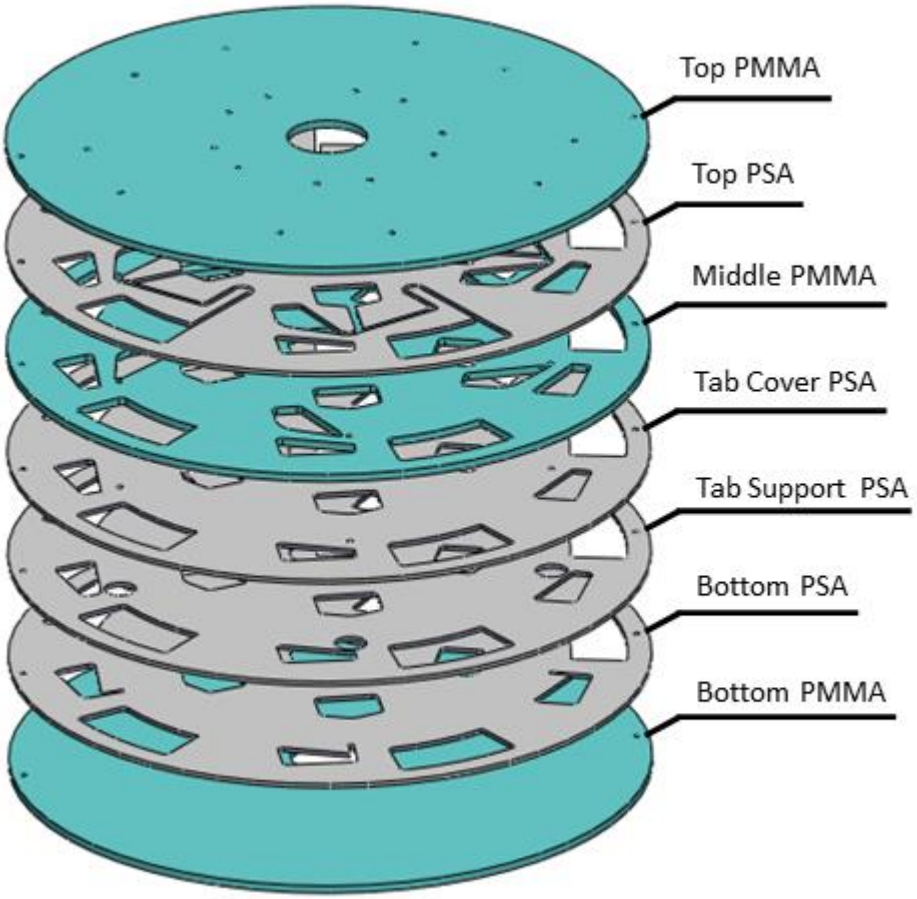

Figure 5.4: Exploded view of disc assembly. The (Ø 120 mm) disc consisted of three layers of PMMA (green) and four layers of PSA (grey). The GO tab was adhered to the underside of the Tab Cover PSA layer.

5.3.2 DNA Preparation

The QiaQuick PCR purification kit (Section 2.2.2) and PicoGreen DNA fluorescence kit (Section 2.4.2.3) were used for the course of these experiments. The lambda DNA standard was taken from the concentrated solution of 100 µg/ml and diluted in 1x TE Buffer to the desired concentration. To test the DNA's interaction with the GO membrane the concentrated solution was diluted to a concentration of 2, 1.5, 1 and 0.5 µg/ml. For validation of the GO router the concentrated

solution was diluted to a concentration of 24 µg/ml. This solution was then split. To measure the pure DNA concentration the 24 µg/ml solution was mixed in a ratio of 1:5 1x TE buffer to bring it to a concentration of 4 µg/ml. For use on the GO router the 24 µg/ml solution was mixed in a ratio of 1:5 Buffer PB. The Qiagen buffers were used on the GO router in order to ensure the correct pH and salt concentrations needed for the DNA to bind to the beads.

For the benchtop spin column test, the standard Qiagen kit protocol was used (Section 2.4.2.3). For the detection 30 µL of dye and sample were used.

5.4 Results and Discussion

5.4.1 Fluidic Operation

Experimental validation was performed in order to determine the optimum spin frequencies required for the operation of the GO router. The final spin frequency profile is shown in Figure 5.5.

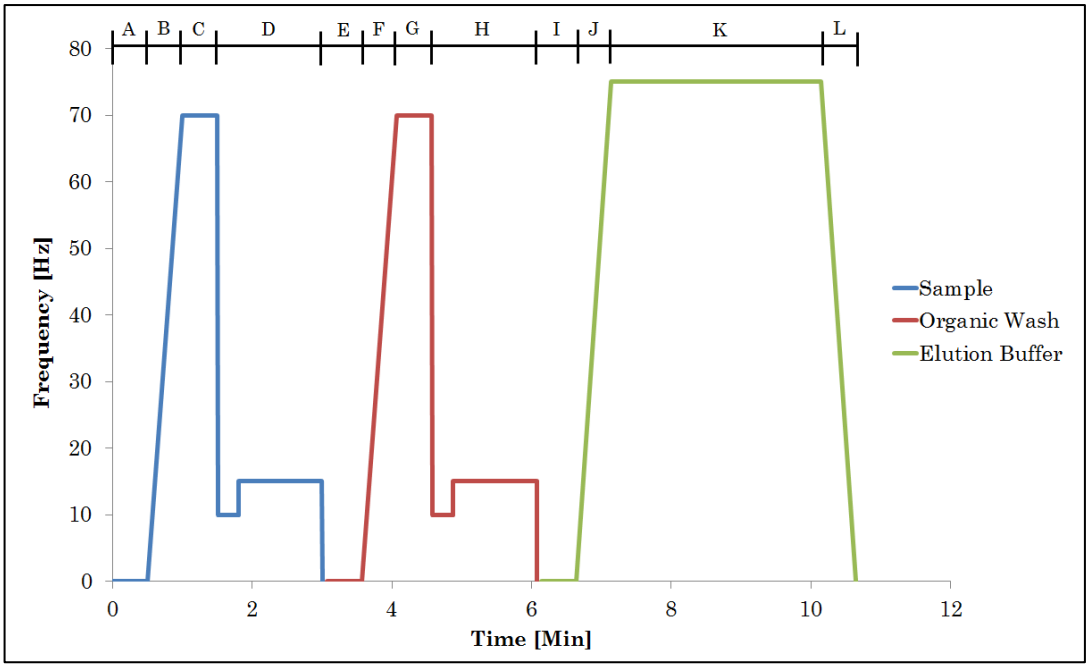

Figure 5.5: Spin frequency profile of GO router versus time for DNA purification protocol. The labels (A – L) refer to the image sequence shown in Figure 5.3. The disc is stopped for each of the solutions to be loaded. The simultaneous purification of five samples can be achieved in less than 11 min.

After loading the 60 µL sample, the disc was initially spun up to 70 Hz to allow the fluid to be pumped into the pneumatic chamber. Upon reduction of the spin frequency to 10 Hz, the expanding gas pocket pushed the fluid to a level higher than the crest of the siphon. The fluid therefore travelled over the siphon to waste. A final burst of speed (up to 15 Hz) was used to ensure the fluid had been fully removed from the siphon channel. The organic washes (60 µL each) followed the same path and spin frequency profile. It should be noted that the both of the first two flows are performed at a frequency below the threshold burst frequency of the GO tab. This is used as a secondary safety feature, as the true barrier is the solvent selectivity of the GO tab. The first sample

is only 1/6th aqueous, mixed with an organic buffer, used to enhance binding to the beads (Section 2.2.2). The second is an EtOH based buffer solution. After the desired number of washing solutions were flowed through the system, the final Elution Buffer (60 μL) was loaded. The disc was spun to 75 Hz, which is above the burst frequency of the GO tab. After approximately 3.5 min the fluid flowed through the GO tab into the collection chamber. The entire process takes approximately 11 min but each disc contains five identical structures, so five samples can be run simultaneously. A stroboscopic frame sequence of this routing is shown in Figure 5.6. Colour dyes were used in this case for clarity.

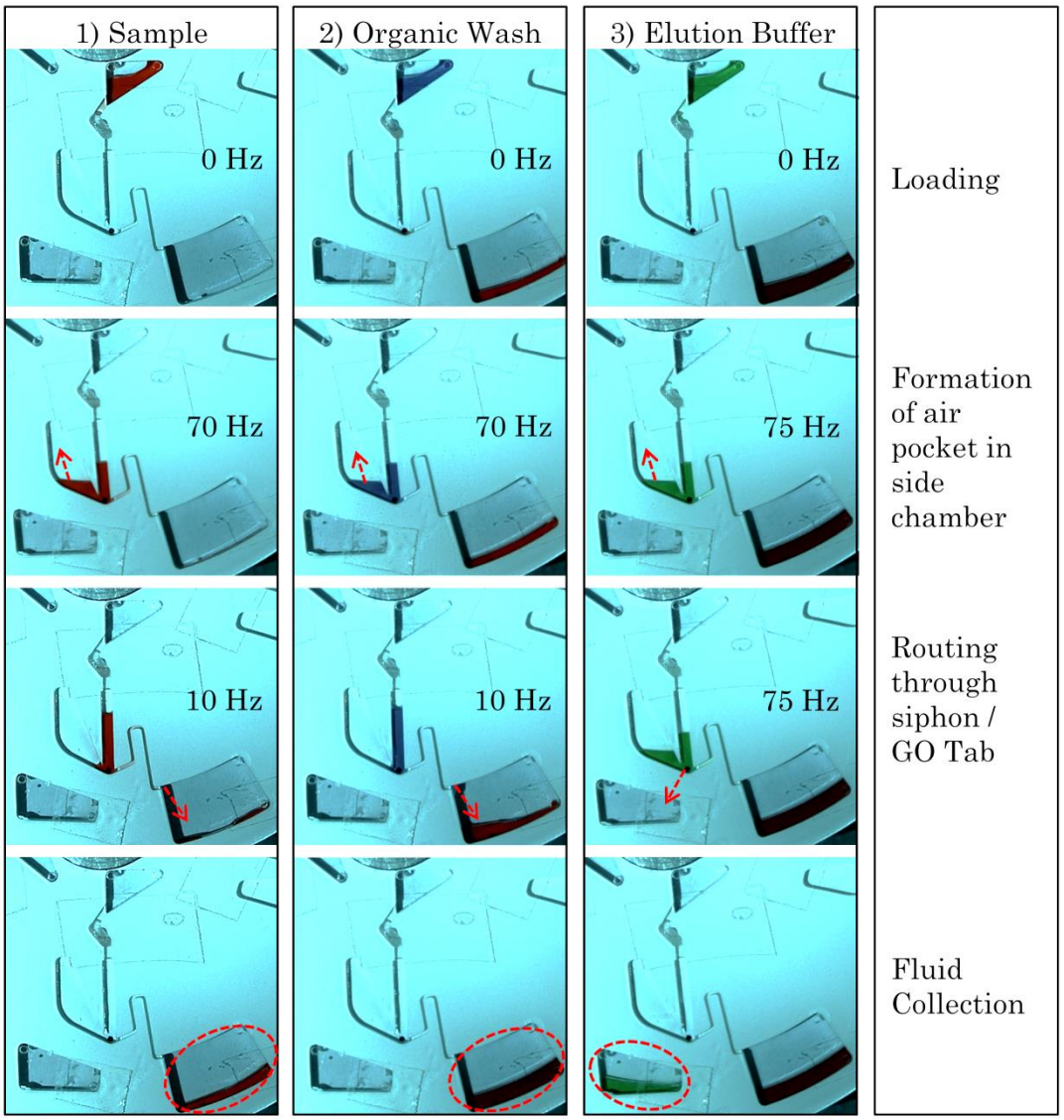

Figure 5.6: Experiment demonstrating solvent-selective routing of flows by the phase- and solvent-selective GO membrane. Arrows indicate the direction of flow and fluids were dyed for clarity.

5.4.2 On-disc DNA Purification

To test the functionality of on-disc SPP of DNA with the GO router, a two-stage validation process was observed.

5.4.2.1 DNA Interaction with GO Membrane

The first step was to ensure that the GO membrane would not interfere with the DNA. There was some concern that the DNA might bind to the GO membrane or that the membrane may somehow damage the DNA. To test if this was the case the flow through structure described in Section 4.3.2 was used. A 10-μm thick tab was used and 60-μL of various dilutions of the DNA concentrations were flowed through the GO membrane. The quantity of DNA present before and after was measured using the PicoGreen fluorescence kit on the TECAN plate reader (Section 2.4.2.3). The results are shown in Figure 5.7.

As can be seen from the graph, there is no discernible negative impact of the GO on the DNA sample at any of the four concentrations. In fact at the highest concentration (1 μg/ml) the DNA signal after flow through the GO membrane is stronger. The author acknowledges that this may be an anomaly which may be due to loss during the dilution process. For all other data points there is no discernible loss of DNA due to the GO. Also tested was the impact of the PMMA disc on the signal strength. This too proved to be negligible. It should also be noted that the error at each point is very small and there is good linearity.

It was thereby concluded that the DNA would not bind to the GO membrane and that the membrane would not damage the DNA in any way that would impede detection using the PicoGreen kit.

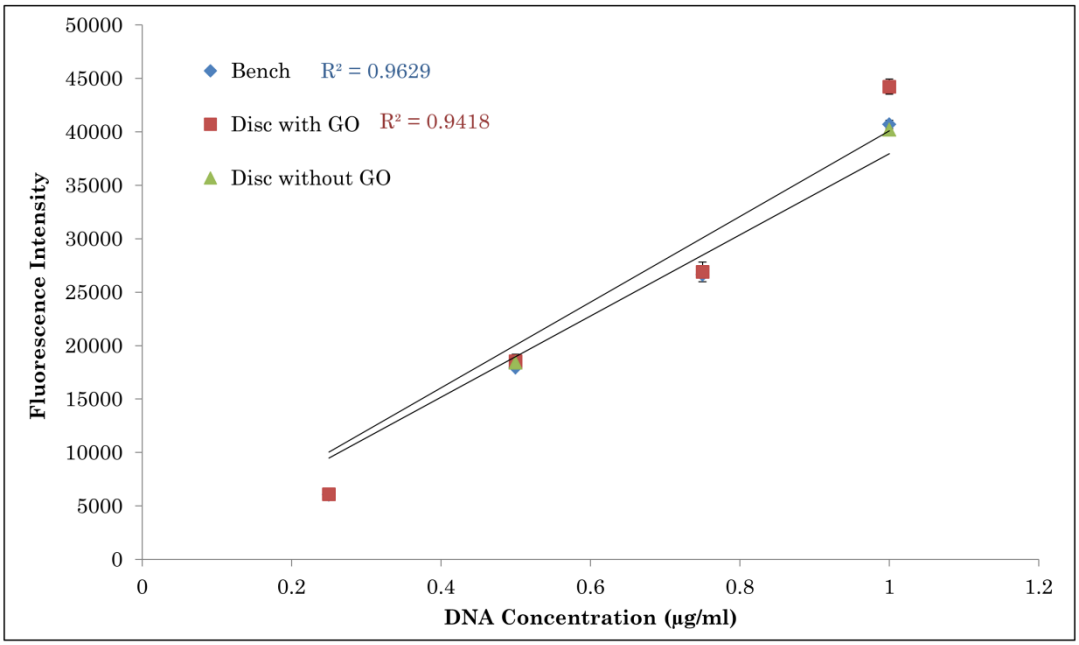

Figure 5.7: Comparison of DNA interaction with GO membrane for a range of DNA concentrations. The quantity of DNA present was measured using the PicoGreen fluorescence assay. The fluorescence intensity readings are arbitrary units assigned by the machine. The blue diamonds represent the DNA sample before flow through the GO membrane, the red squares represent the DNA sample after flow though the GO membrane and the green triangles represent the DNA samples that were flowed through the disc with an open hole (i.e. no GO). Data points are mean ± 1 standard deviation, n=4. The error bars are present on the data points however the error on the lower values is too small to be seen on the figure.

5.4.2.2 DNA Solid Phase Purification using GO Router

To test the viability of the GO Router design shown in Figure 5.1c, Qiagen spin column protocol was also implemented (Section 2.2.2) both on the disc and on the bench. The DNA sample was mixed with five parts Buffer PB solution, which had a pH of less than 7, in order to ensure that the like-charge interactions of the silica beads could be overcome. This gave a DNA concentration of 4-µg/ml in each 60-µL

sample. The samples and corresponding wash and elution procedures (Section 5.4.1) were then implemented on the GO router disc. The first flow through the beads was collected from the waste chamber to determine how much of the DNA sample was not binding to the beads. The final purified sample was also collected from the disc. The benchtop Qiagen spin column procedure was also performed for comparison. The PicoGreen fluorescence kit was used to determine the quantity of DNA present after purification and the results were normalised as a percentage of the total DNA inputted into the system. An aliquot of the original DNA sample used was quantified using the PicoGreen kit and the fluorescence signal generated was taken as 100% of the sample. All other samples were matched against this and their output percentage was calculated. The results are shown in Figure 5.8.

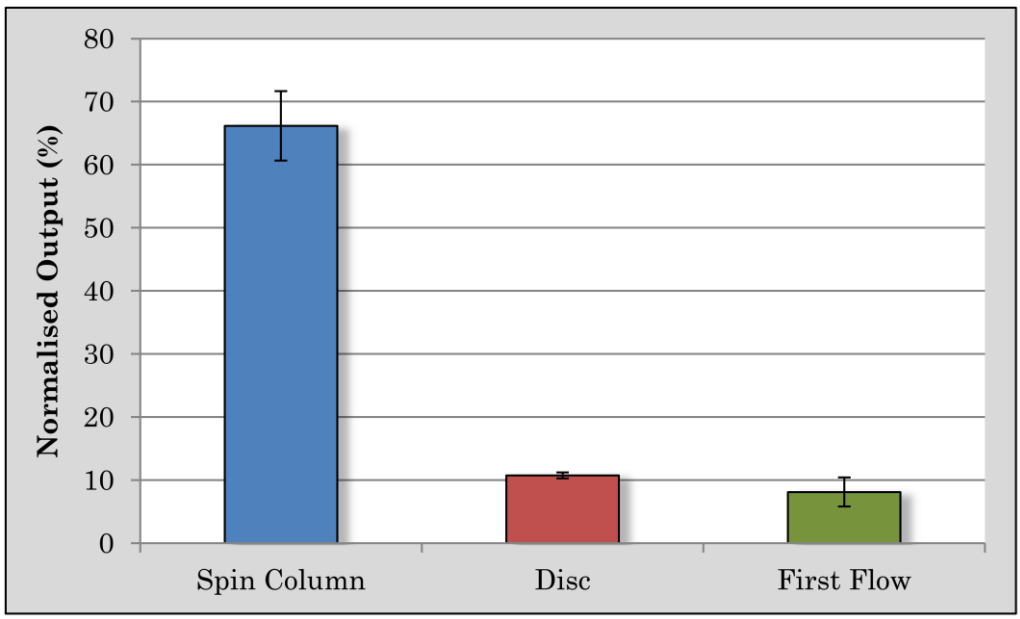

Figure 5.8: Comparison of normalised DNA signal from SPP using benchtop spin column setup and GO router. 66% of the DNA was collected from the spin column versus the 10% from the disc. The first aqueous flow through showed that 8% of the DNA is passing straight through the beads. Data points are mean ± standard deviation, n = 4.

The results show that DNA is collected from the disc after the purification procedure is undertaken, though there is significant loss of the sample. The benchtop 'Spin column' equivalent, which acts as the gold-standard collected an average of 66% of the DNA inputted, whereas the disc collected only an average of 10%. This shows that the GO router system in its current configuration is 16% as efficient as the gold-standard bench-top method. This is an improvement on the 12% achieved using the Solvent-Selective router (Section 3.5.2).

There are numerous points where the loss of DNA may be occurring. The data shows that, on average, 8% of the DNA is flowing

directly to the waste, i.e. not binding to the beads. This number may in-fact be higher as the sample that is extracted from the waste chamber after the first flow through must then be passed through the spin column and eluted in the elution buffer. This is a necessary step as the Buffer PB, which is initially mixed with the sample, inhibits the fluorescence assay. Therefore, knowing that the efficiency of the spin column is 66%, it can be assumed that approximately 12% of the DNA is being lost during the first flow through the beads.

The author notes that further investigation and optimisation of the solid-phase purification protocol should enhance the capture and elution efficiency of the system. Adjustments to the pH and salt concentrations may have an effect. A pH $\leq$ 7.5 is considered optimum for DNA binding to silica beads, whereas a pH of 7.0 - 8.5 is required for elution. Also increasing the time which the sample is in contact with the beads may be useful. The large discrepancy with the gold-standard benchtop method may be related to the difference in using a tightly packed monolith (spin column) and the bead chamber (disc). There may also be some loss due to binding of the DNA to the walls of the plastic disc. Locally washing with a blocking solution, such as Bovine Serum Albumin (BSA), may help reduce the loss (90).

The benefit of the GO router though is not in its capture efficiency but in the movement towards an automated system. The router is a significant improvement on the highly labour-intensive benchtop

equivalent and uses significantly reduced sample volumes. Its ease of manufacturing and simple to use system offers significant benefits for point-of-care uses.

5.5 Conclusions

I have demonstrated for the first time a centrifugo-pneumatic routing of flows based on a centrifugal microfluidic platform which integrated a GO membrane. This membrane is impenetrable to organic solution, but yields at moderate spin rates to an aqueous fluid. This unique solvent-selectiveness of the GO membrane opens new avenues for robust automation of common nucleic acid purification protocols (e.g. “spin columns”) on centrifugal LoaD platforms. The purification of DNA versus the gold-standard benchtop method was demonstrated. Future work should include the optimisation of the router for use with the silica beads in-order to enhance the capture and collection of all nucleic acids.

Chapter 6

Event-triggered Graphene Oxide Router for Automated Nucleic Acid Purification

6.1 General Introduction

The previous chapter described the design and testing of a centrifugo-pneumatic router which used the unique properties of GO for advanced flow control and to perform on-board DNA purification. In this chapter, I show the next stage of this work which is the development of a fully automated system incorporating the GO router which utilises an event-triggered flow control element and incorporates multiple

functional materials to enhance the flow control capabilities of this system.

6.1.1 Event-triggered Valving Mechanisms

Event-triggered valving systems were first developed by Kinahan *et al.* in 2014 as a means by which to overcome the limitations within other valving mechanisms for serialised large-scale integration of microfluidic flow control (27).

The system was developed to allow the release of reagents from a chamber to be triggered by the dissolution of a film in a previous chamber. Figure 6.1 shows the working principle. The main liquid is held in place by an air-locked pressurised channel, sealed by the control film in the bottom chamber. When the ancillary fluid enters the bottom chamber, it dissolves the control film inside. This opens the air-locked pressurised channel to atmosphere. The now vented channel allows the flow of the main fluid onto the load film. The load film is dissolved and the fluid can continue on to trigger the flow of the next solution. Unlike other rotationally actuated valves this event-triggered system is largely independent of the spin rate of the disc and is reliant only on the passage of fluid and the dissolution of the films.

The work described in this chapter integrates this elegant system with the previously described router to develop an automated Event-trigger Graphene Oxide Router (EGOR) and uses it to purify DNA.

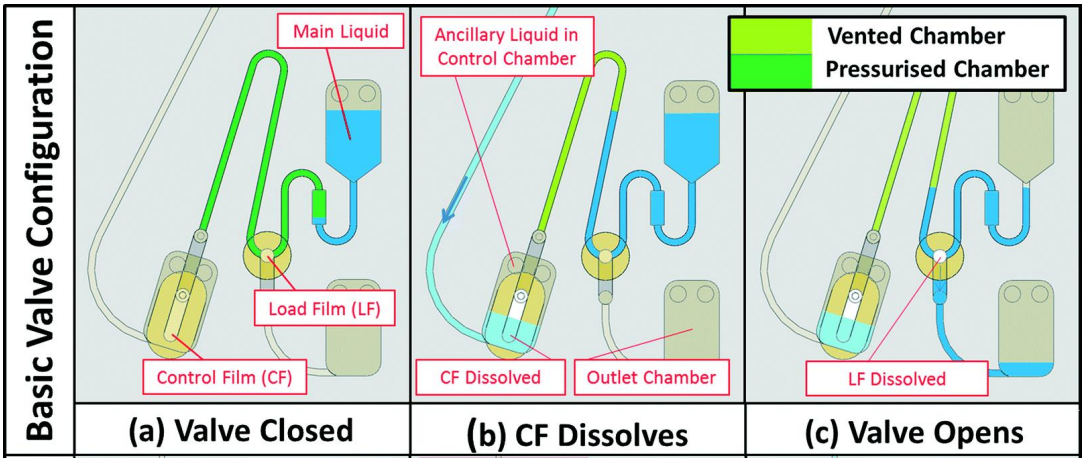

Figure 6.1: Working principle of event-triggered logical flow control system. Ancillary fluid dissolves the control film and vents the pressurised air channel. The main fluid can then travel down the channel to the load film, where it dissolves the film and continues on. Adapted from Kinahan *et al.* 2014 (27).

6.2 System Design

6.2.1 Evolution from first design

Figure 6.2 shows the evolution of the design of the Event-triggered GO Router (EGOR) which incorporates three different membrane tab types for the automated solvent selective routing of flows. The design builds on the work described in Chapter 5. Once again there were a number of iterations but the two main stages are shown here.

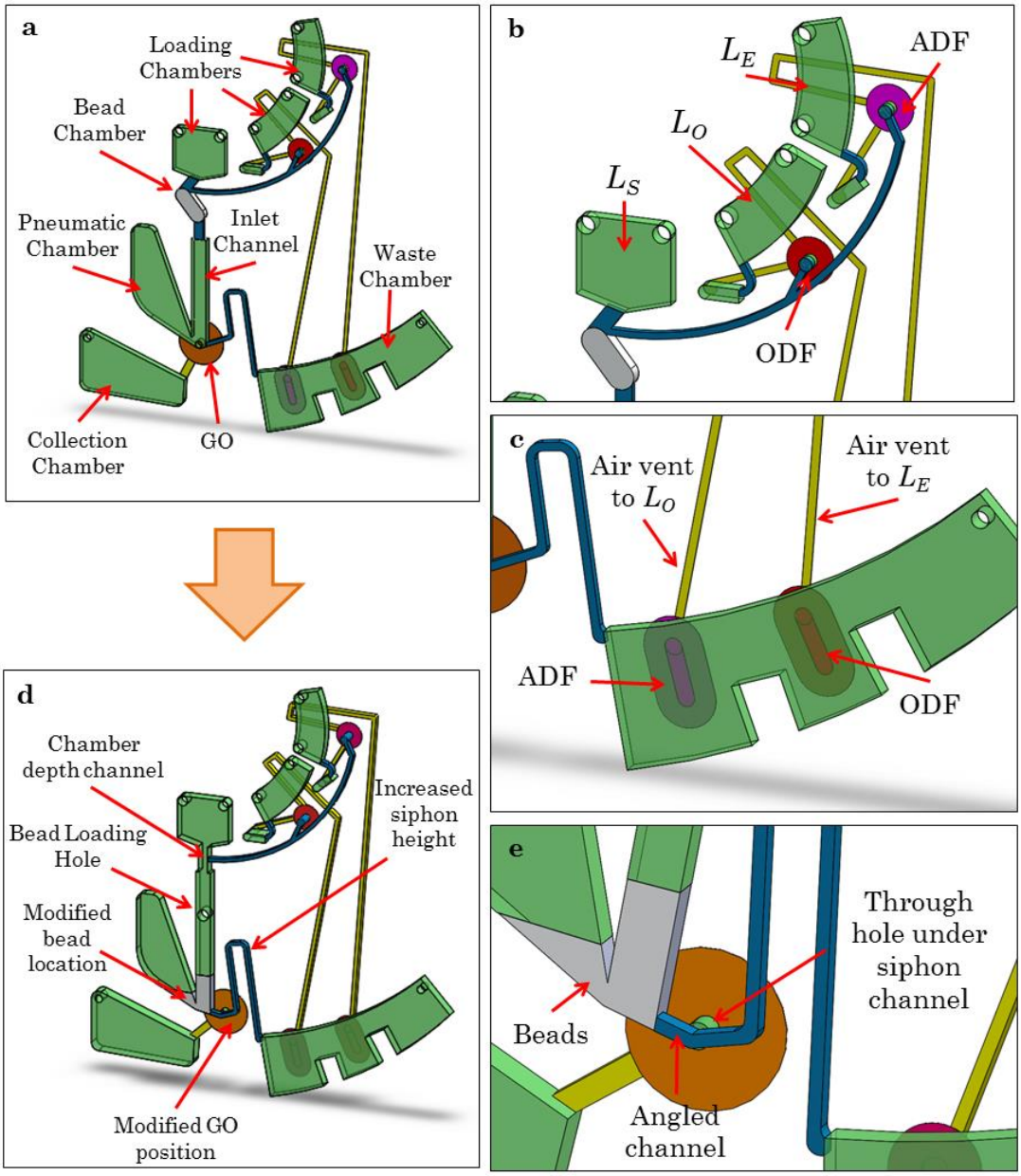

Figure 6.2: Evolution and component parts of design of event-triggered GO router. a) First design iteration with all its functional components. b) Enhanced illustration of the three different loading chambers: the Sample Loading Chamber (L_S), the Organic Loading Chamber (L_O) and the Elution Loading Chamber (L_E). Also shown is the placement of the two dissolvable film tabs: the Organic Dissolvable Film (ODF) and the Aqueous Dissolvable Film (ADF). c) Enhanced illustration of the waste chamber, showing the position of another ADF and ODF tab, also the airtight channels connecting to the loading chambers. d) Second design iteration showing modified parts. e) Enhanced illustration of modified bead's and GO tab's positions.

Initially (Fig. 6.2a), the design consisted of three separate loading chambers, the Sample Loading (L_S), the Organic Wash Loading (L_O) and the Elution Loading (L_E) (Fig. 6.2b). The L_S was connected by a channel to the bead chamber. This channel also connects back to the L_O and L_E. The L_O is sealed by an Organic Dissolvable Film (ODF) which dissolves in the presence of organic solutions. This membrane is also capable of dissolving in aqueous solutions but that feature is not required here. The fluid is maintained within the L_O by an air lock within the connecting channel (shown in yellow). This channel will maintain its air seal so long as the tab in the waste chamber remains intact (Fig. 6.2c). The L_E works in a similar manner however an Aqueous Dissolvable Film (ADF) (used previously in Chapter 3) is used to maintain the air seal and retain the fluid within the chamber. The connecting channel allows for all of the fluids to pass through the bead chamber before being routed onwards. The remainder of the structure is the same as that used in Chapter 5. The bead chamber is connected by a channel to a sealed pneumatic chamber which exhibits a small hole, sealed by a GO tab, at its base. The hole connects to a collection chamber. The chamber is also connected via a siphon channel to a waste chamber. The waste chamber differs slightly from the original design (Fig. 6.2c). It is partitioned to allow only one tab to be triggered per flow and give a more accurate control of the automated process. The waste chamber exhibits two holes in it which are sealed by either an ADF or ODF. These holes connect via an air channel to the L_O and L_E. This design performed fluidically well

but gave low yields for DNA purification; therefore a redesign was performed in an attempt to improve the yield.

Figure 6.2d shows the updated design with the changes highlighted. The main change revolved around the bead chamber. It was postulated that the bead chamber configuration used in Fig. 6.2a, was not ideal for DNA capture onto the beads, as the fluid passes through the chamber very quickly (≤ 15 sec). Therefore, instead the beads were moved down into the base of the pneumatic chamber and inlet channel. This was done as each of the fluids spends considerably longer in this part of the structure and can be pumped back and forth through the area containing the beads as long as the spin frequency is maintained above the siphon burst frequency. The change in bead location led to a number of other modifications. Firstly, the bead chamber was removed entirely and a loading hole was placed over the inlet channel to allow the beads to be packed into the structure. It was placed at the top of the channel to allow for clean emptying over the siphon. The beads were packed into the structure and then the disc was spun in order to position them in the base of the channel. Next, the location of the GO tab and through hole was moved. This was done to ensure that the beads did not block the passage of fluid through the tab. The through hole was shifted to the right, below the siphon channel entrance (Fig. 6.2e). As the beads were larger in diameter than the siphon channel, they would not be able to block the tab. The entrance to the siphon channel was also angled slightly so all fluid could be collected through the GO membrane. Also

due to the space occupied by the beads in the inlet channel and pneumatic chamber, the fluid volume when it enters would reach a higher level. In order to maintain the reliability of the system, the siphon channel was also raised slightly. The final change was unrelated to the bead chamber. It was observed that there was a slight backflow along the blue inlet channel towards L_O and L_E. In order to combat this issue the inlet channel was made entirely chamber depth so that there was a much higher resistance for the fluid to enter the side channel and instead would preferentially travel straight down the inlet channel. All of these changes led to the final working design.

6.2.2 Working Principle

Figure 6.3 shows the flow schemes for the automated sequential routing of aqueous and organic solutions. Initially, the three solutions are loaded: the sample, the organic wash buffer and the elution buffer (A). Under rotation, the sample flows down the inlet channel and up into the pneumatic chamber, trapping and compressing the air inside (B). At this point the beads are suspended within the solution. The high rotational frequency (which is maintained below the threshold burst frequency of the GO tab) ensures that the fluid does not pass over the siphon crest. The other two solutions are retained within their loading chambers due to the air tight channel (shown in yellow) connected to and sealed within the waste chamber. This airlock prevents either fluid

from coming in connect with the DF tabs at their base (Fig. 6.2b, c). Upon reduction of the spin rate, the air within the pneumatic chamber expands, pushing the fluid back up to a level higher than the siphon crest. The fluid therefore travels over the siphon to the waste, where it is collected within the first section of the waste chamber (C).

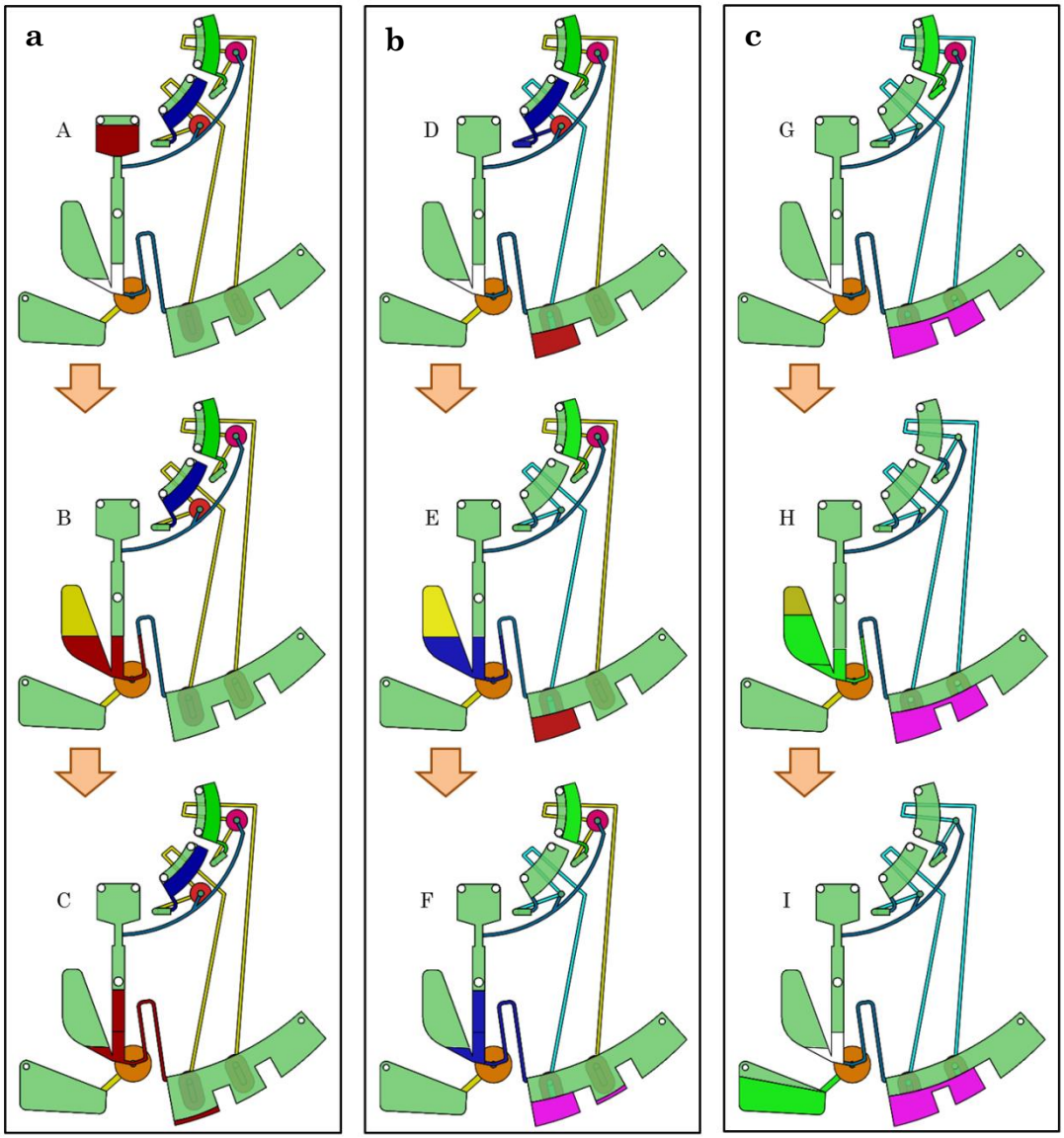

Figure 6.3: Working principle of the EGOR. a) At a high frequency the sample (red) compresses the air within the pneumatic chamber (yellow). Upon deceleration the entrapped air expands to pump the fluid over the siphon to waste. The other two solutions are retained within their loading chambers. b) The dissolution of the first film in the waste chamber triggers the flow of the organic wash buffer. It follows the same pathway as the sample and is routed to the waste chamber. c) In the final stage, the dissolution of the second film in the waste chamber triggers the flow of the elution buffer. The disc is spun at a higher frequency to overcome the threshold burst frequency of the GO tab. The elution buffer is directed to the left collection chamber. The labels (A – I) refer to the spin rates indicated in Figure 6.5.

Once the fluid has been collected within the waste chamber, it is now at a level where it is in contact with the ADF tab. It dissolves the tab, thereby opening the air tight channel to atmosphere and reducing the airlock imposed upon the organic wash buffer. The buffer is therefore free to push into the overflow chamber, down along the channel, where it comes in contact with the ODF at its base (D). Once again the third solution, the elution buffer, is unaffected as its connecting channel is still air-locked. Once the organic wash buffer dissolves the ODF at its base, it travels down the channel, into the inlet channel, and once again under high rotational frequency, is pumped up into the pneumatic chamber, compressing the air inside (E). Upon reduction of the spin rate, the fluid is routed to the waste chamber, where is mixes with the already present solution and flows over into the second section of the waste chamber (F).

Once the entire organic wash buffer has been collected with the waste chamber, it brings the fluid to a level where it is in contact with the ODF. It dissolves the film, thereby releasing the air trap on the elution buffer. The buffer flows from the chamber and encounters the ADF at its base (G). The spin rate is now increased, beyond the threshold burst frequency of the GO tab. The elution buffer travels down the inlet channel and after a short time passes through the GO tab and is collected into the collection chamber (H, I).

6.3 Materials and Methods

6.3.1 Disc Fabrication and Assembly

The disc (Ø 120 mm) consisted of four layers of PMMA and four layers of PSA (Fig. 6.4). The PMMA layers were cut entirely with the laser cutter as described in Section 2.1.2.1 and the PSA layers were cut using the precision knife cutter. The cleaning procedure, as outlined in Section 2.1.3, was observed. The GO tab was fabricated as described in Section 4.2 and was fabricated to a thickness of approximately 45-µm for the fluidic tests and 35-µm for the biological tests. The ADF and ODF tabs (both long tabs placed into the waste chamber and circular tabs placed below the loading chambers) were adhered to PSA with through holes cut out. Prior to assembly (described in Section 2.1.4) all the tabs were adhered to the top side of the 'Tab Cover PMMA' layer, with the 'Tab Support PSA' layer, giving adequate space to house the tabs.

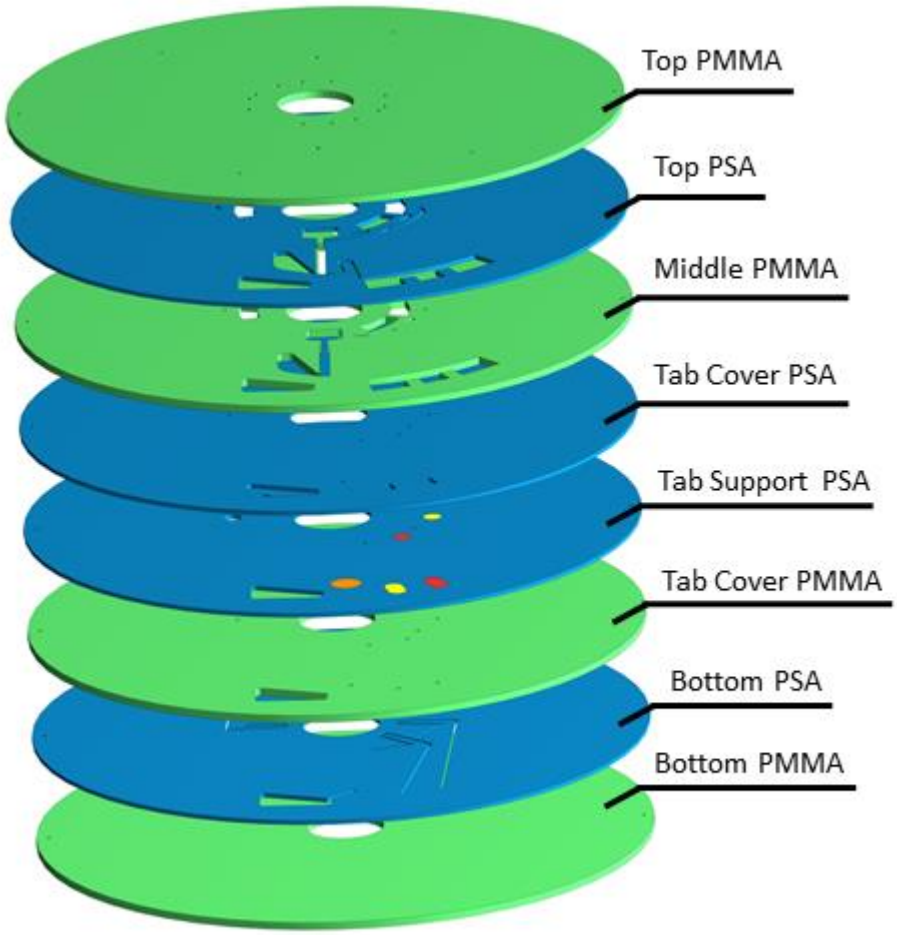

Figure 6.4: Exploded view of EGOR disc assembly. The (Ø 120 mm) disc consisted of four layers of PMMA (green) and four layers of PSA (blue). The GO tab (orange), the ADF (yellow) and the ODF (red) were adhered to the topside of the Tab Cover PMMA layer.

Once assembly of the disc was complete ~30 mg of glass beads (diameter ≤ 106-µm) were added through the hole in the 'Top PMMA' layer (Fig. 6.2d). The hole was then sealed and the disc was spun at a high frequency to encourage the beads to rest at the bottom of the inlet channel/ pneumatic chamber (Fig. 6.2e). Each disc contains two identical structures.

6.3.2 DNA Preparation

The QiaQuick PCR purification kit (Section 2.2.2) and PicoGreen DNA fluorescence kit (Section 2.4.2.3) were used for the course of these experiments. The lambda DNA standard was taken from the concentrated solution of 100 μg/ml and diluted in 1x TE Buffer to a concentration of 12 μg/ml. This solution was then split in three. To measure the pure DNA concentration the 12 μg/ml solution was mixed in a ratio of 1:5 with 1x TE buffer to bring it to a concentration of 2 μg/ml. For use on-disc the 12 μg/ml solution was mixed in a ratio of 1:5 with the PB Buffer. The Qiagen buffers were used on the EGOR in order to ensure the correct pH and salt concentrations needed for the DNA to bind to the beads. For the benchtop spin column test, the standard Qiagen kit protocol was used (Section 2.2.2). For the detection 20 μL of dye and sample was used.

6.4 Experimental Results

6.4.1 Fluidic Operation

Experimental validation was performed in order to determine the optimum spin frequencies and solution volumes required for the operation of the EGOR. The final spin frequency profile is shown in Figure 6.5.

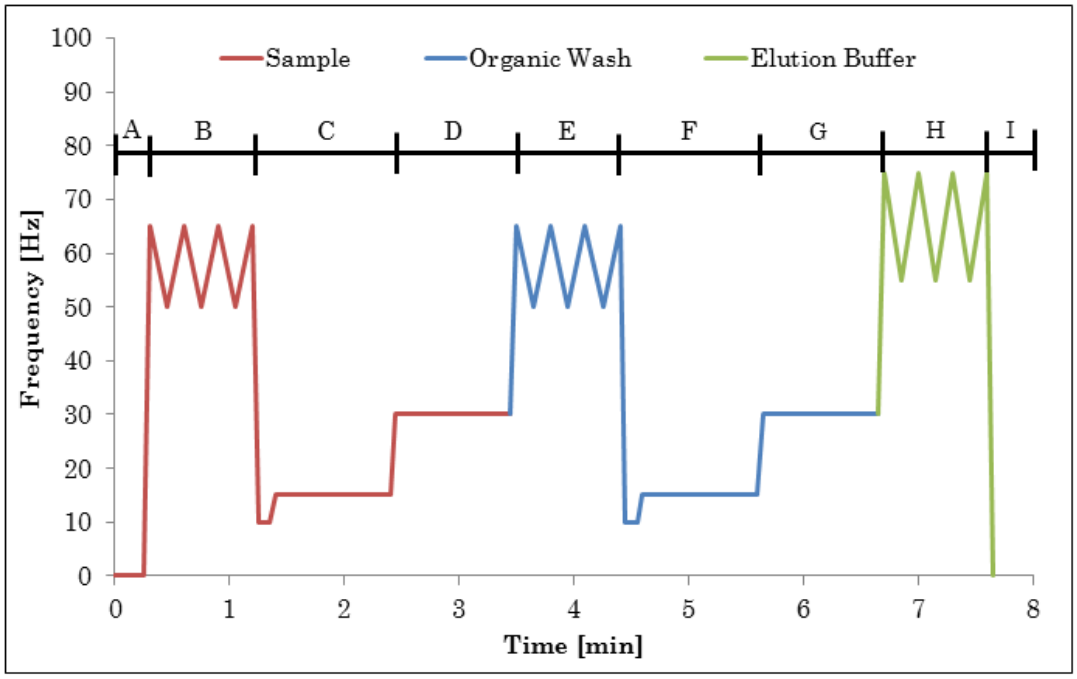

Figure 6.5: Spin frequency profile of EGOR versus time for automated DNA purification protocol. The labels (A – I) refer to the image sequence shown in Figure 6.3. The simultaneous purification of two samples can be achieved in less than eight minutes.

The optimum volume for each of the three solutions was determined to be 50 µL. Any higher volume would sometimes result in the siphon breaking too soon. After the three volumes were loaded into their respective chambers, the disc was initially spun up to 65 Hz, to allow the sample to be pumped into the pneumatic chamber, through the glass beads. The disc frequency was then oscillated between 65 Hz and 50 Hz for one minute. This was done to give the beads maximum exposure to the sample and allow ample binding of the DNA to the bead surface. The 50 Hz spin rate was used to ensure that the fluid did not prematurely pass over the siphon crest. The spin rate was then reduced

to 10 Hz, this caused the gas pocket in the pneumatic chamber to expand and push the fluid to a level higher than the siphon crest. The sample therefore travelled over the siphon to the waste chamber. The speed was then increased to 15 Hz to ensure all the fluid had been removed from the siphon channel. Once the fluid was fully retained in the waste chamber, it came in contact with the ADF tab. At this point the disc was given a small burst in speed, up to 30 Hz to encourage dissolution of the film and open the air-locked back channel. This allowed the second fluid, the organic wash buffer, to leave its loading chamber and come in contact with ODF tab at its base. It took approximately one minute at this frequency for the tab to burst. At any point during this time, the disc was spun back up to 65 Hz and the organic wash followed the same path and spin frequency as the sample. It should be noted that both of the first two flows are performed at a spin frequency below the threshold burst frequency (75 Hz) of the GO tab. Once the second tab in the waste chamber, the ODF tab, was dissolved, and the final elution buffer had come in contacted with and dissolved the ADF tab at its base, the spin frequency was increased to 75 Hz. This is above the threshold burst frequency of the GO tab. It took approximately one minute at this frequency for the fluid to flow through the tab. During this time the frequency was oscillated back and forth between 75 Hz and 55 Hz, to give the beads as much exposure to the elution buffer as possible. The 55 Hz minimum was used as an extra safety measure to ensure that the fluid would not pass over the pre-

wetted siphon. The final eluted solution was then retained within the collection chamber. The entire process takes approximately 8 minutes, which is an improvement on the non-automated version of the structure. This is due to the fact that the disc does not need to be stopped to load the subsequent solutions. A stroboscopic frame sequence of this routing process is shown in Figure 6.6. Coloured dyes were used for the sake of clarity.

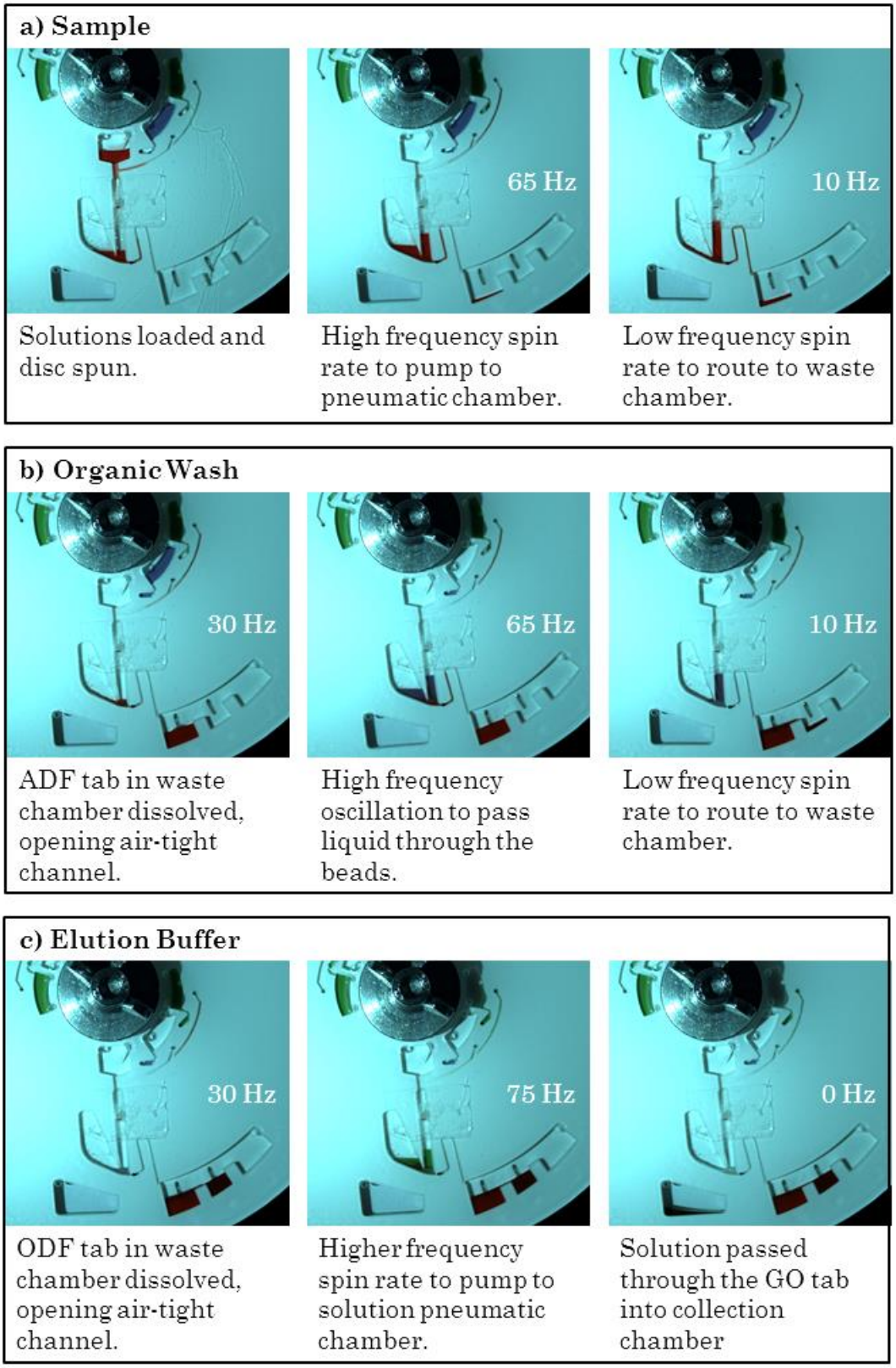

Figure 6.6: Stroboscopic image sequence showing the automated solvent-selective routing of flows. Fluids are dyed for clarity: the sample (red), organic wash buffer (blue) and elution buffer (green).

6.4.2 On-disc Automated DNA Purification

To test the viability of the EGOR system, shown in Figure 6.2d, for automated SPP, the Qiagen spin column protocol (Section 2.2.2) was implemented on-disc and on the bench. The DNA/PB Buffer solution was prepared on bench and the 50 μL solution was loaded unto the disc, along with 50 μL PE Buffer and 50 μL EB Buffer. The automated routing process was observed and a final purified sample was collected from the disc. The benchtop Qiagen spin column procedure was also performed for comparison. The PicoGreen fluorescence kit was used to determine the quantity of DNA present after purification and the results were normalised as a percentage of the total DNA inputted into the system. The results are shown in Figure 6.7.

The results show that there is DNA recovered from the disc after the purification process has taken place though there is still significant loss of sample. The benchtop 'Spin column' equivalent, which acts as the gold-standard collected an average of 33% of the DNA inputted, whereas the disc collected only an average of 3%. The lower yield from the spin column in this experiment may have been due to a loss during the dilution phase of the experiment (Section 6.3.2). This shows that the EGOR system in its current configuration is 10% as efficient as the gold-standard bench-top method.

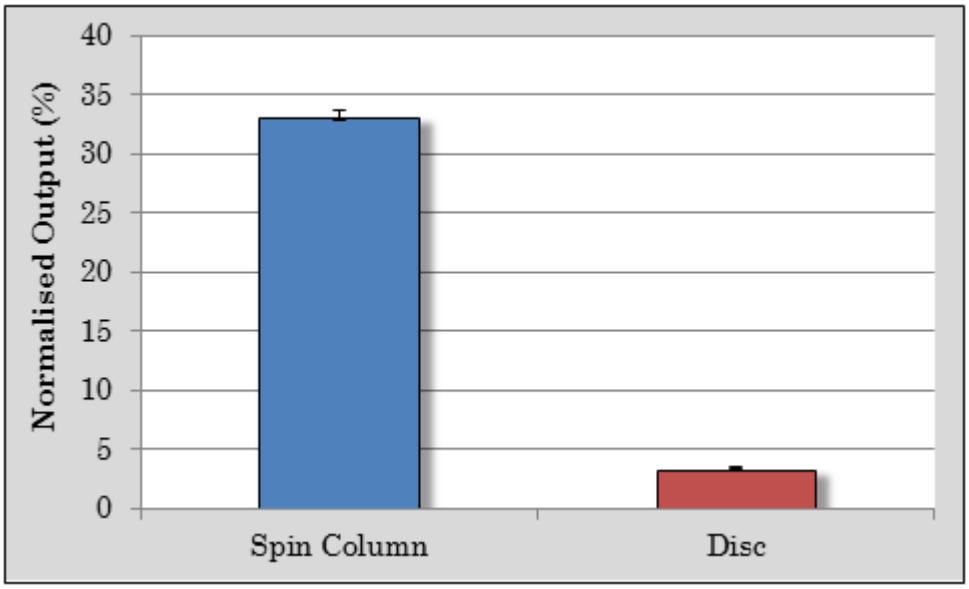

Figure 6.7: Comparison of normalised DNA signal from SPP using benchtop spin column setup and EGOR. 33% of the DNA was collected from the spin column versus the 3% from the disc. Data points are mean ± 1 standard deviation, n=4 for the spin column and n=3 for the disc.

6.5 Discussion

The 10% efficiency of the EGOR systems is less than the 16% shown in Chapter 5. There are a number of possible reasons for this low yield. The biggest variation from the former non-automated design is the position of the beads within the disc. The earlier version had a bead chamber, which was packed to capacity. In the current EGOR version the beads are placed at the base of the pneumatic chamber/inlet channel (Fig. 6.2e). The process of loading the beads within the disc involves placing a pipette tip into the loading hole to act as a funnel. The beads are then poured into the tip. The beads however are highly static and can stick to the tip surface; therefore one tip was only ever used once.

With the earlier design, due to the dimensions of bead chamber, the beads had no option but to remain within the bead chamber. However, with the EGOR design the beads are placed into a much more open space and, due to their static nature, some would be prone to moving to other parts of the disc that all the fluid would not be exposed to, such as the sample loading chamber or the top of the pneumatic chamber. If this happens then some of the DNA may bind to beads that do not encounter the elution buffer and so cannot be re-suspended.

Another issue may be with the Pressure Sensitive Adhesive (PSA). The base of the loading chambers, inlet channel and pneumatic chamber (Fig. 6.2d) are all comprised of the exposed sticky PSA. This may be part of the reason the beads are not packing to the base of the chamber but the DNA may also be adhering to the sticky surface.

Finally, the last change in protocol from the earlier to non-automated version to the EGOR system was that only one organic wash was performed in the latter, versus two in the former. If some of the salts are not being removed from the beads, this may be interfering with the fluorescence assay and reducing the signal strength.

However, there are some positive points to note. Firstly, the error bars indicated in Figure 6.6 are very small, showing that though the system is outputting a small yield, it is doing so consistently, in fact more consistently than the benchtop method. This could therefore be considered a systematic error and it may be possible to use this to

correlate how much DNA was in fact added to the system. If the output fluorescence signal is known to be approximately 3% of the actual DNA present then the true DNA quantity could be calculated.

Next, with the DNA concentration chosen (2 μg/ml) and the 50 μL volume inputted for each iteration, this gives an inputted quantity of 100 ng of DNA per sample. If during the detection process, each well of the 96-well plate receives 30 μL of solution, this equates to 60 ng per well. If the disc gives a signal that is 3% that of the pure DNA sample then this would equate to 2.05 ng on average per well. However, an average of 35 μL is extracted from the collection chamber so if 100 ng of DNA is inputted into the disc, 2.39 ng of DNA is extracted. This quantity is more than sufficient for such detection techniques as PCR. The *New England BioLabs* recommends 1 pg – 1ng of DNA for plasmid or viral DNA, which the lambda DNA standard used in this experiment is, when performing *Taq* DNA Polymerase (91).

Furthermore, this process is entirely automated. All of the solutions are pre-loaded at the beginning of testing. In fact, due to the air-tight under-channel sealed by the ADF and ODF tabs in the waste chamber (Fig. 6.2c), the organic wash buffer and elution buffer could be pre-loaded at a much early time and sealed within the chamber. This pre-storage of reagents is extremely useful for use in Point-of-Care systems. Also, as the disc works reliably within the spin frequency profile outlined, an automated spin profile could be implemented which

would minimise the user input required and therefore the training needed for its operation. The EGOR is therefore a significant improvement over the highly labour-intensive benchtop equivalent.

6.6 Conclusion

In this chapter I have demonstrated an event-triggered centrifugo-pneumatic routing system which utilises three different functional materials: graphene oxide, an organic dissolvable film and an aqueous dissolvable film. The functionality of this system was demonstrated as was its ability to purify DNA with low yield but highly repeatable output.

Chapter 7

Nucleic Acid Extraction Systems

7.1 General Introduction

In the previous results chapters 3, 4, 5 and 6 the work focused on the development of sample preparation systems for the downstream purification of nucleic acids. The work in this chapter looks at upstream concepts of the nucleic acid testing process, NA extraction. Two distinct extraction methods will be discussed: chemical extraction of RNA and mechanical extraction of NAs.

7.2 Fluid-fluid Extraction of Total RNA

As discussed in Section 1.5.2.1, chemical cell lysis is a highly useful method of NA extraction, and has been a method of choice for

some time. This section details the development and optimisation of a centrifugo-pneumatic microhomogenizer, which is based on the work of Linares *et al.* (53). They overcame the limitation of microRNA extraction, by using the μHomogenizer, which used a pneumatically assisted pumping design to create turbulent conditions for the efficient lysis and chemical extraction of RNA from whole blood.

The idea is simple; by mixing blood with TRI Reagent an aqueous phase containing the RNA can be extracted from whole blood (Fig. 7.1). TRI Reagent is a patented solution used for the extraction and isolation of total RNA (92). It can also be used to isolate DNA and proteins. The solution contains phenol and guanidine thiocyanate which allows for the separation of the aqueous phase and the denaturing of proteins (93). The aqueous phase can then be removed for further downstream processing using the devices shown in the previous chapters.

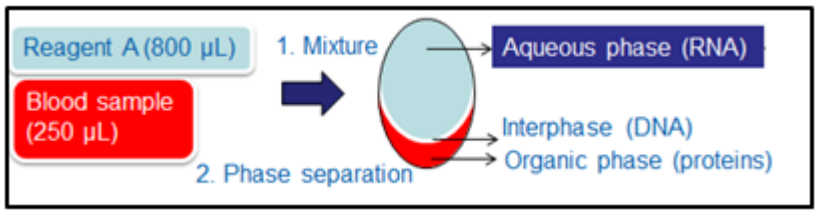

Figure 7.1: Separation of RNA from whole blood procedure.

7.2.1 Evolution of System Design

Figure 7.2 shows the evolution of the design of the μHomogenizer to its currently working model. There were multiple iterations, but the three main steps are shown here.

Initially, the design by Linares *et al.* consisted of a central mixing chamber connected to two air-tight pneumatic side arms. There is a loading hole at the top of the mixing chamber and a small turbulence area at the base of the chamber. This nozzle-like area is smaller than the rest of the design and was optimised to enhance mixing through the introduction of turbulence (Fig.7.2a). This design worked well but retrieval of the sample after use was difficult. It was therefore necessary to design a method of extracting the aqueous phase but leaving the remainder of the fluid within the side arms.

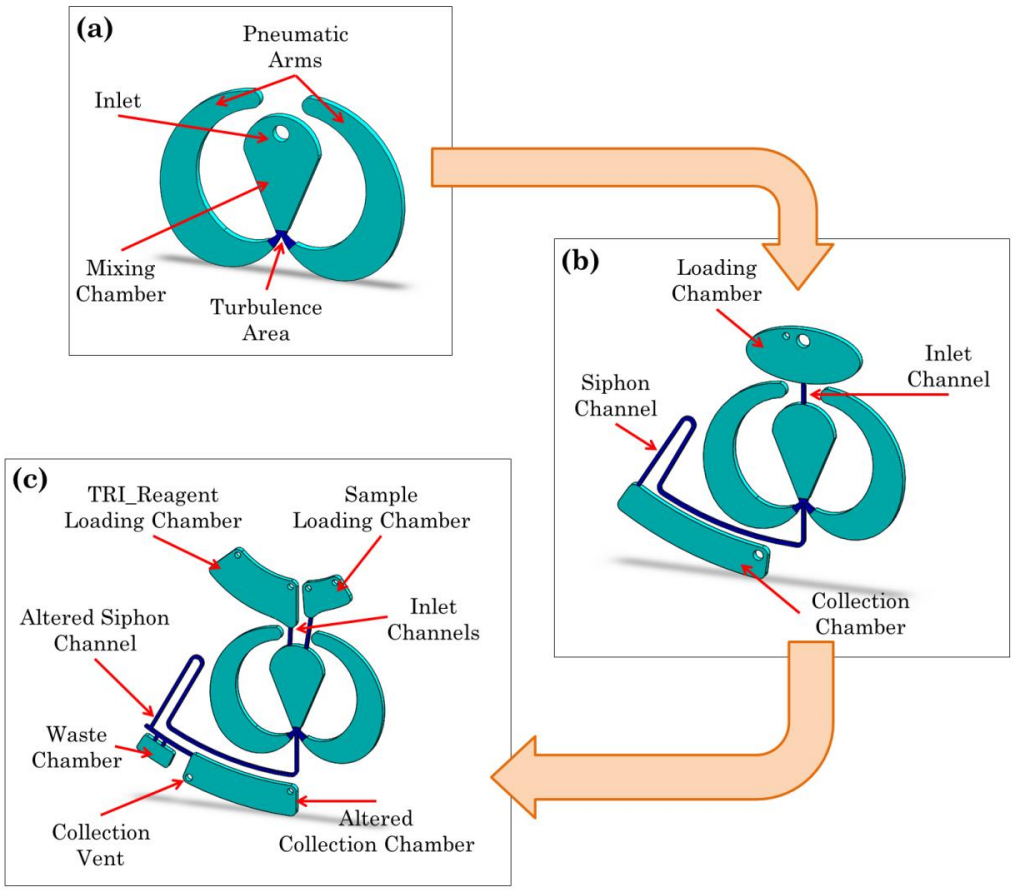

Figure 7.2: Evolution of design of µHomogenizer from original design. a) First iteration designed by Linares *et al.* with all its functional components. b) Second design iteration showing the introduction of a loading chamber, siphon channel and collection chamber. c) Third and final design iteration showing the introduction of a second loading chamber and waste chamber.

These issues were attempted to be addressed in the second iteration (Fig. 7.1b). Some significant changes were introduced. Firstly, a designated loading chamber was added, along with an inlet channel linking it to the mixing chamber. The central structure remained the same, apart from the removal of the inlet hole. Secondly, a siphon channel was added which connected with the base of the turbulence area. Finally, a collection chamber was added, connecting to the siphon

channel. Once again this system had a number of issues. The loading chamber was only large enough to load one solution at a time (TRI-Reagent or sample) and so the disc had to be stopped to load the second solution. The low pass siphon valve allowed the mixing to occur at high speeds but premature priming of the siphon was a problem. This seemed to occur when the disc was stopped for the second loading. This meant that some of the solution would break the crest and enter the collection chamber before full mixing could occur. It was also a problem during the initial loading phase. The fluid would go straight into the siphon channel and not be correctly mixed. During emptying this would go straight to the collection chamber and could contaminate the final extracted sample (Fig. 7.3).

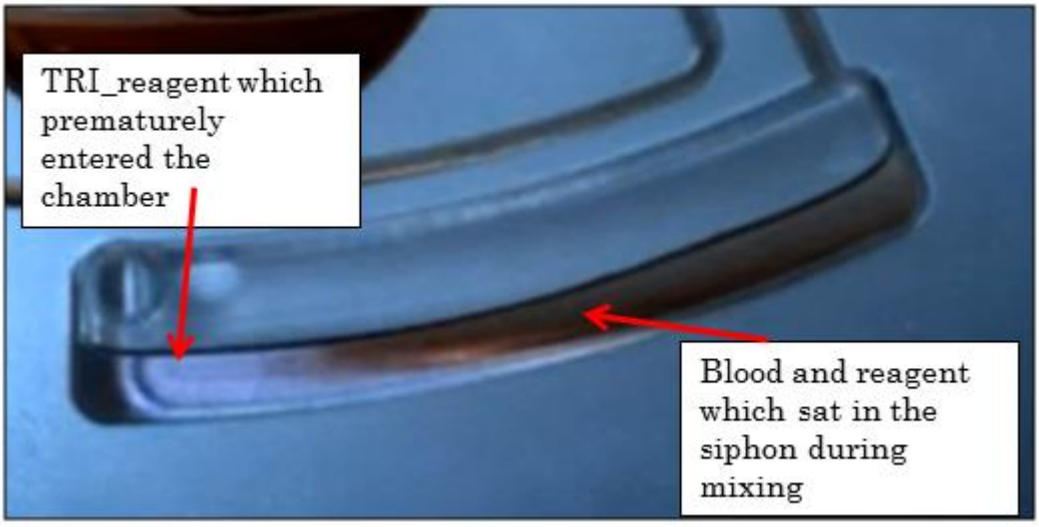

Figure 7.3: Contamination of extracted aqueous phase in collection chamber. Some TRI-reagent prematurely burst the siphon and entered the chamber when the disc was stopped. Some blood and reagent sat in the siphon during mixing and was not correctly separated.

The final design change attempted to address these issues (Fig. 7.2c). As the main problem with premature priming seemed to occur when the disc was stopped to load the second solution, two separate loading chambers were included to overcome this issue. To address the problem of the solutions sitting in the siphon channel, a waste chamber was added. The volume of this waste chamber was calculated to hold the fluid from the siphon channel, before the crest back to the turbulence area. This equated to approximately 10 μL. For the two channels leading onto the waste: one acted as inlet, while the other as the air vent. The size of the collection chamber was altered also and a collection vent was added to the base of the chamber to allow easier removal of the aqueous phase, for further processing. All of these changes lead to the final working design.

7.2.2 Working Principle

Figure 5.4 shows the flow schemes for the μHomogenizer. Initially, 25 μL of blood/sample is loaded into the small loading chamber and 80 μL of TRI Reagent is added to the large loading chamber, along with 5 μL of 4-Bromoindole (BAN). The BAN acts as a separating agent to help enhance the separation of the aqueous phase (A). Next the disc is spun to a high frequency to push all the fluid from the loading chambers to the mixing chamber and up into the pneumatic arms, trapping and compressing the air inside (B). The disc spin frequency is then reduced

and the air within the pneumatic chamber pushes back, forcing the fluid back through the small turbulence area into the mixing chamber (C). This induces effective mixing of the three solutions and begins the phase separation. This compression/relaxation cycle can be performed as many times as is required as along as the disc is maintained above the burst frequency of the siphon channel. Once phase separation occurs, the aqueous phase resides on top, in the mixing chamber, leaving the interphase and organic phase in the pneumatic arms (D). Once the sample is ready for collection, the disc is spun to a lower frequency; the air expands even more within the pneumatic arms, pushing the fluid to a level in the mixing chamber that is higher than the siphon crest (E). The contents of the siphon that were unmixed are collected in the waste chamber (F) and the aqueous phase is collected in the collection chamber and can be extracted from the disc for further downstream processing and detection (G).

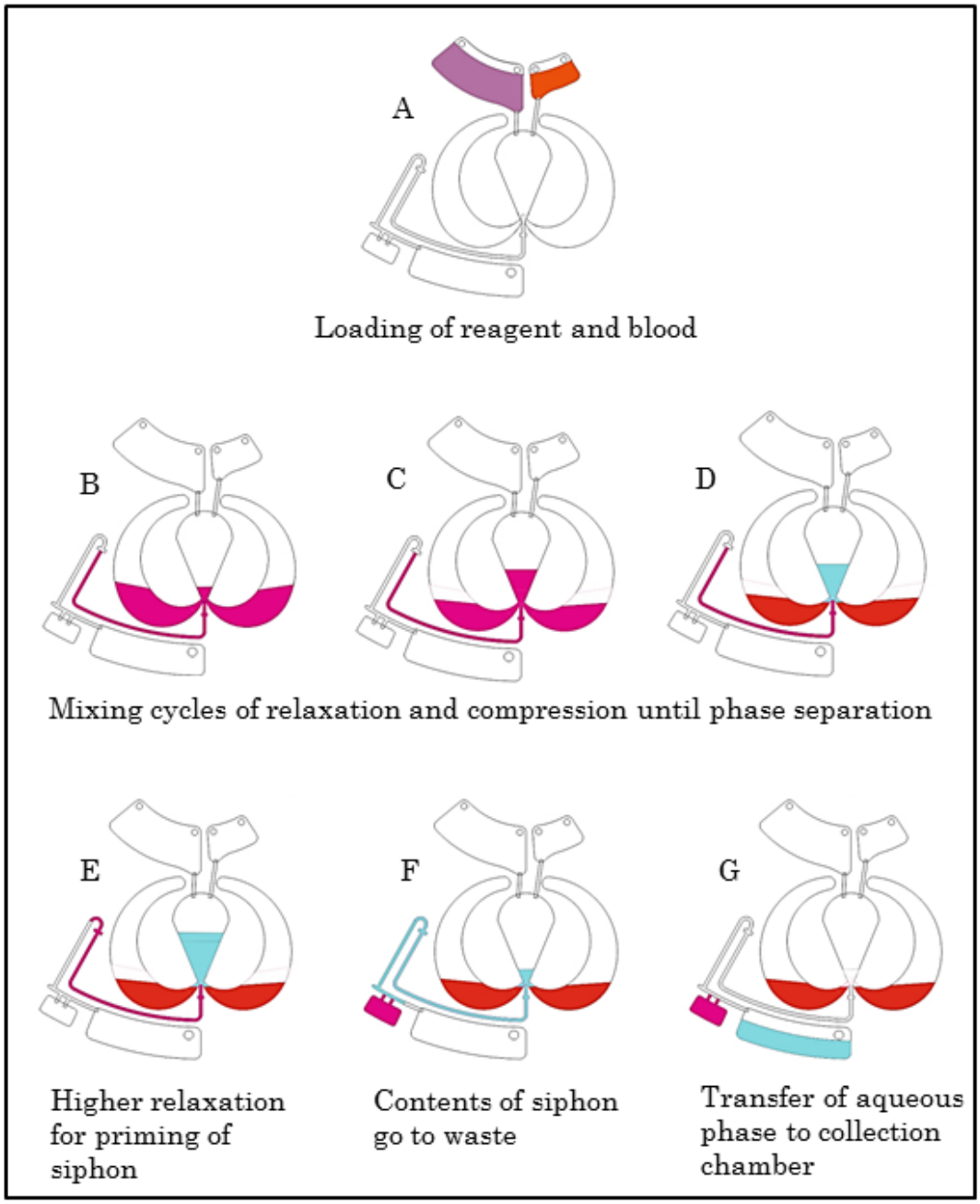

Figure 7.4: Working principle of µHomogenizer. Once solutions are loaded, the disc undergoes multiple cycles or compression and relaxation until phase separation occurs. The disc is then spun slower and the separated aqueous phase is transported over the siphon to the collection chamber. The waste chamber collects the not lysed mixture contained within the siphon.

7.2.3 Materials and Methods

7.2.3.1 Disc Fabrication

The disc (Ø 120 mm) consisted of two layers of Zeonor (Section 2.1.1) and two layers of PSA, one white, one clear. Zeonor was chosen as the polymer of choice as most other plastics offer poor chemical resistance to the harsh organic solvents (TRI Reagent and BAN) used in these experiments. The disc features were milled into a 1.5mm thick Zeonor layer using CNC machining (Section 2.1.2.2). The Zeonor discs cannot be cut using laser ablation as it absorbs too strongly in the IR and melts giving a very unclean cut. Also precision milling of various depths for the individual parts is required. This could not be achieved with the laser.

The precision knife cutter was used to cut the silhouette of the structures into the white PSA layer. These two layers were adhered with a 0.6 mm thick Zeonor layer as a base layer. Finally, a clear PSA layer was added to the top of the disc as an added protection against the harsh chemicals and to seal the collection vent (Fig. 7.5).

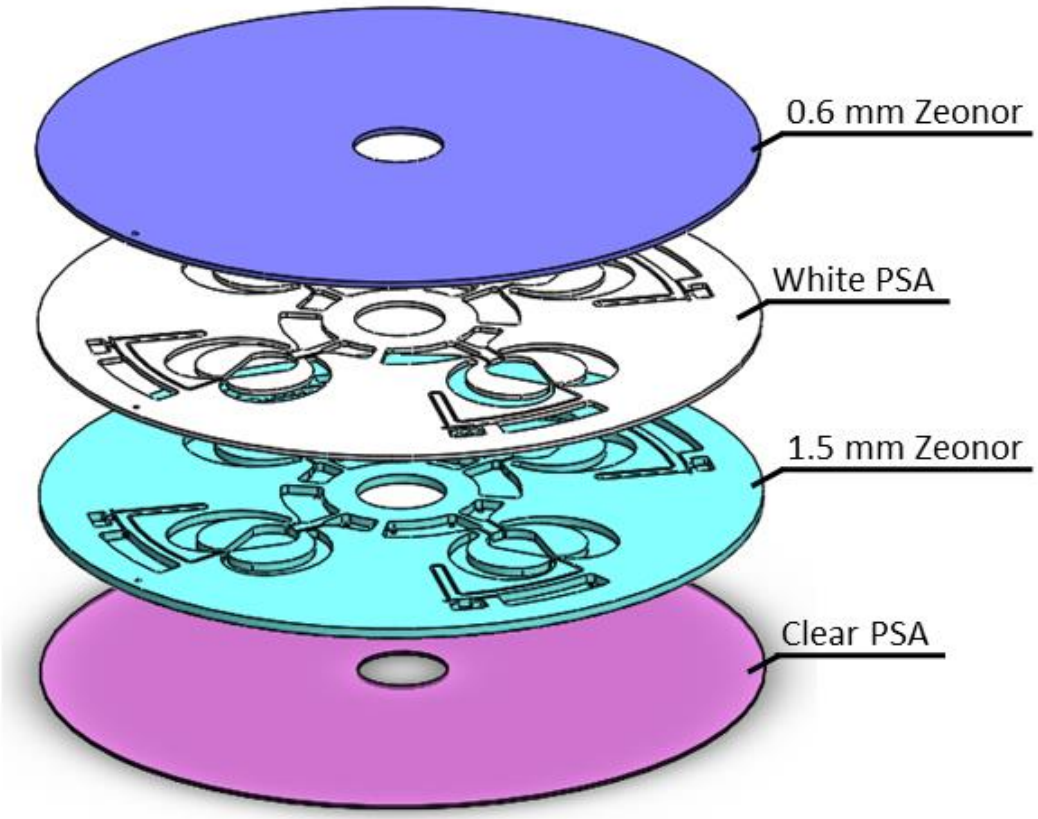

Figure 7.5: Exploded view of µHomogenizer disc. The four layer disc is made up of a 0.6 mm thick Zeonor base (blue), an 86 µm thick white PSA adhesive layer (white), a 1.5 mm thick Zeonor layer (green) which contains the milled structures and a 50 µm thick clear PSA support layer (pink).

7.2.3.2 Off-Chip Sample Processing

The extracted aqueous sample required purification before analysis. This was done on-bench. The aqueous phase was removed from the collection chamber of the disc and placed into a fresh Eppendorf tube. The RNA was then precipitated by adding 100 µL isopropanol. The sample was incubated at room temperature for 5 minutes and then spun

at 14,000 rpm for 8 minutes. The RNA precipitated in a gel-like transparent pellet at the bottom of the tube.

Without disturbing the pellet, the supernatant was exchanged to 100 µL solution of 75% ethanol (EtOH). The tubes were centrifuged for another 5 minutes. Then the EtOH was exchanged and the step was repeated.

The ethanol wash was removed and the pellet was briefly air-dried. A final water solution was added to each sample up to its initial volume and the RNA was left to dissolve at room temperature for 5 minutes. Before analysis samples were vortexed and spun down for 10 seconds.

To measure the concentration and integrity of the purified total RNA the spectrophotometer was used (Section 2.4.2.2).

7.2.4 Results and Discussion

7.2.4.1 Fluidic Validation

Experimental validation was performed to determine the optimum spin frequencies for the operation of the µHomogenizer. The final spin frequency is shown in Figure 7.6.

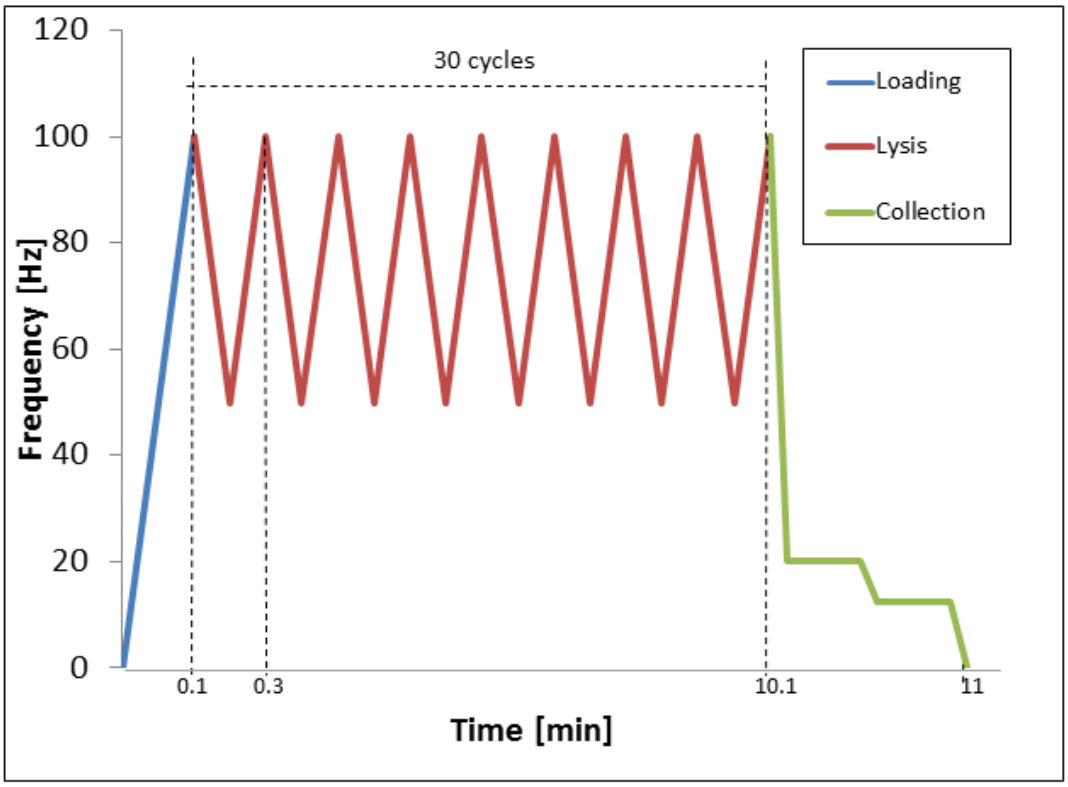

Figure 7.6: Spin frequency profile of µHomogenizer versus time. The blue line indicates the initial loading phase, the red line represents the cycling back and forth between high and low frequencies for 30 cycles and the green line show the shows the emptying and collection of the aqueous phase.

After loading the 80 µL of TRI-reagent, the 5 µL BAN and the 25 µL of sample, the disc was spun up to 100 Hz at an acceleration of 10 Hz/s, to allow the fluids to enter the mixing chamber and pneumatic arms. The compression/relaxation cycles were then performed to mix the solutions and separate the phases. The spin frequency was alternated between 100 Hz and 45 Hz, in ten second intervals for 30 cycles (for a total of 10 minutes), to allow adequate separation of the aqueous phase. The frequency was then reduced from 100 Hz to 20 Hz, the air in the pneumatic chambers pushed back even more, forcing the fluid to a level

higher than the siphon crest. The fluid therefore travelled over the siphon to the waste and collection chamber. Once the aqueous phase was fully retained with the collection chamber the spin frequency was then slowly reduced to zero to ensure no undesired mixing of the waste and collection chamber. The entire process takes ~11 minutes but each disc contains four identical structures so up to four samples can be extracted simultaneously.

7.2.4.2 Mixing Test

In order to validate the functionality of the mixing process of the μHomogenizer, a fluidic test was performed using two chemicals, potassium thiocyanate and iron nitrate, which change colour when mixed. The second iteration of the design (Fig. 7.2b) was used for the experiments. A stroboscopic fame sequence of the mixing is shown in Figure 7.7.

The image sequence shows that the mixing process worked very well on this disc, the two fluids (originally clear) were successfully mixed. It took three compression/relaxation cycles for complete mixing to occur. However, this test clearly shows the issue with having to stop the disc. The premature breaking of the siphon resulted in some of the unmixed fluid entering the collection chamber (Fig. 7.7B).

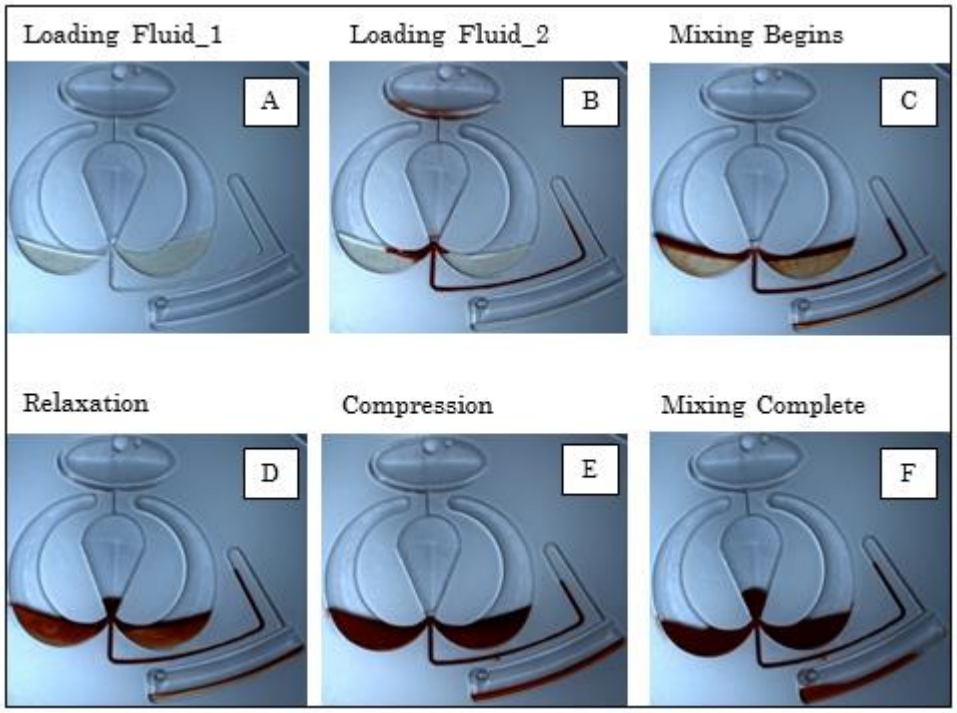

Figure 7.7: Fluidic mixing validation test of μHomogenizer. A) 80μL of Iron nitrate is loaded and the disk is spun, B) Disk is stopped and 25μL of Potassium thiocyanate is loaded and the disk is spun again, C) Mixing processes begins with compression of the air in the pneumatic arms, D) The spin speed is then reduced and the fluid relaxes, E) The disk is spun up and again the fluid compress the air and F) After multiple cycles of compression/relaxation the two fluids have successfully mixed.

7.2.4.3 TRI Reagent Extraction Test

Figure 7.8 shows the demonstration of separation of the aqueous phase from a whole blood sample using the final design iteration (Fig. 7.2c). Once again, good mixing of the TRI Reagent and blood was achieved through cycling between 100 Hz and 45 Hz. After 30 compression/relaxation cycles, separation of the aqueous phase was achieved. The disc spin frequency was then reduced and the contents of the siphon were deposited in the waste chamber and the aqueous phase

was directed to collection chamber (Fig. 7.8f). The remaining organic phase remained in the mixing arms. The extracted sample could then be removed from the disc for analysis.

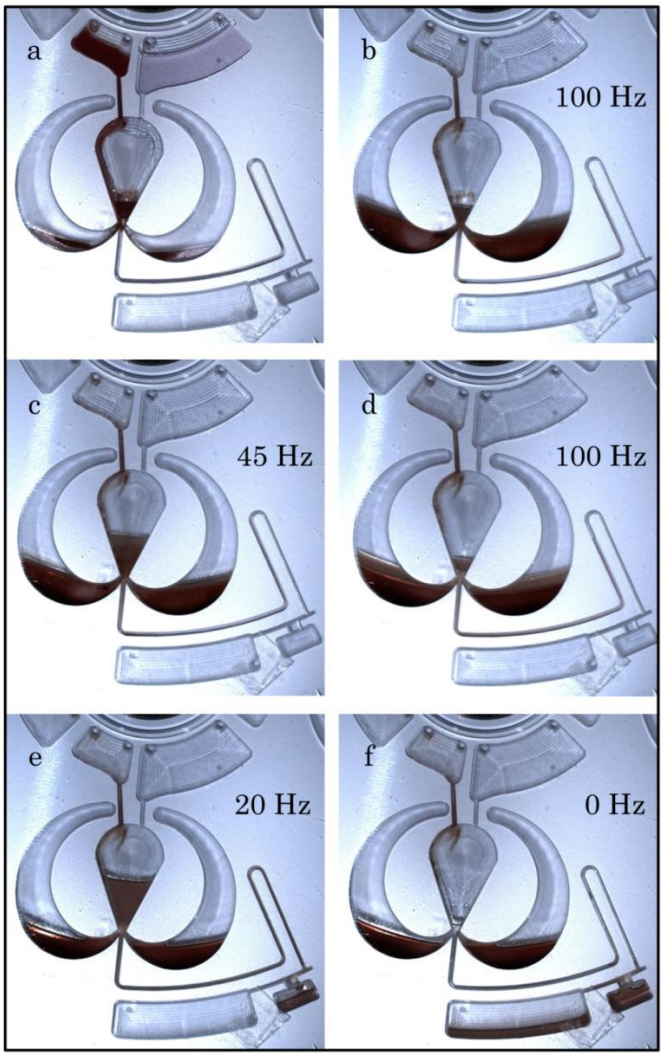

Figure 7.8: Image sequence of aqueous phase extraction from whole blood using TRI Reagent. a) Blood and TRI Reagent are loaded and the disc is spun. b, c) Mixing processes begins with the relaxation and compression of the air in the pneumatic arms. d) After 30 cycles of compression/relaxation the aqueous phase separates. e) The disc is relaxed further and the siphon primes. f) The aqueous phase from the central mixing chamber enters the separation chamber, with the waste chamber retaining the un-mixed contents of the siphon.

7.2.4.4 Biological Analysis

To determine the functionality of the system for biological testing, various quantities of *E. coli* were spiked into whole blood and total RNA was extracted into the aqueous phase using the μHomogenizer. The samples were acquired by the author and run through the Nanodrop (Section 2.4.2.2) by Dr. Nikolay Dimov (94).

Table 7.1: Average amount of total RNA extracted from whole blood spike with *E. coli*, using μHomogenizer and conventional benchtop methods. Samples were measured using the Nanodrop and each value was normalised to the initially extracted volume of the aqueous phase (n = 8) (94).

Method of sample preparation	**Volume of *E.coli* spiked into whole blood**			
	10 μL	**5 μL**	**2.5 μL**	**0 μL**
μHomogenizer	5.3 ng μL^{-1}	3.9 ng μL^{-1}	3.5 ng μL^{-1}	3.4 ng μL^{-1}
On bench	3.4 ng μL^{-1}	1.2 ng μL^{-1}	0.9 ng μL^{-1}	1.2 ng μL^{-1}

Table 7.1 shows the outcome comparison of the μHomogenizer versus benchtop methods for the extraction of total RNA from blood samples spiked with *E. coli*. The whole blood was spiked off-chip with 10 μL, 5 μL, 2.5 μL or 0 μL of *E. coli* to reach a total sample volume of 25 μL. The results show that the μHomogenizer consistently recovered higher amounts of total RNA when directly compared to the benchtop equivalent. It should be noted that the Nanodrop is incapable of differentiating between nucleic acids from the blood or the bacteria which is the reason a signal even at 0 μL of *E. coli.*

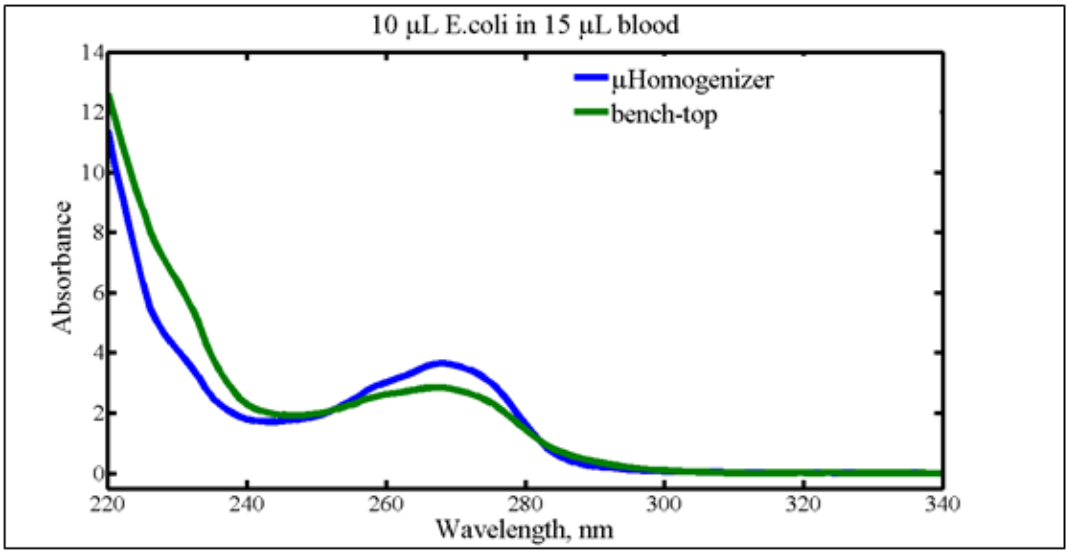

Figure 7.9: Spectra obtained from analysis of *E. coli* spiked blood using Nanodrop.

Table 7.2: Spectrophotometer ratios based on absorbance values from analysis of *E. coli* spiked blood. 260/280 & 260/230 ratios are given respectively.

Method of sample preparation	**Absorbance values**				
	230 nm	**260 nm**	**280 nm**	**260/280**	**260/280**
µHomogenizer	4.23	3.13	1.69	1.85	0.74
bench-top	6.80	2.79	1.54	1.81	0.41

The spectra shown in Figure 7.9 and the associated spectrophotometer ratios (Table 7.2) give information about the purity of the extracted samples and the efficiency of the system. Pure RNA has a 260/280 ratio of 2. The sample extracted from the µHomogenizer has a 260/280 ratio of 1.85. This indicates that there is some small contamination, possibly a result of some small amount of phenol still present in the aqueous phase. A 260/230 ratio value less than 1 indicates residual guanidine (which is part of the TRI_Reagent)

contamination. The 0.74 value obtained from the μHomogenizer sample indicates that further downstream purification is required. It should be noted though that the samples obtained from the μHomogenizer show a higher purity than the standard benchtop equivalent (94).

7.2.4.5 Inconsistency in Milling Technology

As mentioned previously, the premature priming of the siphon was an issue with this design structure. The inclusion of dual loading chambers somewhat addressed this issue, by allowing the disc to never go below the 45 Hz during the cycling phases. However, this sometimes was not fully effective, the siphon would still prime at the 45 Hz frequency. It was determined that the reason for this was inconsistency in the milling of the disc using the CNC milling machine. This inconsistency was due to mounting issues of the disc within the machine (Section 2.1.2.2). Coolant would spread in between the substrate and the machine base. This could create a compressible area whereby the tool-part would not mill away the structure but instead just push it away. If the disc was milled correctly, to the correct depths then the siphon acted as desired and the aqueous phase could be 'cleanly', extracted.

In order to determine the extent of the inconsistency of the milling procedure, the milled depths of the siphon channels on three discs were measured and compared. The siphons were labelled 1 – 4 and

a direct comparison of each siphons position within the milling device was observed. The results are shown in Figure 7.10.

Figure 7.10 shows that large variation in milled depths of the siphons even within one disc. The siphon channel was programmed to be milled to a depth of 500 μm but only one of the twelve siphons measured reached this and in-fact exceeded it. It seems that unless a disc was milled to within some small tolerance of this value the siphon could prematurely prime. The large and unpredictable variation within the siphon depths is indicative of the variation within other structures within the design. If the mixing chamber, for example, was milled too shallow then, during the relaxation phase, the fluid level would be higher than the siphon and it would prime.

This data shows an inherent limitation within the in-house milling capabilities of our lab and therefore a means by which to overcome this problem was devised.

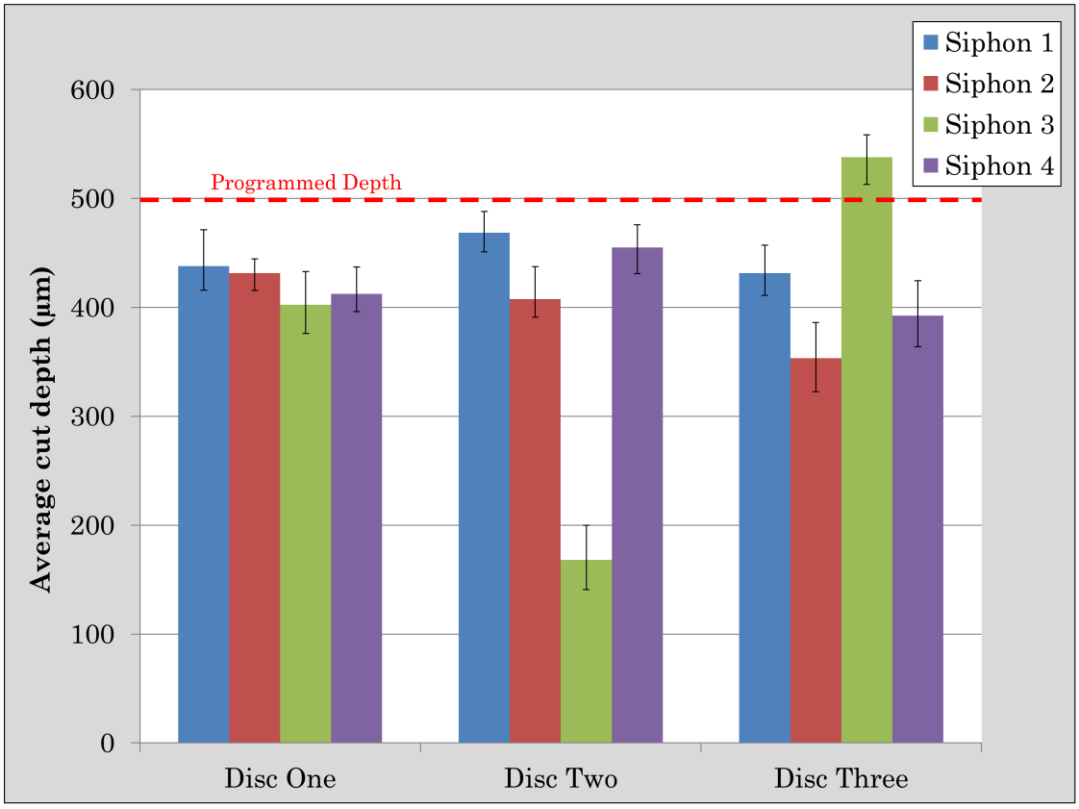

Figure 7.10: Variation in milled siphon depth for three different discs using CNC milling machine. The siphons cut in the same position on each disc were compared. The dotted red line indicates depth programmed into the CNC (500 µm). Error bars show variation with n = 3 measurements taken on the one siphon.

7.2.4.6 Event-triggered µHomogenizer System

The largest issue with the current design of the µHomogenizer is: if the discs are not milled to the correct depths then premature priming of the siphon can sometimes occur. To overcome this problem the air vent in the collection chamber was sealed at the beginning of the experiment, which created an air-trap within the siphon channel, preventing the fluid from travelling over the siphon even at low spin frequencies. This fix was not ideal, however, for two reasons. Firstly, the

disc must be stopped, and the air vent manually opened and then the disc is recommenced spinning. This is not ideal when considering the desired 'user-free' automated system. Secondly, as the disc must be stopped, the fluid level reaches a point within the mixing chamber where the organic solution is reintroduced to the aqueous phase and is ultimately collected.

In order to overcome the manufacturing limitations and the negative side-effects of the 'quick-fix', the μHomogenizer design was integrated with a variation of the previously described event-triggered valves. An image of the system is shown in Figure 7.11.

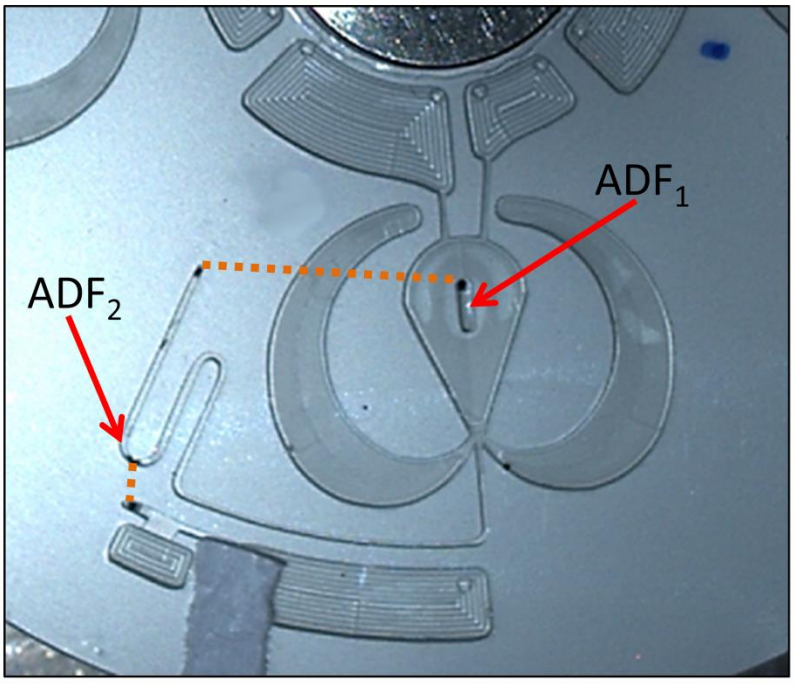

Figure 7.11: Design of event-trigger μHomogenizer. The dotted orange lines indicate channel cut into the lower layer of the discs and connecting to the holes shown.

The disc was made up of eight layers: three 0.6 mm Zeonor layers, one 1.2 mm Zeonor layer and four white PSA layers. The design was based on the μHomogenizer with some additions. An aqueous dissolvable film (ADF) tab, ADF_1, was placed within the mixing chamber. This tab sealed an air channel connected to the siphon. At the base of the siphon is a second, ADF_2, tab which blocks the entrance to the waste and collection chambers. As long as both tabs remain closed the siphon channel is air-locked and fluid will not be able to pass the crest of the siphon channel, even at low frequencies. However, once ADF_1 is dissolved, the siphon channel is open to atmosphere and the fluid can travel over the siphon and come in contact with ADF_2. The operating principle is shown in Figure 7.12 using a stroboscopic frame sequence. Note that the colour change solutions, potassium thiocyanate and iron nitrate were used.

Initially, the two solutions were loaded and the disc was spun to 100 Hz. The combined fluid entered the mixing chamber and was forced up into the side arms. Some fluid travelled down the channel at the base of mixing chamber but does not approach the siphon crest (Fig. 7.12a). This is due to the air-lock achieved by ADF_1 located in the mixing chamber. The compression/relaxation cycling was then performed, cycling back and forth between 100 Hz and 50 Hz (Fig. 7.12b, c). During this time the fluid remained far from the siphon crest. Once mixing was achieved, the frequency was reduced to 10 Hz to push the fluid to a level within the mixing chamber where it came in contact with ADF_1. The

frequency was maintained at 10 Hz for approximately 1.5 minutes to allow the film time to dissolve (Fig. 7.12d). The frequency was then increased to 20 Hz to pump the fluid up over the siphon crest and down onto ADF_2 (Fig. 7.12e). After approximately one minute the tab dissolved and the fluid travelled through the channel in the bottom layer to the waste and collection chamber. An increase in spin frequency to 50 Hz was used to enhance emptying (Fig. 7.12f).

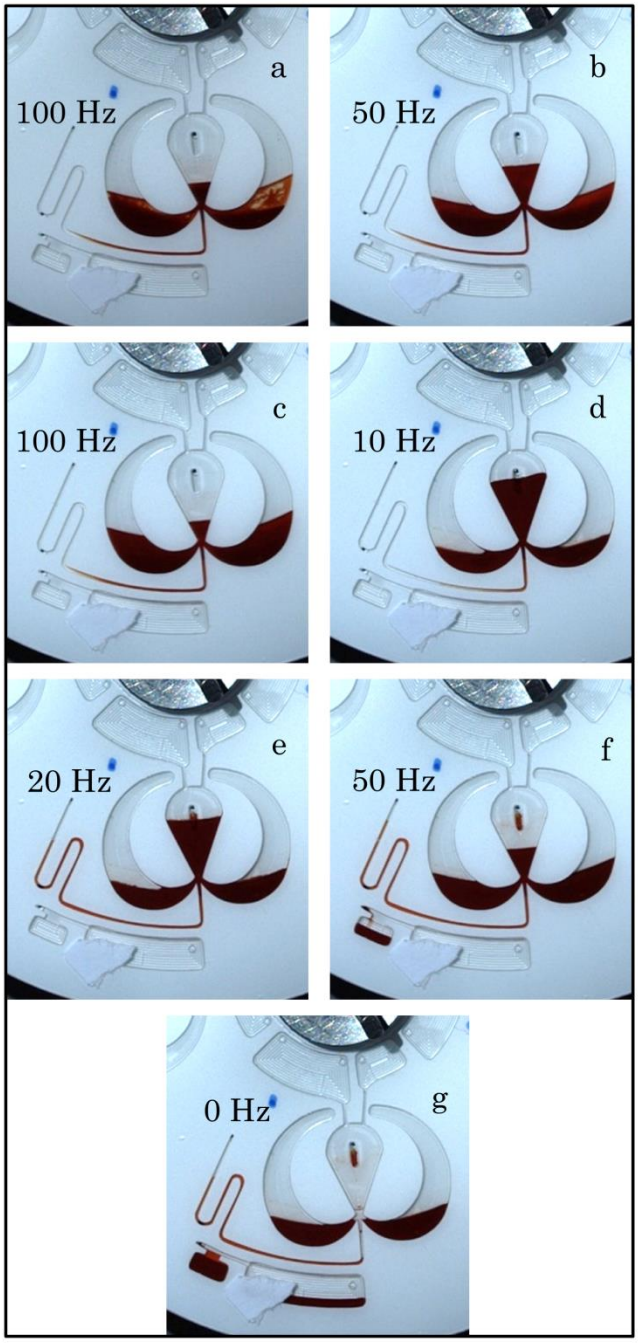

Figure 7.12: Image sequence of operating principle of event-triggered µHomogenizer. a) At high spin frequency air is compressed within pneumatic arms by the fluid. b) Upon reduction of spin rate, air pushes back and fluid is pushed back into central mixing chamber. c) Compression/relaxation cycle continues with fluid still air-locked away from siphon crest. d) Spin rate further reduced and fluid contacts with ADF_1. e) Slight increase in spin rate to encourage fluid over the now open siphon. f) Fluid dissolves ADF_2. g) Fluid is directed into waste and collection chambers.

This novel modification of the event-triggered system allows the dissolution of the valve to be achieved not by an ancillary fluid but by the aqueous phase of the extracted sample and it eliminates errors associated with limitations of milling technologies.

7.3 Mechanical Cell Lysis of Nucleic Acids

An alternative method of nucleic acid extraction to the chemical cell lysis is mechanical cell lysis. Mechanical lysis involves the rupturing of the cell wall through piercing, breaking or tearing to allow the access the inner contents of the cell.

Mechanical lysis is of particular importance when dealing with cell-types that have rigid cell walls. Mammalian cells tend to be more shear-sensitive and require far less energy to disrupt the cell wall. Yeast and similar fungi, as well as gram positive bacteria, in contrast, have a much stronger cell membrane and are far more resistant to disruption.

Some methods of mechanical cell lysis were discussed in Section 1.5.2.1. A recent advancement of particular interest to the author was described by Millis *et al.* (95). The work presented a new method of mechanical cell lysis of algae cells, based on the ancient 'Norse Mill' design. The Norse Mill is a horizontal mill used to grind flour using a water driven stone millstone. Millis designed a microscale lab-on-a-chip technology based on this concept (Fig. 7.13).

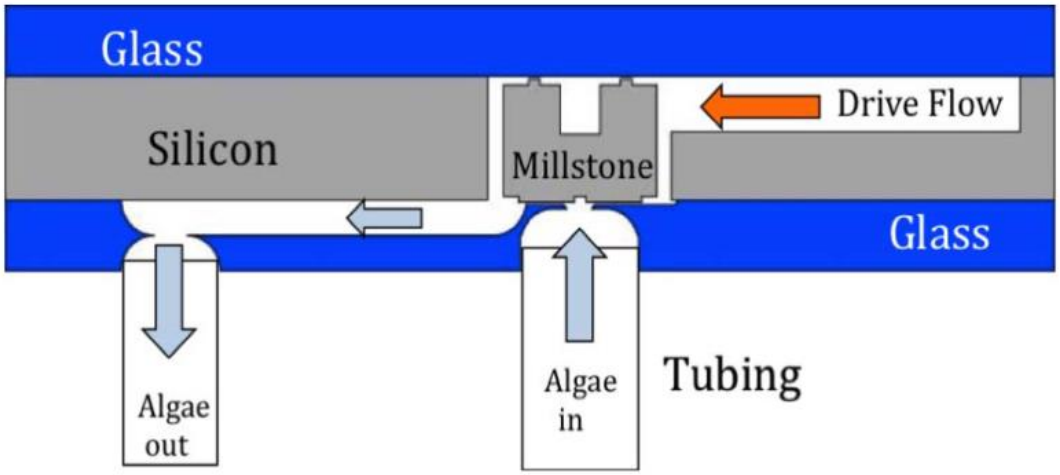

Figure 7.13: Schematic of cross-section of flow driven mill. Algae sample enters at the base of the millstone and exits through the adjacent channel. The millstone's rotation is driven by a flow on the top. Adapted from Millis *et al.* 2015 (95).

A rotating microfabricated millstone is embedded within the chip. Two microchannels connect to the top and bottom of the mill: one to provide the fluid flow to rotate the mill (using a set of vanes on the mill's upper side) and one channel that supplies the algae sample to the grinding surface. The system was determined to have a 70% lysing efficiency, even with a smooth mill stone surface.

The main disadvantage of this system is its time consuming and high cost manufacturing requirements. The millstone, including the vanes and grinding surface, with any texturing required, must be fabricated out of a single silicon wafer using photolithography and Deep Reactive Ion Etching, both of which are time consuming processes (95). Also the use of an ancillary fluid, used to rotate the millstone, adds a secondary source of complexity and possible source of contamination.

A design concept was devised based on this system which utilises a rotor stator grinding mill driven by the spindle motor. The system uses the inherent rotation of our spin stand, which acts against a concentrically held stator, through which the sample is loaded. This system would be useful for a general lysis/ homogenization scheme used, for example in the area of food or environment samples with prior unknown viscosity/consistency. This type of system would also be beneficial in reducing the need for potentially harmful chemical reagents, which may interfere with downstream assays.

This work is predominantly proof-of-principle, and I demonstrate the design of a working fluidic model.

7.3.1 System Design

As shown in Figure 7.14, the system consists of a standard disc (Ø 120 mm) with three 1.5 mm thick PMMA layers, held together using two 86 μm thick white PSA layers. Embedded within the disc is a 2 mm thick PMMA layer which acts as the stator. The entire underside of the stator has been rastered, using the laser cutter, to increase the surface roughness.

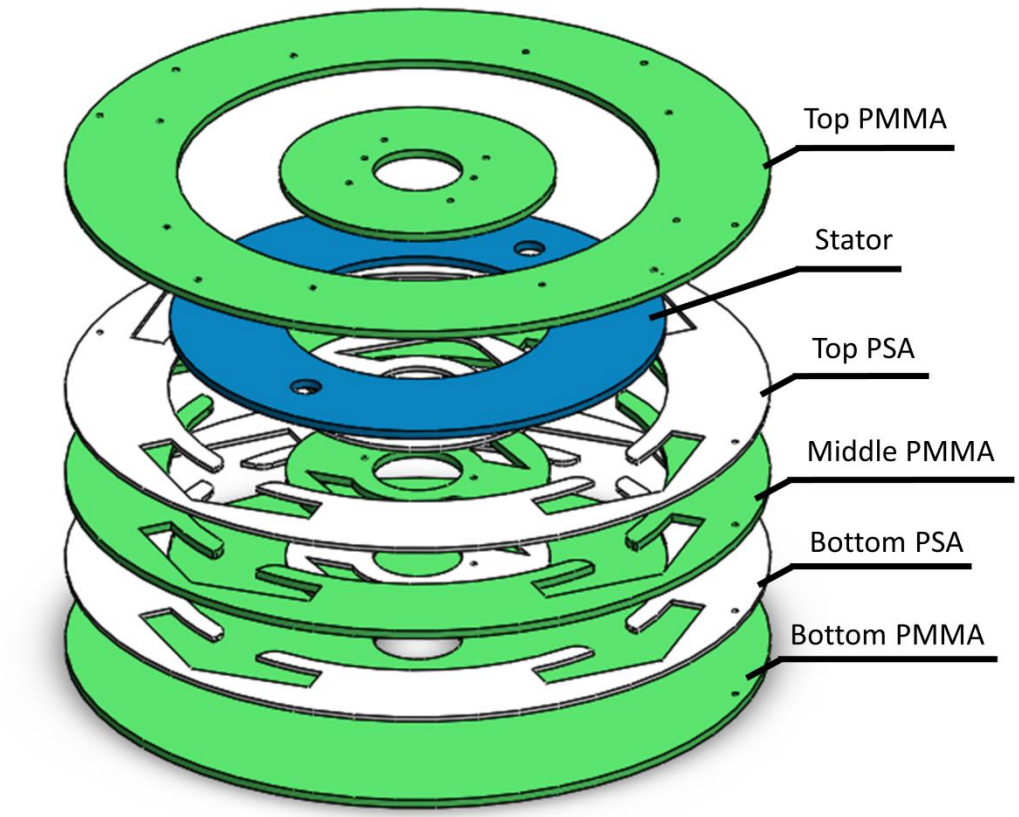

Figure 7.14: Exploded view of stator rotor disc design. The disc consists of three PMMA layers (green) held together by two PSA layers (white). The PMMA stator (blue) is embedded within the device.

A top down view of the system can be seen in Figure 7.15a. The design consists of a two loading chambers connected via channels on the Bottom PSA layer to the underside of the stator ring. At the outer edge of the disc are four collection chambers, evenly dispersed around the disc. The collection chambers are not in direct line with the loading chambers so as to increase the fluids time in contact with the stator ring. The stator ring contains two holes which are used to hold the ring stationary, while the rest of the disc spins around it.

A cross-sectional view of the structure can be seen in Figure 7.15b. It shows one side of the disc and the arrows indicate the direction of fluid flow. Note that the fluid flows under the stator ring which is in direct contact with the Bottom PMMA layer.

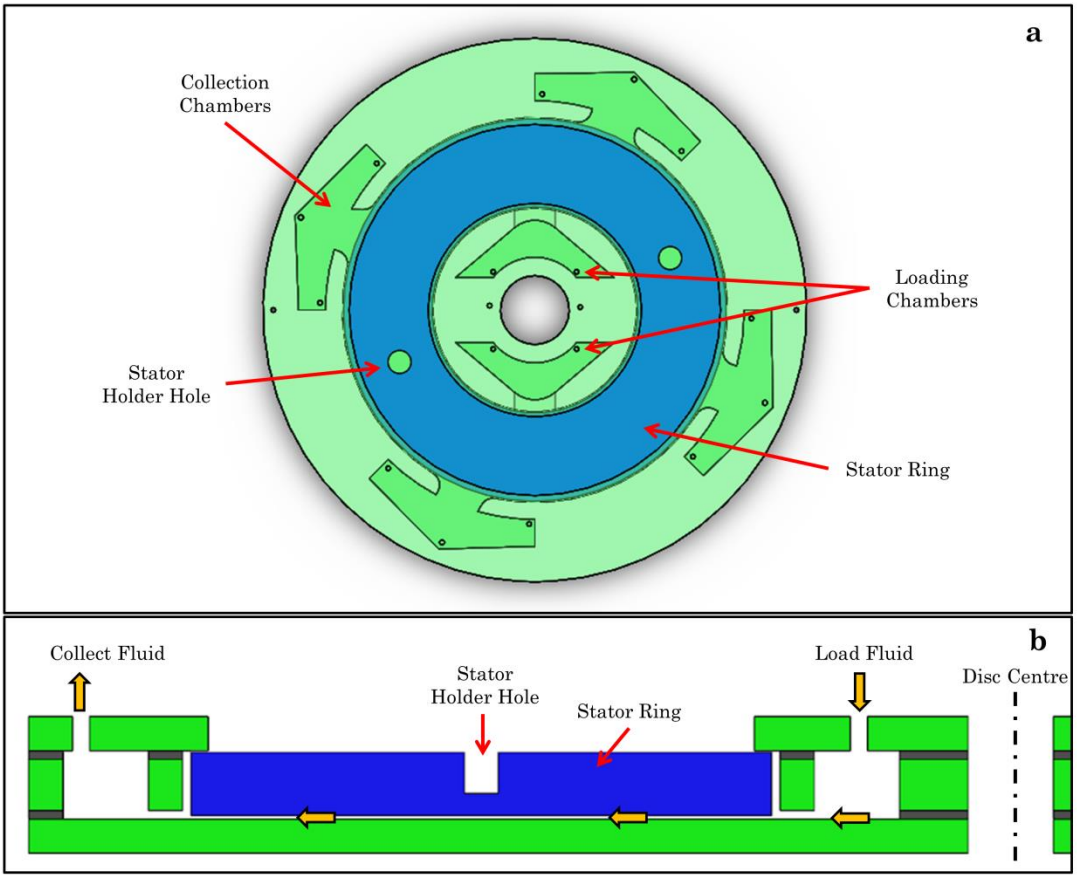

Figure 7.15: Schematic of stator rotor disc. a) Top down view of disc design showing all the functional part. b) Cross-sectional view of system design. Yellow arrows indicate the direction of fluid flow.

7.3.2 Working Principle

The stator rotor disc design works by using the inherent spin capabilities of the spin stand. In order for the design to work the central

stator ring must be held stationary while the remainder of the disc turns in the conventional manor. To achieve this, a holder was designed which could be attached to the spin stand (Section 2.3). The holder assembly is shown in Figure 7.16.

The holder is comprised of four parts: an upper mount, a lower mount and two PMMA sections. The lower and upper mounts are 3D printed (Section 2.1.2.4) and the PMMA sections are cut using the laser cutter. The lower mount contains two plugs which are inserted into the holes of the stator ring. It also has two insets to align it with the upper mount. The position of the lower mount with the upper mount can be adjusted manually to allow for best contact with the disc. The hole in the centre of the upper and lower mount allows space for the disc to be screwed to the spindle motor of the spin stand. The two L-shaped PMMA sections are 3 mm thick and slot into the upper mount. These PMMA sheets are then screwed to the metal box surrounding the spindle motor (Section 2.3, Fig. 2.5). The clear PMMA sheets allow visibility of the collection chambers.

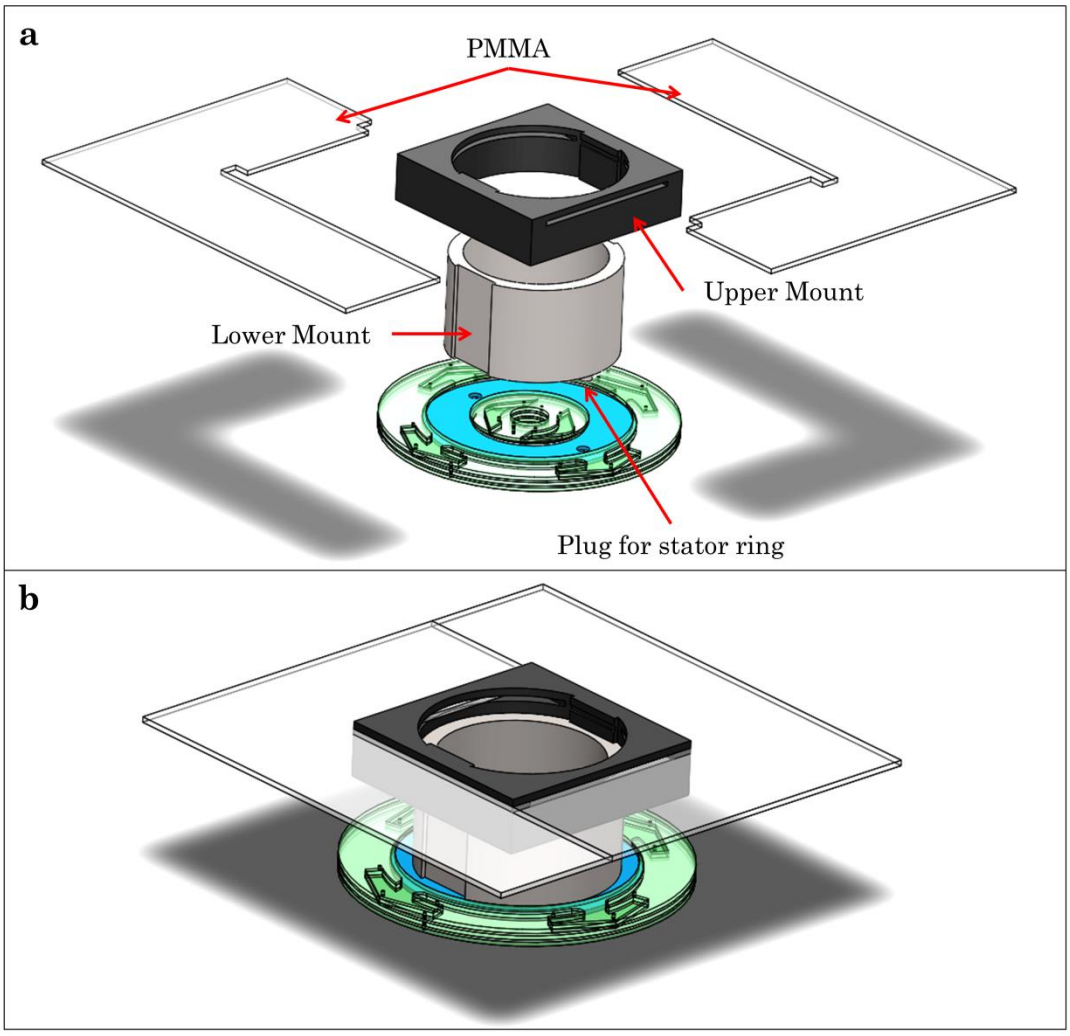

Figure 7.16: Schematic of stator rotor holder which attached to the spin stand. a) Exploded view of the functional components of the holder. b) Assembled view of the holder.

A 400 µL volume, containing cells to be lysed, can be loaded into each of the loading chambers. Under centrifugation the stator ring remains stationary while the rest of the disc rotates. As the disc spins, the fluid leaves the loading chamber and travels below the stator ring. The ring offers some resistance to the fluids passage outwards and it travels around the surface somewhat before entering the collect chambers. This was tested by adding one of the two colour change

chemicals, potassium thiocyanate and iron nitrate, to each loading chamber. The fluids collected from the collection chamber had completely mixed, showing that the fluids do not travel directly outwards.

7.3.3 Bio-Analysis Possibilities

In order to test the viability of the system for cell lysis, *E. coli* cells in LB broth media were passed through the system. The efficacy of cell lysing was accessed using a traditional microscope and a 3D microscope (Section 2.4.1.1) and a hemocytometer (Section 2.4.2.4). The quantities of cells in a 7 µL volume (assuming good homogeneity of the sample) were counted before and after passing through the stator rotor disc.

Unfortunately, this test was unsuccessful as the number of cells counted before and after was almost identical. It was determined that *E. coli* cells are too small to be lysed using this system. An average *E. coli* cell has a size of ~ 1 x 3 µm (96) versus the size of Alexandrium tamarense (the algae used by Millis *et al.*) of 22 – 51 µm in length and 17 – 44 µm in width (97). It was therefore determined that a larger cell type would be needed to demonstrated the viability of this system.

7.4 Conclusion

This chapter described the development of two separate nucleic acid extraction platforms. The first is a novel centrifugo-pneumatic 'μHomogenizer', which implements a 3-phase fluid extraction protocol of RNA. This system builds on the work of Linares *et al.* (53) to integrate chemical lysis and separation of the RNA containing aqueous phase and show significant improvement over its time-consuming and labour intensive benchtop alternate. The second is the development of a mechanical lysis method that utilises a rotor stator grinding mill driven by the spindle motor. This system could be used for general lysis of a wide range of cell types but would be of significant benefit for armoured cells. It would also be beneficial in reducing the need for potentially harmful chemical reagents, which might interfere with downstream assays.

Chapter 8

Conclusion and Future Work

8.1 Conclusions

In this work the development of novel flow control methods on centrifugal microfluidic platforms for nucleic acid testing was shown. Flow control is of the utmost importance in centrifugal microfluidics, where the centrifugal field acts concurrently on all parts of the disc.

The inclusion of functional materials within these Lab-on-a-Disc structures opens up new avenues for sample-to-answer devices. This is especially important in biological diagnostics, such as nucleic acid testing, where the main bottleneck in performing these processes on microfluidic devices is in sample preparation.

Nucleic acid testing can be broken into three stages: extraction purification and detection. The solid-phase purification process requires

the sequential handling of multiple aqueous and organic solutions. The difficulty lies in being able to sequentially handle all these different fluids, but to ultimately collect a sample which is uncontaminated by them.

To that end, the work demonstrated in this report focused on two separate methods of nucleic acid purification. The first was the development of a solvent-selective router which integrated two solvent specific valves into a multilayer microfluidic disc: a dissolvable film membrane, which dissolves when it comes in contact with an aqueous solution but is completely resistance to organic solutions and a PTFE-supported hydrophobic membrane, which is impermeable to aqueous solutions but allows water to pass through. The development of the system from a simple router to the more complex design, capable of handling the four fluids, was demonstrated. The performance of the system was evaluated for the purification of total RNA from MCF7 cell homogenate. The capability of the system to purify total RNA with significant integrity and concentration through an automated, rotationally controlled process was shown.

The second method of solid-phase purification arose from the integration of multilayer Graphene Oxide (GO) membranes into our microfluidic structures. GO offers unique properties as a flow control element in microfluidics. Notably, I demonstrated two such properties of the GO membranes: their solvent selectivity and air impermeability.

Beyond a specific burst pressure, GO membranes allow water to pass through with very low flow resistance; however, it completely blocks organic solutions or air, even at high pressure heads. I first developed a method for inclusion of the GO into polymeric microfluidic systems. I then used those devices to investigate and characterise the capabilities of the GO.

A novel, centrifugo-pneumatic scheme for solvent-selective routing of organic and aqueous flows based on an integrated GO membrane was demonstrated. I then implemented a sequential, multi-reagent protocol geared towards automated solid-phase purification of nucleic acids with a sequence of washing and elution steps with aqueous and organic fluids. This second routing system improved on the first in that the integration of a single membrane is capable of handling all the various fluids needed for this complex process, as well as significantly reducing manufacturing and fabrication processes. The GO router was further developed by combining it with an event-triggered valving scheme first developed by Kinahan *et al.* (27). The router system was used to purify DNA and it was shown that, despite the low yield of DNA, the router is a significant improvement on the highly labour-intensive benchtop equivalent and uses significantly reduced sample volumes. Its ease of manufacturing and simple to use system offers significant benefits for point-of-care uses.

The final chapter focused on the upstream part of the nucleic acid testing protocol, extraction. To this end, two separate extraction platforms were developed. The first was a novel centrifugo-pneumatic 'μHomogenizer', which implements a 3-phase fluid extraction protocol of RNA. This system built on the work of Linares *et al.* (53) to integrate chemical lysis and separation of the RNA containing aqueous phase and showed significant improvement of its time-consuming and labour intensive benchtop alternate. The system was further advanced by combining it with a modified event-triggered system. This novel modification of the event-triggered system allows the dissolution of the valve to be achieved not by an ancillary fluid but by the aqueous phase of the extracted sample and it eliminates errors associated with limitations of milling technologies.

The second extraction system showed the design of a mechanical lysis method that utilises a rotor stator grinding mill driven by the spindle motor. This system could be used for general lysis of a wide range of bacteria but would be of significant benefit for armoured cells. It would also be beneficial in reducing the need for potentially harmful chemical reagents, which might interfere with downstream assays.

8.2 Future Work

Building on this work, there are several strands which could be explored.

8.2.1 Further Investigation of GO Capabilities

Though a significant number of capabilities of the GO membranes were investigated during the course of this thesis, there are still a range of areas which could be explored. The possibly of using the membranes for filtration purposes may be useful in environmental analysis where it is important to remove larger particulates before testing. The capability of using the membranes for desalination could also be investigated. Desalination is currently a very slow process in microfluidics (98); Cohen-Tanugi *et al.* theorised the use of graphene membranes for this purpose (99). Also, though it was shown that DNA passed freely through the GO membranes, it was not clear whether all sizes of DNA would do so. The GO could possibly be used for size separation of DNA. Finally, the interaction of RNA with the GO membrane should be investigated. RNA is far more susceptible to degradation and so may be affected by the membrane.

8.2.2 Increase of NA Purification Yield

The results given in Chapters 3, 5 and 6 shows that relatively small quantities of DNA and RNA are being recovered from the discs after purification. The possible reasons for this are discussed in the relevant chapters but there are some broad solutions which may help to enhance the yield:

1. An investigation of the possible points of loss of the DNA should be undertaken. By fluorescently tagging the DNA and performing the experiments, the discs could then be viewed under a fluorescent microscope to show the positions on the disc where DNA is being trapped.
2. In the case of the GO Router system, the first flowed through solution was analysed but the organic washes were not collected and tested (Section 5.4.2.2). By passing this solution through a spin column the loss due to the organic washes could be determined.
3. The solid phase could be changed. The use of silica beads may not be the most efficient capture media. The integration of a silica membrane, such as those used in the spin columns, may help improve the capture efficiency.
4. There is a possibly that the DNA is binding to the polymer surfaces. The use of a blocking agent such as BSA may help prevent this.
5. In the case of the EGOR (Chapter 6), the DNA may be sticking to the PSA base. Removing that PSA layer may stop this from happening.
6. In order to try and enhance the binding and release efficiency, the contact time of the fluids with the beads could be increased and drying steps could be implemented. Adjustments to the pH or salt concentrations may also have an effect.

8.2.3 NA Extraction Advancement

The NA extraction systems shown in Chapter 7 could be further advanced. With the μHomogenizer, the functionality of the system for RNA extraction was shown, however there is further optimisation and characterisation that can be undertaken. The optimum number of compression relaxation cycles needs to be biologically validated. The 30 cycle number was determined through visual inspection of the separating solutions but the point at which optimum extraction efficiency occurs should be determined.

The mechanical rotor system, shown here, was a proof of principle concept that has only been shown to work fluidically, and its inability to lyse *E.coli* cells was discussed. The next stage in the process should be to characterise the system fully to determine the effect of varying raster depths, to show cell lysis with larger and/or armoured cells and to determine if the mechanical grinding will damage the DNA/RNA.

8.2.4 Design of Full Sample-to-Answer System

The systems described in this thesis are all individual parts capable of performing the sample preparation aspects of NA testing The ultimate goal is to combine these aspects together into a singular device. The device should be capable of taking in a sample, running all the necessary extraction (using the μHomogenizer or Stator rotor) and purification (using the EGOR system) steps and performing on-board

detection. In order to allow for POC capabilities, instrumentation needs to be developed that would allow the operation of this integrated system, in a simple and straight-forward manner.

References

1. Clerc O, Greub G. Routine use of point-of-care tests: usefulness and application in clinical microbiology. Clin Microbiol Infect. 2010 Aug;16(8):1054–61.

2. Chen WY. Measuring the Effectiveness of Mammography. JAMA Oncol. American Medical Association; 2015 Oct 20;1(8):1.

3. Saravolatz LD, Manzor O, VanderVelde N, Pawlak J, Belian B. Broad-range bacterial polymerase chain reaction for early detection of bacterial meningitis. Clin Infect Dis. 2003 Jan 1;36(1):40–5.

4. Yager P, Domingo GJ, Gerdes J. Point-of-care diagnostics for global health. Annu Rev Biomed Eng. 2008 Jan;10:107–44.

5. Diabetes.co.uk. Blood Glucose Testing [Internet]. 2015 [cited 2015 Dec 26]. Available from: http://www.diabetes.co.uk/blood-glucose/blood-glucose-testing.html

6. Siemens. Point of Care Testing.

7. Radisen Diagnostics. Radisens Diagnostics – Integrated Multi-mode Point-of-Care Diagnostics » Radisens Technology [Internet]. [cited 2015 Dec 26]. Available from: http://www.radisens.com/technology/

8. Abraxis. Piccolo Xpress [Internet]. [cited 2015 Dec 26]. Available from: http://www.piccoloxpress.com/products/piccolo/overview/

9. Lee BS, Lee J-N, Park J-M, Lee J-G, Kim S, Cho Y-K, et al. A fully automated immunoassay from whole blood on a disc. Lab Chip. The Royal Society of Chemistry; 2009 Jun 7;9(11):1548–55.

10. Lee BS, Lee YU, Kim H-S, Kim T-H, Park J, Lee J-G, et al. Fully

integrated lab-on-a-disc for simultaneous analysis of biochemistry and immunoassay from whole blood. Lab Chip. The Royal Society of Chemistry; 2011 Jan 7;11(1):70–8.

11. Dineva MA, MahiLum-Tapay L, Lee H. Sample preparation: a challenge in the development of point-of-care nucleic acid-based assays for resource-limited settings. Analyst. 2007 Dec;132(12):1193–9.

12. Lee HH, Dineva MA, Chua YL, Ritchie A V, Ushiro-Lumb I, Wisniewski CA. Simple amplification-based assay: a nucleic acid-based point-of-care platform for HIV-1 testing. J Infect Dis. 2010 Apr 15;201 Suppl(Supplement_1):S65–72.

13. Park BH, Jung JH, Zhang H, Lee NY, Seo TS. A rotary microsystem for simple, rapid and automatic RNA purification. Lab Chip. The Royal Society of Chemistry; 2012 Oct 21;12(20):3875–81.

14. Sun Y, Høgberg J, Christine T, Florian L, Monsalve LG, Rodriguez S, et al. Pre-storage of gelified reagents in a lab-on-a-foil system for rapid nucleic acid analysis. Lab Chip. The Royal Society of Chemistry; 2013 Apr 21;13(8):1509–14.

15. Cordray MS, Richards-Kortum RR. Emerging nucleic acid-based tests for point-of-care detection of malaria. Am J Trop Med Hyg. 2012 Aug;87(2):223–30.

16. Chin CD, Linder V, Sia SK. Commercialization of microfluidic point-of-care diagnostic devices. Lab Chip. 2012 Jun 21;12(12):2118–34.

17. Chakraborty S. Microfluidics and Microfabrication. 1st ed. New York Springer; 2010.

18. Ducrée J, Haeberle S, Lutz S, Pausch S, Stetten F Von, Zengerle

R. The centrifugal microfluidic Bio-Disk platform. J Micromechanics Microengineering. 2007 Jul 1;17(7):S103–15.

19. Gorkin R, Park J, Siegrist J, Amasia M, Lee BS, Park J-M, et al. Centrifugal microfluidics for biomedical applications. Lab Chip. 2010 Jul 21;10(14):1758–73.

20. Oh KW, Ahn CH. A review of microvalves. J Micromechanics Microengineering. 2006;16(5):R13–39.

21. Siegrist J, Gorkin R, Clime L, Roy E, Peytavi R, Kido H, et al. Serial siphon valving for centrifugal microfluidic platforms. Microfluid Nanofluidics. 2009 Nov;9(1):55–63.

22. Chen JM, Huang P-C, Lin M-G. Analysis and experiment of capillary valves for microfluidics on a rotating disk. Microfluid Nanofluidics. 2007 Jul 27;4(5):427–37.

23. Siegrist J, Gorkin R, Clime L, Roy E, Peytavi R, Kido H, et al. Serial siphon valving for centrifugal microfluidic platforms. Microfluid Nanofluidics. 2009 Nov 4;9(1):55–63.

24. Gorkin R, Nwankire CE, Gaughran J, Zhang X, Donohoe GG, Rook M, et al. Centrifugo-pneumatic valving utilizing dissolvable films. Lab Chip. 2012 Aug 21;12(16):2894–902.

25. Park J, Cho Y, Lee B, Lee J, Ko C. Multifunctional microvalves control by optical illumination on nanoheaters and its application in centrifugal microfluidic devices. Lab Chip. 2007;7:557–64.

26. van der Linden HJ, Herber S, Olthuis W, Bergveld P. Stimulus-sensitive hydrogels and their applications in chemical (micro)analysis. Analyst. The Royal Society of Chemistry; 2003 Apr 7;128(4):325–31.

27. Kinahan DJ, Kearney SM, Dimov N, Glynn MT, Ducrée J. Event-triggered logical flow control for comprehensive process integration

of multi-step assays on centrifugal microfluidic platforms. Lab Chip. 2014 Jul 7;14(13):2249–58.

28. Mishra R, Alam R, Kinahan DJ, Anderson K, Ducree J. Lipophilic-membrane based routing for centrifugal automation of heterogeneous immunoassays. 2015 28th IEEE International Conference on Micro Electro Mechanical Systems (MEMS). IEEE; 2015. p. 523–6.

29. Kim J, Hee Jang S, Jia G, Zoval J V, Da Silva NA, Madou MJ. Cell lysis on a microfluidic CD (compact disc). Lab Chip. The Royal Society of Chemistry; 2004 Oct 7;4(5):516–22.

30. Brenner T, Glatzel T, Zengerle R, Ducrée J. Frequency-dependent transversal flow control in centrifugal microfluidics. Lab Chip. The Royal Society of Chemistry; 2005 Jan 24;5(2):146–50.

31. Haeberle S, Pausch S, Burger R, Lutz S, Stetten F von, Zengerle R, et al. Automation of nucleic acid extraction by a Coriolis-force actuated droplet router. Proceedings of the 11th International Conference on Miniaturized Systems for Chemistry and Life Sciences (μTAS 2007). Paris; 2007. p. 1231–3.

32. Kloke A, Fiebach AR, Zhang S, Drechsel L, Niekrawietz S, Hoehl MM, et al. The LabTube - a novel microfluidic platform for assay automation in laboratory centrifuges. Lab Chip. 2014 May 7;14(9):1527–37.

33. Haeberle S, Zengerle R. Microfluidic platforms for lab-on-a-chip applications. Lab Chip. 2007 Sep;7(9):1094–110.

34. Madou M, Zoval J, Jia G, Kido H, Kim J, Kim N. Lab on a CD. Annu Rev Biomed Eng. Annual Reviews; 2006 Jan 11;8:601–28.

35. Gorkin R, Clime L, Madou M, Kido H. Pneumatic pumping in centrifugal microfluidic platforms. Microfluid Nanofluidics. 2010

Feb 17;9(2-3):541–9.

36. Noroozi Z, Kido H, Micic M, Pan H, Bartolome C, Princevac M, et al. Reciprocating flow-based centrifugal microfluidics mixer. Rev Sci Instrum. 2009 Jul;80(7):075102.

37. Grumann M, Geipel A, Riegger L, Zengerle R, Ducrée J. Batch-mode mixing on centrifugal microfluidic platforms. Lab Chip. 2005 May;5(5):560–5.

38. Ng AHC, Uddayasankar U, Wheeler AR. Immunoassays in microfluidic systems. Anal Bioanal Chem. 2010;397(3):991–1007.

39. Pratt ED, Huang C, Hawkins BG, Gleghorn JP, Kirby BJ. Rare Cell Capture in Microfluidic Devices. Chem Eng Sci. 2011 Apr 1;66(7):1508–22.

40. Zare RN, Kim S. Microfluidic Platforms for Single-Cell Analysis. Annual Reviews; 2010 Jul 9;

41. Dineva MA, Mahilum-Tapay L, Lee H. Sample preparation: a challenge in the development of point-of-care nucleic acid-based assays for resource-limited settings. Analyst. The Royal Society of Chemistry; 2007 Nov 19;132(12):1193.

42. Sidransky D. Nucleic Acid-Based Methods for the Detection of Cancer. Science (80-). 1997 Nov 7;278(5340):1054–8.

43. McCalla SE, Tripathi A. Microfluidic reactors for diagnostics applications. Annu Rev Biomed Eng. Annual Reviews; 2011 Aug 15;13:321–43.

44. Heneghan HM, Miller N, Kelly R, Newell J, Kerin MJ. Systemic miRNA-195 differentiates breast cancer from other malignancies and is a potential biomarker for detecting noninvasive and early stage disease. Oncologist. 2010 Jan;15(7):673–82.

45. Wheelwright SM. Protein Purification: Design and Scale Up of Downstream Processing. Hanser-Gardner Publications; 1991. 228 p.

46. Dahm R. Discovering DNA: Friedrich Miescher and the early years of nucleic acid research. Hum Genet. 2007 Sep 28;122(6):565–81.

47. TRI Reagent® Protocol | Sigma-Aldrich [Internet]. [cited 2015 Dec 28]. Available from: http://www.sigmaaldrich.com/technical-documents/protocols/biology/tri-reagent.html

48. Boom R, Sol CJ, Salimans MM, Jansen CL, Wertheim-van Dillen PM, van der Noordaa J. Rapid and simple method for purification of nucleic acids. J Clin Microbiol. 1990 Mar;28(3):495–503.

49. O'Connor L, Glynn B. Recent advances in the development of nucleic acid diagnostics. Expert Rev Med Devices. Taylor & Francis; 2014 Jan 9;

50. Cho Y-K, Lee J-G, Park J-M, Lee B-S, Lee Y, Ko C. One-step pathogen specific DNA extraction from whole blood on a centrifugal microfluidic device. Lab Chip. The Royal Society of Chemistry; 2007 May 2;7(5):565–73.

51. Than Linh Quyen, Sun Yi, Wei Hoe Chin, Tran Quang Hung, Sannah Jardenbæk AW and DDB. Eight-chamber microfluidic device with integrated loop mediated isothernmal amplification (LAMP) for multiple detection of Campylobacter spp from pig at slaughter. Proceedings of The18th International Conference on Miniaturized Systems for Chemistry and Life Sciences. 2014. p. 1930–2.

52. Sun Y, Quyen TL, Hung TQ, Chin WH, Wolff A, Bang DD. A lab-on-a-chip system with integrated sample preparation and loop-mediated isothermal amplification for rapid and quantitative detection of Salmonella spp. in food samples. Lab Chip. The Royal

Society of Chemistry; 2015 Apr 21;15(8):1898–904.

53. Linares A V, Iii RG, Glynn B, Godino N, Miller N, Kerin M, et al. Purification of miRNA from whole blood by chemical lysis and phase separation in a centrifugo-pnuematic micro-homogenizer. Proceedings of the 15th International Conference on Miniaturized Systems for Chemistry and Life Sciences (μTAS). Seattle; 2011. p. 1460–2.

54. SOLIDWORKS. 3D CAD Design Software SOLIDWORKS [Internet]. [cited 2016 May 2]. Available from: http://www.solidworks.com/

55. Herold KE, Rasooly A. Lab on a Chip Technology: Fabrication and microfluidics, Volume 1. 1st Ed. Horizon Scientific Press; 2009. 409 p.

56. Zhang W, Lin S, Wang C, Hu J, Li C, Zhuang Z, et al. PMMA/PDMS valves and pumps for disposable microfluidics. Lab Chip. 2009 Nov 7;9(21):3088–94.

57. Chen Y, Zhang L, Chen G. Fabrication, modification, and application of poly(methyl methacrylate) microfluidic chips. Electrophoresis. 2008 May;29(9):1801–14.

58. Becker H, Gärtner C. Polymer microfabrication technologies for microfluidic systems. Anal Bioanal Chem. 2008 Jan;390(1):89–111.

59. Cheng J-Y, Wei C-W, Hsu K-H, Young T-H. Direct-write laser micromachining and universal surface modification of PMMA for device development. Sensors Actuators B Chem. 2004 Apr;99(1):186–96.

60. Lee S-JJ, Sundararajan N. Microfabrication for Microfluidics. Artech House; 2010. 276 p.

61. Nunes PS, Ohlsson PD, Ordeig O, Kutter JP. Cyclic olefin

polymers: emerging materials for lab-on-a-chip applications. Microfluid Nanofluidics. 2010 Apr 7;9(2-3):145–61.

62. Yi L, Xiaodong W, Fan Y. Microfluidic chip made of COP (cyclo-olefin polymer) and comparion to PMMA (polymethylmethacrylate) microfluidic chip. J Mater Process Technol. 2008 Nov;208(1-3):63–9.

63. Jagota A, Bennison SJ. Mechanics of adhesion through a fibrillar microstructure. Integr Comp Biol. 2002 Dec 1;42(6):1140–5.

64. Klank H, Kutter JP, Geschke O. CO(2)-laser micromachining and back-end processing for rapid production of PMMA-based microfluidic systems. Lab Chip. The Royal Society of Chemistry; 2002 Nov 22;2(4):242–6.

65. Nayak NC, Lam YC, Yue CY, Sinha AT. CO 2 -laser micromachining of PMMA: the effect of polymer molecular weight. J Micromechanics Microengineering. 2008 Sep 1;18(9):095020.

66. Jensen MF, Noerholm M, Christensen LH, Geschke O. Microstructure fabrication with a CO2 laser system: characterization and fabrication of cavities produced by raster scanning of the laser beam. Lab Chip. 2003 Nov;3(4):302–7.

67. Chung CK, Lin YC, Huang GR. Bulge formation and improvement of the polymer in CO 2 laser micromachining. J Micromechanics Microengineering. 2005 Oct 1;15(10):1878–84.

68. Gibbs D, Crandell TM. An Introduction to CNC Machining and Programming. Industrial Press; 1991. 537 p.

69. Leatham-Jones B. Introduction to computer numerical control. Pitman; 1986. 245 p.

70. Milling Machines MODELA MDX-40A >> Specifications | Roland DG [Internet]. [cited 2015 Dec 21]. Available from:

http://www.rolanddg.com/product/3d/3d/mdx-40a/specifications.html

71. Mecomber JS, Stalcup AM, Hurd D, Halsall HB, Heineman WR, Seliskar CJ, et al. Analytical performance of polymer-based microfluidic devices fabricated by computer numerical controlled machining. Anal Chem. American Chemical Society; 2006 Feb 1;78(3):936–41.

72. Rengier F, Mehndiratta A, von Tengg-Kobligk H, Zechmann CM, Unterhinninghofen R, Kauczor H-U, et al. 3D printing based on imaging data: review of medical applications. Int J Comput Assist Radiol Surg. 2010 Jul;5(4):335–41.

73. He Y, Qiu J, Fu J, Zhang J, Ren Y, Liu A. Printing 3D microfluidic chips with a 3D sugar printer. Microfluid Nanofluidics. 2015 Apr 2;19(2):447–56.

74. VHX-5000 Digital Microscope | KEYENCE CORPORATION [Internet]. [cited 2015 Dec 22]. Available from: http://www.keyence.com/ss/products/microscope/vhx5000/

75. Bhushan B, editor. Encyclopedia of Nanotechnology. Dordrecht: Springer Netherlands; 2012. 2273-2280 p.

76. Schroeder A, Mueller O, Stocker S, Salowsky R, Leiber M, Gassmann M, et al. The RIN: an RNA integrity number for assigning integrity values to RNA measurements. BMC Mol Biol. 2006 Jan;7:3.

77. Thermo Scientific NanoDrop Products – Nucleic Acids [Internet]. [cited 2015 Dec 22]. Available from: http://www.nanodrop.com/ND1/NucleicAcid-Booklet.html

78. Wilfinger WW, Mackey K, Chomczynski P. Effect of pH and ionic strength on the spectrophotometric assessment of nucleic acid

purity. Biotechniques. 1997 Mar;22(3):474–6, 478–81.

79. Adams RL. Cell Culture for Biochemists. 2nd Editio. Amsterdam; Oxford: Elsevier Science; 1990. 122-123 p.

80. ThermoFisher. Guidelines for Maintaining Cultured Cells [Internet]. [cited 2016 May 5]. Available from: https://www.thermofisher.com/im/en/home/references/gibco-cell-culture-basics/cell-culture-protocols/maintaining-cultured-cells.html

81. Kim J, Kido H, Rangel RH, Madou MJ. Passive flow switching valves on a centrifugal microfluidic platform. Sensors Actuators B Chem. 2008 Jan;128(2):613–21.

82. Copois V, Bibeau F, Bascoul-Mollevi C, Salvetat N, Chalbos P, Bareil C, et al. Impact of RNA degradation on gene expression profiles: assessment of different methods to reliably determine RNA quality. J Biotechnol. 2007 Jan 20;127(4):549–59.

83. Hiorns LR, Bradshaw TD, Skelton LA, Yu Q, Kelland LR, Leyland-Jones B. Variation in RNA expression and genomic DNA content acquired during cell culture. Br J Cancer. Cancer Research UK; 2004 Jan 26;90(2):476–82.

84. Dimov N, Gaughran J, Auley DM, Boyle D, Kinahan DJ, Ducree J. Centrifugally automated solid-phase purification of RNA. 2014 IEEE 27th International Conference on Micro Electro Mechanical Systems (MEMS). IEEE; 2014. p. 260–3.

85. Novoselov KS, Geim a K, Morozov S V, Jiang D, Zhang Y, Dubonos S V, et al. Electric field effect in atomically thin carbon films. Science. 2004 Oct 22;306(5696):666–9.

86. Pumera M, Ambrosi A, Bonanni A, Chng ELK, Poh HL. Graphene for electrochemical sensing and biosensing. TrAC Trends Anal

Chem. Elsevier Ltd; 2010 Oct;29(9):954–65.

87. Ang PK, Li A, Jaiswal M, Wang Y, Hou HW, Thong JTL, et al. Flow sensing of single cell by graphene transistor in a microfluidic channel. Nano Lett. 2011 Dec 14;11(12):5240–6.

88. Lo C-W, Zhu D, Jiang H. An infrared-light responsive graphene-oxide incorporated poly(N-isopropylacrylamide) hydrogel nanocomposite. Soft Matter. 2011;7(12):5604.

89. Nair RR, Wu H a, Jayaram PN, Grigorieva I V, Geim a K. Unimpeded permeation of water through helium-leak-tight graphene-based membranes. Science. 2012 Jan 27;335(6067):442–4.

90. Taylor S. Impact of surface chemistry and blocking strategies on DNA microarrays. Nucleic Acids Res. 2003 Aug 15;31(16):87e – 87.

91. PCR Protocol for Taq DNA Polymerase with Standard Taq Buffer (M0273) | NEB [Internet]. [cited 2015 Dec 14]. Available from: https://www.neb.com/protocols/1/01/01/taq-dna-polymerase-with-standard-taq-buffer-m0273

92. Molecular Research Centre I. TRI Reagent® / TRI Reagent® BD / TRI Reagent® LS [Internet]. [cited 2016 May 22]. Available from: http://mrcgene.com/rna-isolation/tri-reagent

93. Chomczynski P, Sacchi N. Single-step method of RNA isolation by acid guanidinium thiocyanate-phenol-chloroform extraction. Anal Biochem. 1987 Apr;162(1):156–9.

94. Dimov N, Gaughran J, Clancy E, Barry T, Smith TJ, Ducree J. Automated on-disc total RNA extraction from whole blood towards point-of-care for early stage diagnostics. 2013 Transducers & Eurosensors XXVII: The 17th International Conference on Solid-State Sensors, Actuators and Microsystems (TRANSDUCERS &

EUROSENSORS XXVII). IEEE; 2013. p. 2548–51.

95. Millis J, Connell L, Collins SD, Smith RL. A microfabricated, flow driven mill for the mechanical lysis of algae. 2015 28th IEEE International Conference on Micro Electro Mechanical Systems (MEMS). IEEE; 2015. p. 188–91.

96. Reshes G, Vanounou S, Fishov I, Feingold M. Cell shape dynamics in Escherichia coli. Biophys J. 2008 Jan 1;94(1):251–64.

97. EOS - Phytoplankton Encyclopedia Project [Internet]. [cited 2015 Dec 21]. Available from: http://www.eos.ubc.ca/research/phytoplankton/dinoflagellates/alexandrium/a_tamarense.html

98. Roelofs SH, van den Berg A, Odijk M. Microfluidic desalination techniques and their potential applications. Lab Chip. The Royal Society of Chemistry; 2015 Aug 11;15(17):3428–38.

99. Cohen-Tanugi D, Grossman JC. Water desalination across nanoporous graphene. Nano Lett. 2012 Jul 11;12(7):3602–8.

Appendix A: List of Materials and Manufactures

ADF	Adhesives Research, Limerick, Ireland
BAN	Sigma Aldrich, Arklow, Ireland
Coloured food dyes	Goodalls, Cork, Ireland
DF Films	Adhesives Research, Limerick, Ireland
GO flakes	Bluestone, Manchester, UK
Iron (III) nitrate nnahydrate	Sigma Aldrich, Arklow, Ireland
LB Broth	Sigma Aldrich, Arklow, Ireland
Nuclease free water	VWR, Blanchardstown, Ireland
ODF	Adhesives Research, Limerick, Ireland
Potassium thiocyinate	Sigma Aldrich, Arklow, Ireland
PTFE-membrane	Merck Millipore, Cork Ireland
QiaQuick PCR Purification Kit	Qiagen, Manchester, UK
Quant-iT PicoGreeen dsDNA Assay	Life Technologies, Dublin, Ireland
Trizol Reagent	Sigma Aldrich, Arklow, Ireland
Zeonor	Zeonex, Düsseldorf, Germany